

UCSF

UC San Francisco Electronic Theses and Dissertations

Title

Recruited Monocytes and Type 2 Cytokines Promote Lung Regeneration

Permalink

<https://escholarship.org/uc/item/6bj342z5>

Author

Lechner, Andrew John

Publication Date

2017

Peer reviewed|Thesis/dissertation

Recruited Monocytes and Type 2 Cytokines
Promote Lung Regeneration

by

Andrew J Lechner

DISSERTATION

Submitted in partial satisfaction of the requirements for the degree of

DOCTOR OF PHILOSOPHY

in

Biomedical Sciences

in the

GRADUATE DIVISION

of the

UNIVERSITY OF CALIFORNIA, SAN FRANCISCO

Acknowledgements

The completion of this work would not have been possible without the constant support of mentors, friends, and family. Specifically, Andrew would like to thank Jason Rock and his committee members Zena Werb, Michael Matthay, and Tony Defranco for their guidance and insights. Andrew would like to thank his laboratory members Ian Driver, Matt Donne, Cindy Kanegai, Gorica Amidzic, Carmen Maria Conroy, Abigail Nagle, Raymond Ho, and Tyler Kim for assisting in the laboratory, as well as Eric Dang and Jinwoo Lee for continuous technical assistance and friendship. Andrew would like to thank Jason Chung and Kathy Wai for emotional support, and his beautiful wife, Narges Alipanah, for her unwavering love and patience. Finally, Andrew would like to thank his sister, Melissa, and his parents, Andy and Victoria, for instilling him with a love a science a long time ago and guiding him all the way.

Abstract

The only current treatment for end stage lung diseases is a full lung transplant. This procedure is limited by poor survival and an inadequate supply of donor lungs. An alternative is to promote regeneration of normal lung tissue from endogenous progenitor cells. Partial pneumonectomy (PNX), the surgical removal of one or more lobes, stimulates compensatory lung growth in the remaining lobes. This model of adult alveologenesis is mediated by proliferation of several progenitor populations, including alveolar epithelial type 2 cells (AEC2s), which are distal lung epithelial stem cells. Recently macrophages have been implicated in tissue repair and regeneration, but little is knownpdf about their role in lung regeneration. Significant questions remain regarding the regenerative potential of human lungs, the identities of human lung epithelial stem cells, the molecular signals that control their activation, and the influences of the microenvironment on regeneration. Our objective is to apply data from murine studies to stimulate regeneration of human lungs.

We used fluorescent reporters and genetic gain- and loss-of function in mice to identify populations of immune cells that modulate epithelial stem cell behaviors in adult lung regeneration. We hope to identify molecular targets that mediate these effects that might be exploited to stimulate lung regeneration and may be developed into novel therapies for patients with end-stage lung disease.

We found that CD115+ monocytes and macrophages accumulate in the remaining uninjured lung lobes during the peak of proliferation of type 2 alveolar epithelial stem cells (AEC2s). Single cell RNA sequencing identified myeloid subpopulations in regenerating lungs, including CCR2+ monocytes and M2-like macrophages. Genetic loss of function in mice and adoptive transfer studies revealed that bone marrow-derived macrophages are recruited to the lung through a CCL2-CCR2 chemokine axis and are required for optimal lung regeneration. Bone marrow chimerism demonstrated that IL-4R α -mediated signaling is required on leukocytes for polarization of Arginase1+ M2-like macrophages that are also required for lung regeneration.

Our data suggest that these cells modulate AEC2 proliferation and differentiation. Finally, we provide evidence that ILC2s are a source of IL13 that polarizes M2-like macrophages. Together, our data highlight the potential for immunomodulatory therapies to stimulate alveologenesis in adults.

Table of Contents

Chapter 1: Introduction	1
References.....	8
Figures	14
Chapter 2: Emerging niche components of the alveolar type 2 stem cell niche	16
References.....	27
Figures	35
Chapter 3: Recruited monocytes and Type-2 cytokines promote lung regeneration.....	37
Introduction	38
Results	41
Discussion.....	52
Methods	55
References.....	67
Figures	77
Chapter 4: Alveolar epithelial lung stem cells are vulnerable to exhaustion after injury	108
Introduction	109
Results	110
Discussion.....	112
Methods	114
References.....	116
Figures	117
Chapter 5: Conclusions	123
References.....	127

List of Figures

Chapter 1:

Figure 1: Schematic of the major epithelial progenitor populations and their niches in the distal lung alveolus.....	14
Figure 2: Unilateral pneumonectomy procedure	15

Chapter 2:

Figure 1: Selected niche-stem cell interactions in lung repair/regeneration	35
---	----

Chapter 3:

Figure 1. Increased numbers of myeloid cells in the lungs of mice after PNX.....	77
Figure 2. CCR2+ monocytes are recruited to the lung post-PNX.	79
Figure 3. CCR2+ monocytes are required for lung regeneration post-PNX	81
Figure 4. Macrophages are sufficient to support alveolar stem cells.....	83
Figure 5. M2-like macrophages are required for lung regeneration.....	85
Figure 6. ILC2s accumulate and produce IL-13 post-PNX	87
Figure S1. Related to Figure 1. CD115+ macrophages are the dominant myeloid population in regenerating lung tissue post-PNX	89
Figure S2. Related to Figure 2. CCR2+ monocytes are recruited and local macrophages proliferate post-PNX.....	91
Figure S3. Related to Figure 3. Impaired lung regeneration in CCR2-deficient mice persists long-term.....	93
Figure S4. Related to Figure 4. Lung and bone marrow-derived macrophages support lung regeneration <i>in vivo</i> and <i>in vitro</i>	94
Figure S5. Related to Figure 5. CCR2-deficiency impairs the generation of IL4-dependent M2-like macrophages, which are required for lung regeneration and locally proliferate post-PNX.....	97
Figure S6: Related to Figure 6. ILC2s accumulate and produce IL-13 post-PNX	99

Chapter 4:

Figure 1. Genetic depletion model for lung alveolar epithelial stem cells 117

Figure 2. Lung alveolar epithelial stem cells recover after targeted depletion 119

Figure 3. Repeated AEC2s depletion results in diminished AEC2 recovery 121

List of Tables:

Chapter 3:

Table 1. Key Resources Table.....	101
Table S1. Primer sequences used for mouse genotyping	106
Table S2. Primer sequences used for quantitative RT-PCR analysis.....	107

Chapter 1
Introduction

1.1 The burden of lung disease and the need for alternative therapies

There are no cures for end-stage lung diseases and the only long-term option remains a full lung transplant. The effectiveness of this procedure is limited by both poor survival and an inadequate supply of donor lungs. An alternative to lung transplant is to promote regeneration of normal lung tissue from endogenous progenitor cells. Significant questions remain regarding the regenerative potential of human lungs, the identities of human lung epithelial stem cells, the molecular signals that control their activation, and the influences of the microenvironment on regeneration. Our eventual goal is to apply basic biological discoveries to stimulate the regeneration of lungs in patients with pulmonary diseases.

While relatively quiescent at steady-state, several lung epithelial stem cell populations are activated by different models of regeneration and repair (Rock and Hogan, 2011). Partial pneumonectomy (PNX), or the removal of one or more lung lobes, induces alveolar epithelial type 2 cell (AEC2) proliferation and adult alveologenesis to compensate for the lost surface area for gas exchange (Thane et al., 2014). In this model of lung regeneration, the niche components assisting lung epithelial stem cell proliferation have begun to be elucidated (Hogan et al., 2014). Recently, macrophages have been shown to play roles in regenerating spinal cord, skin, heart, skeletal muscle, liver, colon, kidney, and limbs (Arnold et al., 2007; Aurora and Olson, 2014; Aurora et al., 2014; Boulter et al., 2012; Duffield et al., 2005; Epelman et al., 2014; Godwin et al., 2013; Lin et al., 2010; Lucas et al., 2010; Pull et al., 2005; Ramachandran et al., 2012; Ruffell et al., 2009; Shechter et al., 2013), but little is known about their role in lung regeneration. These pro-regenerative macrophages are often derived from circulating monocytes recruited to injured tissues (Dutta et al., 2015; Gibbons et al., 2011; Ramachandran et al., 2012). Their abundance, proximity to AEC2s, and functional versatility make lung macrophages good candidates as integral niche components regulating lung epithelial stem cells. Preliminary data from our lab demonstrates that macrophages increase in the regenerating alveolar tissue, with a peak at 7 days after pneumonectomy. At present, little is

known about how macrophages respond to PNx-induced lung regeneration, how macrophages may regulate AEC2 behavior during injury and repair, and how AEC2s respond to macrophage-derived signals.

One goal of regenerative medicine is to harness the endogenous potential of an organ for self-repair in order to restore normal function during disease states (Dimmeler et al., 2014). To ensure the safety and efficacy of stem cell therapies in the clinic, we must first understand the mechanisms that govern stem cell behaviors including the role of the stem cell niche (Lane et al., 2014). The epithelial lining of the respiratory tract is subjected to continuous environmental insults and acute injuries, both requiring local cell turnover and repair. A number of incurable respiratory conditions, including emphysema and idiopathic pulmonary fibrosis, are characterized by irreparable damage to lung epithelia that compromises lung function. Thus, the development of new therapies for repairing and regenerating lung epithelium holds great promise for the field of pulmonary medicine.

1.2 Distal lung epithelial stem cells

Although several putative alveolar epithelial stem cell populations have been described, historic and recent evidence suggests that AEC2s (which express surfactant associated protein C, *Sftpc*) are capable of long-term self-renewal and generation of AEC1s (Barkauskas et al., 2013; Rock et al., 2011). While AEC2s far outnumber AEC1s, 97% of the alveolar epithelial surface is lined by AEC1s, which until recently were thought to be completely terminally differentiated (Jain et al., 2015). AEC1s lie in apposition to endothelial capillaries, creating a thin diffusion membrane that maximizes the efficiency of gas exchange. An alveolar population of *Itga6b4*⁺, *Sftpc*⁻ cells that is also capable of self renewal and of generating AEC1 in vitro or under the kidney capsule was recently identified, but their endogenous capacity for self-renewal and differentiation in vivo awaits genetic lineage tracing experiments (Chapman et al., 2011). Additional putative alveolar progenitor populations include lineage-negative epithelial

progenitors (LNEPs) and distal alveolar stem cells (DASCs), which express Keratin5 and Trp63 (Kumar et al., 2011; Vaughan et al., 2015; Zuo et al., 2015). In the mouse, the bronchioalveolar duct junction (BADJ) harbors putative progenitors called bronchioalveolar stem cells (BASCs) that can give rise to both airway and alveolar lineages in vitro and under some injury conditions (Kim et al., 2005). BASCs express both Sftpc and Scg1a1, but to date, no human counterpart of this cell type has been identified. Putative niche components for the distal lung stem cells described above include stromal cells and various immune cell populations (Figure 1). Surrounding the alveolus, mesenchymal cell types include fibroblasts, smooth muscle cells, and pericytes. Lung resident alveolar macrophages patrol the alveolar space and are easily identified by their characteristic morphology and expression of CD11c. Other local immune cell populations include dendritic cells, eosinophils, basophils, neutrophils, interstitial macrophages and monocytes, innate lymphoid cells, and lymphocytes.

1.3 Pneumonectomy-induced lung regeneration

The lung is a relatively quiescent organ, with less than 1% of cells proliferating under steady-state conditions. Therefore, it is common to induce injury/repair paradigms to study cell lineage relationships in the lung. The type and severity of induced lung injury likely determines the specific lung epithelial stem cell that will respond. In partial pneumonectomy (PNX) the removal of healthy lung tissue results in compensatory growth of the remaining lobes to compensate for lost alveolar surface area (Figure 2). Dogma asserts that this process is initiated by the stretch that PNX causes on the remaining lung tissue. This PNX-induced regenerative response can be quantified by increased lung weight, alveolar number, and proliferation of epithelial, mesenchymal, and vascular progenitor cell populations. AEC2s are the major proliferating epithelial stem cell contributing to new alveolar tissue, with a peak in proliferation at 7 days post-PNX in mice (Hoffman et al., 2010; Nolen-Walston et al., 2008). AEC2 niche

components such as PDGFR-A⁺ fibroblasts and VEGFR3⁺ endothelial cells have essential roles in PNX-induced lung regeneration (Chen et al., 2012; Ding et al., 2011). However, the role of immune cells in this process is not clear.

1.4 Macrophages in tissue repair and regeneration

Macrophages are heterogeneous in origin, marker expression, and functions, with important roles in tissue development, homeostasis, disease, and injury repair (Davies et al., 2013; Murray and Wynn, 2011; Wynn et al., 2013). Most tissue resident macrophages are derived from hematopoietic progenitors during embryogenesis and are maintained by self-renewal; however, circulating monocytes are able to replenish macrophages during states of inflammation and regeneration (Arnold et al., 2007; Aurora and Olson, 2014; Aurora et al., 2014; Boulter et al., 2012; Duffield et al., 2005; Epelman et al., 2014a; Godwin et al., 2013; Lin et al., 2010; Lucas et al., 2010; Pull et al., 2005; Ramachandran et al., 2012; Ruffell et al., 2009; Shechter et al., 2013). Micro-environmental cues polarize macrophages towards different phenotypes to execute specific functions (Mosser and Edwards, 2008; Murray et al., 2014; Sica and Mantovani, 2012). Classically activated macrophages (M1) are typically induced by bacterial infections and respond by producing pro-inflammatory cytokines TNF- α , IL-6, IL-1 β , interferons, and reactive oxygen species that promote pathogen clearance. Alternatively activated macrophages (M2) are associated with parasitic helminthic infections and wound healing. Through their secretion of IL-10, M2s promote type-2 anti-inflammatory immunity that contributes to matrix remodeling and attenuates inflammation. M2s are regulated internally by Stat6 signaling, and express key genes like *Arg1*, *Fizz1*, *Ym1*, *MRC1*, and *PPAR- γ* (Gordon and Martinez, 2010).

In models ranging from *Axolotl* limbs to mammalian liver, kidney, and heart, macrophages are essential for tissue regeneration (Arnold et al., 2007; Aurora and Olson, 2014;

Aurora et al., 2014; Boulter et al., 2012; Duffield et al., 2005; Epelman et al., 2014a; Godwin et al., 2013; Lin et al., 2010; Lucas et al., 2010; Pull et al., 2005; Ramachandran et al., 2012; Ruffell et al., 2009; Shechter et al., 2013). During bleomycin-induced lung fibrosis in mice, the disease process worsened when macrophages were depleted during the recovery stage and improved when macrophages were depleted during the fibrotic stage (Gibbons et al., 2011). In PNX-induced lung regeneration, alveolar macrophages proliferate, and upregulate pro-angiogenic and matrix-remodeling genes (Chamoto et al., 2012). Researchers also identified increases in CD11b⁺ cells in regenerating lung tissue post-PNX and provided some evidence that CD18-deficient mice fail to generate new lung tissue post-PNX (Chamoto et al., 2013). However, no study has characterized immune cells over the course of the regenerative response, described their activation states, or proposed a mechanism of how myeloid cells may regulate AEC2s or their niche during lung regeneration. While macrophages regulate other epithelial stem cells during injury and repair, their precise action on AEC2s during lung regeneration is unknown.

1.5 Macrophages as components of the lung epithelial stem cell niche

Lung macrophages are essential for clearing proteinaceous debris from airway lumens, killing pathogens that evade the mucociliary escalator, priming lymphocytes, and modulating the inflammatory milieu in homeostasis and disease (Hussell and Bell, 2014; Li et al., 2003; Shibata et al., 2001). Lung macrophages are M2-polarized during postnatal alveologenesi and transgenic activation of NF- κ B signaling in these cells disrupts branching lung morphogenesis, highlighting the importance of lung macrophage activation states (Blackwell et al., 2011; Jones et al., 2013). Lung macrophages may prolong chronic airway injury through pro-inflammatory cytokine secretion, or attenuate immune responses by phagocytizing neutrophils (Aggarwal et al., 2014; Herold et al., 2011). While their role in protecting the respiratory epithelium is well established, little is known about how macrophages may influence AEC2 behaviors during lung

regeneration and adult alveologenesis. Considering their alveolar localization, ability to modulate inflammatory microenvironments, and their contribution to stem cell niches in other organs, we hypothesize that macrophages in the lung comprise an essential part of the AEC2 regenerative niche. We have shown that these cells increase post-PNX, but it is unclear how macrophages interact with AEC2s and it is not known how lung epithelial stem cells respond to immune signals post-PNX.

References:

- Aggarwal, N.R., King, L.S., and D'Alessio, F.R. (2014). Diverse macrophage populations mediate acute lung inflammation and resolution. *Am. J. Physiol. Lung Cell Mol. Physiol.* *306*, L709–25.
- Arnold, L., Henry, A., Poron, F., Baba-Amer, Y., van Rooijen, N., Plonquet, A., Gherardi, R.K., and Chazaud, B. (2007). Inflammatory monocytes recruited after skeletal muscle injury switch into antiinflammatory macrophages to support myogenesis. *J. Exp. Med.* *204*, 1057–1069.
- Aurora, A., and Olson, E. (2014). Immune Modulation of Stem Cells and Regeneration. *Cell Stem Cell* *15*, 1425.
- Aurora, A.B., Porrello, E.R., Tan, W., Mahmoud, A.I., Hill, J.A., Bassel-Duby, R., Sadek, H.A., and Olson, E.N. (2014). Macrophages are required for neonatal heart regeneration. *J. Clin. Invest.* *124*, 1382–1392.
- Barkauskas, C.E., Counce, M.J., Rackley, C.R., Bowie, E.J., Keene, D.R., Stripp, B.R., Randell, S.H., Noble, P.W., and Hogan, B.L. (2013). Type 2 alveolar cells are stem cells in adult lung. *J. Clin. Invest.* *123*, 3025–3036.
- Blackwell, T.S., Hipps, A.N., Yamamoto, Y., Han, W., Barham, W.J., Ostrowski, M.C., Yull, F.E., and Prince, L.S. (2011). NF- κ B signaling in fetal lung macrophages disrupts airway morphogenesis. *J. Immunol.* *187*, 2740–2747.
- Boulter, L., Govaere, O., Bird, T.G., Radulescu, S., Ramachandran, P., Pellicoro, A., Ridgway, R.A., Seo, S.S., Spee, B., Van Rooijen, N., et al. (2012). Macrophage-derived Wnt opposes Notch signaling to specify hepatic progenitor cell fate in chronic liver disease. *Nat. Med.* *18*, 572–579.
- Chamoto, K., Gibney, B.C., Ackermann, M., Lee, G.S., Lin, M., Kondering, M.A., Tsuda, A., and Mentzer, S.J. (2012). Alveolar macrophage dynamics in murine lung regeneration. *J. Cell. Physiol.* *227*, 3208–3215.
- Chamoto, K., Gibney, B.C., Lee, G.S., Ackermann, M., Kondering, M.A., Tsuda, A., and

Mentzer, S.J. (2013). Migration of CD11b⁺ accessory cells during murine lung regeneration. *Stem Cell Res* 10, 267–277.

Chapman, H.A., Li, X., Alexander, J.P., Brumwell, A., Lorizio, W., Tan, K., Sonnenberg, A., Wei, Y., and Vu, T.H. (2011). Integrin $\alpha 6\beta 4$ identifies an adult distal lung epithelial population with regenerative potential in mice. *J. Clin. Invest.* 121, 2855–2862.

Chen, L., Acciani, T., Le Cras, T., Lutzko, C., and Perl, A.-K.T.K. (2012). Dynamic regulation of platelet-derived growth factor receptor α expression in alveolar fibroblasts during realveolarization. *Am. J. Respir. Cell Mol. Biol.* 47, 517–527.

Davies, L., Jenkins, S., Allen, J., and Taylor, P. (2013). Tissue-resident macrophages. *Nature Immunology* 14, 986–995.

Dimmeler, S., Ding, S., Rando, T.A., and Trounson, A. (2014). Translational strategies and challenges in regenerative medicine. *Nat. Med.* 20, 814–821.

Ding, B.-S.S., Nolan, D.J., Guo, P., Babazadeh, A.O., Cao, Z., Rosenwaks, Z., Crystal, R.G., Simons, M., Sato, T.N., Worgall, S., et al. (2011). Endothelial-derived angiocrine signals induce and sustain regenerative lung alveolarization. *Cell* 147, 539–553.

Duffield, J.S., Forbes, S.J., Constandinou, C.M., Clay, S., Partolina, M., Vuthoori, S., Wu, S., Lang, R., and Iredale, J.P. (2005). Selective depletion of macrophages reveals distinct, opposing roles during liver injury and repair. *J. Clin. Invest.* 115, 56–65.

Dutta, P., Sager, H.B., Stengel, K.R., Naxerova, K., Courties, G., Saez, B., Silberstein, L., Heidt, T., Sebas, M., Sun, Y., et al. (2015). Myocardial Infarction Activates CCR2(+) Hematopoietic Stem and Progenitor Cells. *Cell Stem Cell* 16, 477–487.

Epelman, S., Lavine, K.J., Beaudin, A.E., Sojka, D.K., Carrero, J.A., Calderon, B., Brija, T., Gautier, E.L., Ivanov, S., Satpathy, A.T., et al. (2014a). Embryonic and adult-derived resident cardiac macrophages are maintained through distinct mechanisms at steady state and during inflammation. *Immunity* 40, 91–104.

Epelman, S., Lavine, K.J., and Randolph, G.J. (2014b). Origin and functions of tissue

macrophages. *Immunity* 41, 21–35.

Gibbons, M.A., MacKinnon, A.C., Ramachandran, P., Dhaliwal, K., Duffin, R., Phythian-Adams, A.T., van Rooijen, N., Haslett, C., Howie, S.E., Simpson, A.J., et al. (2011). Ly6Chi monocytes direct alternatively activated profibrotic macrophage regulation of lung fibrosis. *Am. J. Respir. Crit. Care Med.* 184, 569–581.

Godwin, J.W., Pinto, A.R., and Rosenthal, N.A. (2013). Macrophages are required for adult salamander limb regeneration. *Proc. Natl. Acad. Sci. U.S.A.* 110, 9415–9420.

Gordon, S., and Martinez, F. (2010). Alternative Activation of Macrophages: Mechanism and Functions. *Immunity* 32, 593–604.

Hashimoto, D., Chow, A., Noizat, C., Teo, P., Beasley, M.B., Leboeuf, M., Becker, C.D., See, P., Price, J., Lucas, D., et al. (2013). Tissue-resident macrophages self-maintain locally throughout adult life with minimal contribution from circulating monocytes. *Immunity* 38, 792–804.

Herold, S., Mayer, K., and Lohmeyer, J. (2011). Acute lung injury: how macrophages orchestrate resolution of inflammation and tissue repair. *Front Immunol* 2, 65.

Hoffman, A.M., Shifren, A., Mazan, M.R., Gruntman, A.M., Lascola, K.M., Nolen-Walston, R.D., Kim, C.F., Tsai, L., Pierce, R.A., Mecham, R.P., et al. (2010). Matrix modulation of compensatory lung regrowth and progenitor cell proliferation in mice. *Am. J. Physiol. Lung Cell Mol. Physiol.* 298, L158–68.

Hogan, B.L., Barkauskas, C.E., Chapman, H.A., Epstein, J.A., Jain, R., Hsia, C.C., Niklason, L., Calle, E., Le, A., Randell, S.H., et al. (2014). Repair and regeneration of the respiratory system: complexity, plasticity, and mechanisms of lung stem cell function. *Cell Stem Cell* 15, 123–138.

Hussell, T., and Bell, T.J. (2014). Alveolar macrophages: plasticity in a tissue-specific context. *Nat. Rev. Immunol.* 14, 81–93.

Jain, R., Barkauskas, C.E., Takeda, N., Bowie, E.J., Aghajanian, H., Wang, Q., Padmanabhan, A., Manderfield, L.J., Gupta, M., Li, D., et al. (2015). Plasticity of Hopx(+) type I alveolar cells to

regenerate type II cells in the lung. *Nat Commun* 6, 6727.

Jakubzick, C., Gautier, E.L., Gibbings, S.L., Sojka, D.K., Schlitzer, A., Johnson, T.E., Ivanov, S., Duan, Q., Bala, S., Condon, T., et al. (2013). Minimal differentiation of classical monocytes as they survey steady-state tissues and transport antigen to lymph nodes. *Immunity* 39, 599–610.

Jones, C.V., Williams, T.M., Walker, K.A., Dickinson, H., Sakkal, S., Rumballe, B.A., Little, M.H., Jenkin, G., and Ricardo, S.D. (2013). M2 macrophage polarisation is associated with alveolar formation during postnatal lung development. *Respir. Res.* 14, 41.

Kim, C.F., Jackson, E.L., Woolfenden, A.E., Lawrence, S., Babar, I., Vogel, S., Crowley, D., Bronson, R.T., and Jacks, T. (2005). Identification of bronchioalveolar stem cells in normal lung and lung cancer. *Cell* 121, 823–835.

Kumar, P.A., Hu, Y., Yamamoto, Y., Hoe, N.B., Wei, T.S., Mu, D., Sun, Y., Joo, L.S., Dagher, R., Zielonka, E.M., et al. (2011). Distal airway stem cells yield alveoli in vitro and during lung regeneration following H1N1 influenza infection. *Cell* 147, 525–538.

Lane, S.W., Williams, D.A., and Watt, F.M. (2014). Modulating the stem cell niche for tissue regeneration. *Nat. Biotechnol.* 32, 795–803.

Li, M., Sarkisian, M., Mehal, W., Rakic, P., and Flavell, R. (2003). Phosphatidylserine Receptor Is Required for Clearance of Apoptotic Cells. *Science* 302, 1560–1563.

Lin, S.-L.L., Li, B., Rao, S., Yeo, E.-J.J., Hudson, T.E., Nowlin, B.T., Pei, H., Chen, L., Zheng, J.J., Carroll, T.J., et al. (2010). Macrophage Wnt7b is critical for kidney repair and regeneration. *Proc. Natl. Acad. Sci. U.S.A.* 107, 4194–4199.

Lucas, T., Waisman, A., Ranjan, R., Roes, J., Krieg, T., Müller, W., Roers, A., and Eming, S. (2010). Differential Roles of Macrophages in Diverse Phases of Skin Repair. *The Journal of Immunology* 184, 3964–3977.

Mosser, D.M., and Edwards, J.P. (2008). Exploring the full spectrum of macrophage activation. *Nat. Rev. Immunol.* 8, 958–969.

Murray, P.J., and Wynn, T.A. (2011). Protective and pathogenic functions of macrophage

subsets. *Nat. Rev. Immunol.* *11*, 723–737.

Murray, P.J., Allen, J.E., Biswas, S.K., Fisher, E.A., Gilroy, D.W., Goerdt, S., Gordon, S., Hamilton, J.A., Ivashkiv, L.B., Lawrence, T., et al. (2014). Macrophage activation and polarization: nomenclature and experimental guidelines. *Immunity* *41*, 14–20.

Nolen-Walston, R.D., Kim, C.F., Mazan, M.R., Ingenito, E.P., Gruntman, A.M., Tsai, L., Boston, R., Woolfenden, A.E., Jacks, T., and Hoffman, A.M. (2008). Cellular kinetics and modeling of bronchioalveolar stem cell response during lung regeneration. *Am. J. Physiol. Lung Cell Mol. Physiol.* *294*, L1158–65.

Pull, S.L., Doherty, J.M., Mills, J.C., Gordon, J.I., and Stappenbeck, T.S. (2005). Activated macrophages are an adaptive element of the colonic epithelial progenitor niche necessary for regenerative responses to injury. *Proc. Natl. Acad. Sci. U.S.A.* *102*, 99–104.

Ramachandran, P., Pellicoro, A., Vernon, M.A., Boulter, L., Aucott, R.L., Ali, A., Hartland, S.N., Snowden, V.K., Cappon, A., Gordon-Walker, T.T., et al. (2012). Differential Ly-6C expression identifies the recruited macrophage phenotype, which orchestrates the regression of murine liver fibrosis. *Proc. Natl. Acad. Sci. U.S.A.* *109*, E3186–95.

Rock, J.R., and Hogan, B.L. (2011). Epithelial progenitor cells in lung development, maintenance, repair, and disease. *Annu. Rev. Cell Dev. Biol.* *27*, 493–512.

Rock, J.R., Barkauskas, C.E., Counce, M.J., Xue, Y., Harris, J.R., Liang, J., Noble, P.W., and Hogan, B.L. (2011). Multiple stromal populations contribute to pulmonary fibrosis without evidence for epithelial to mesenchymal transition. *Proc. Natl. Acad. Sci. U.S.A.* *108*, E1475–83.

Ruffell, D., Mourkioti, F., Gambardella, A., Kirstetter, P., Lopez, R., Rosenthal, N., and Nerlov, C. (2009). A CREB-C/EBP β cascade induces M2 macrophage-specific gene expression and promotes muscle injury repair. *Proceedings of the National Academy of Sciences* *106*, 17475–17480.

Shechter, R., Miller, O., Yovel, G., Rosenzweig, N., London, A., Ruckh, J., Kim, K.-W.W., Klein, E., Kalchenko, V., Bendel, P., et al. (2013). Recruitment of beneficial M2 macrophages to

injured spinal cord is orchestrated by remote brain choroid plexus. *Immunity* 38, 555–569.

Shibata, Y., Berclaz, P.Y., Chroneos, Z.C., Yoshida, M., Whitsett, J.A., and Trapnell, B.C. (2001). GM-CSF regulates alveolar macrophage differentiation and innate immunity in the lung through PU.1. *Immunity* 15, 557–567.

Sica, A., and Mantovani, A. (2012). Macrophage plasticity and polarization: in vivo veritas. *J Clin Invest* 122, 787–795.

Thane, K., Ingenito, E., and Hoffman, A. (2014). Lung regeneration and translational implications of the postpneumonectomy model. *Translational Research* 163, 363376.

Vaughan, A.E., Brumwell, A.N., Xi, Y., Gotts, J.E., Brownfield, D.G., Treutlein, B., Tan, K., Tan, V., Liu, F.C., Looney, M.R., et al. (2015). Lineage-negative progenitors mobilize to regenerate lung epithelium after major injury. *Nature* 517, 621–625.

Wynn, T., Chawla, A., and Pollard, J. (2013). Macrophage biology in development, homeostasis and disease. *Nature* 496, 445–455.

Zuo, W., Zhang, T., Wu, D.Z., Guan, S.P., Liew, A.-A.A., Yamamoto, Y., Wang, X., Lim, S.J., Vincent, M., Lessard, M., et al. (2015). p63(+)Krt5(+) distal airway stem cells are essential for lung regeneration. *Nature* 517, 616–620.

Figure 1: Schematic of the major epithelial progenitor populations and their niches in the distal lung alveolus (modified from Rock and Hogan, 2010).

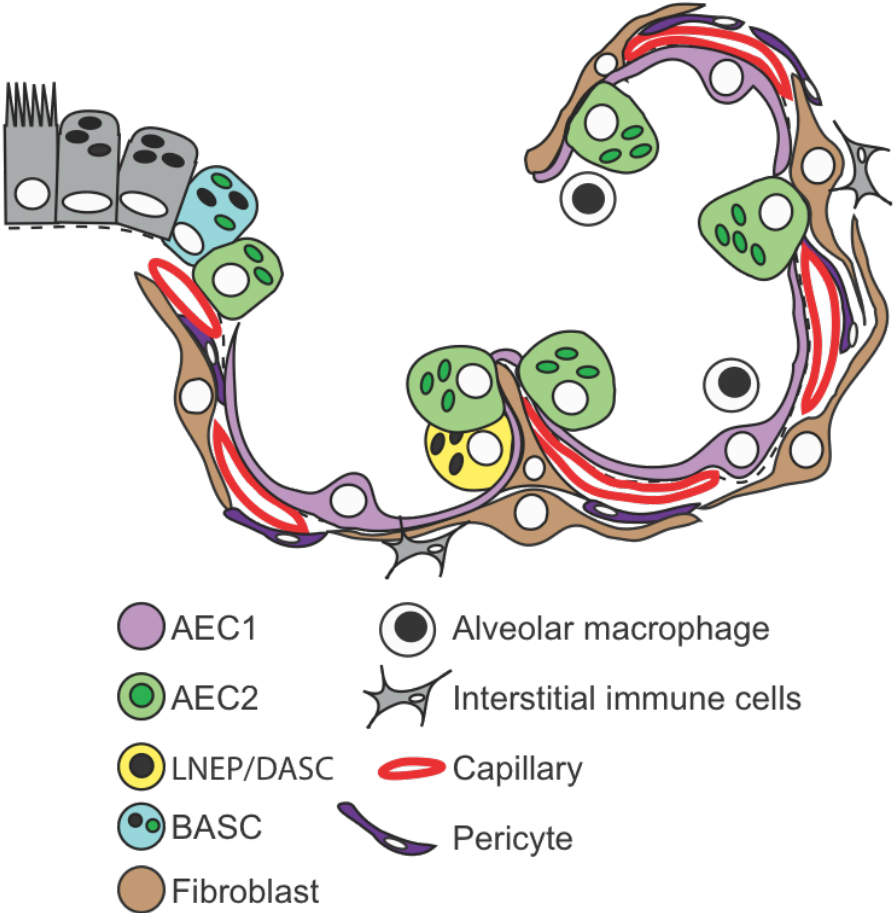
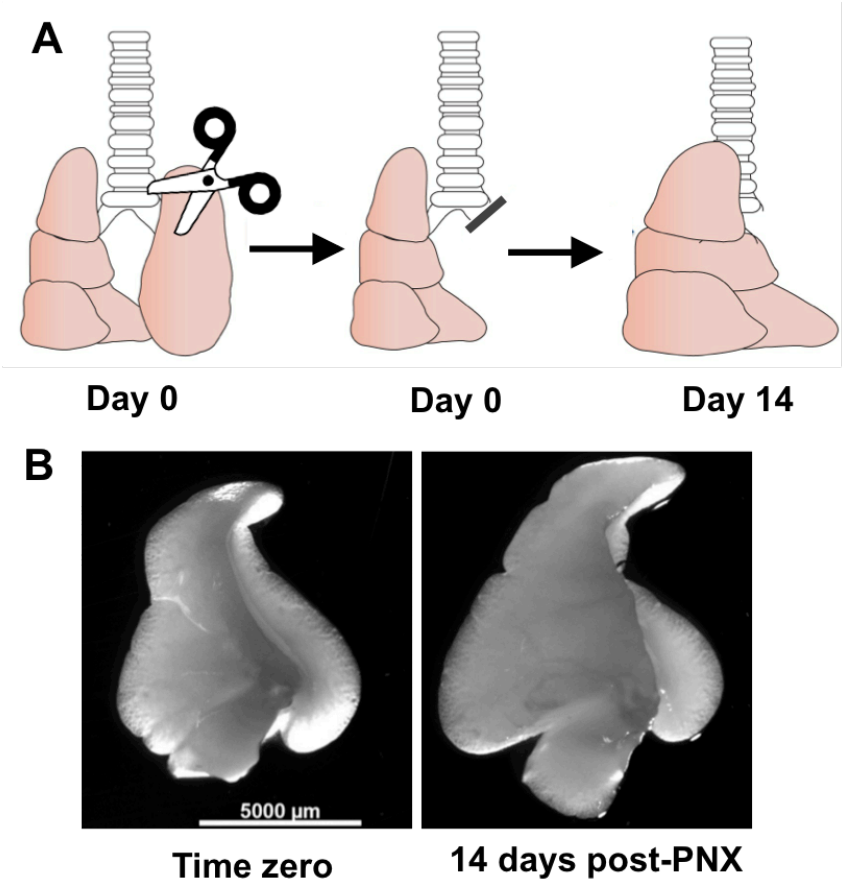


Figure 2: Unilateral pneumonectomy procedure (A) Schematic of pneumonectomy procedure in mice. **(B)** Whole mount image of accessory lobe at time zero or 14 days post-pneumonectomy.



Chapter 2

Evidence for lung epithelial stem cell niches

2.1 Regulatory niches for lung epithelial stem cells

Recent studies have identified epithelial stem and progenitor cell populations of the lung. We are just beginning to understand the mechanisms that regulate their homeostatic, regenerative and maladaptive behaviors. Here, we discuss evidence of regulatory niches for epithelial stem cells of the lung. Unfortunately, curative therapies do not exist for many end stage lung diseases and the final option is often a full lung transplant. The success of this procedure is limited by an inadequate supply of suitable donor organs and chronic allograft rejection in recipients. In vitro studies and animal models have demonstrated that the lung, like some other solid organs, has an endogenous capacity for maintenance and repair (reviewed in [1]). One potential alternative strategy for the management of lung disease would be to harness this reparative potential to prevent or reverse the debilitating effects of pathologic remodeling of the lung. This will require a better understanding of the stem/progenitor cell populations and the cellular and molecular mechanisms that regulate their behaviors.

2.2 Lung structure and cellular composition

The cellular composition of the epithelial lining of the respiratory tract varies along its proximo-distal axis [2]. The conducting airways from the trachea to bronchioles of human lungs consist of pseudostratified epithelium, comprising roughly equal proportions of basal cells, secretory cells, and ciliated cells, as well as some neuroendocrine cells. The smallest bronchioles, known as terminal and respiratory bronchioles, are lined with a simple columnar or cuboidal epithelium containing secretory and ciliated cells with fewer basal cells. The epithelia of these conducting airways form a tight barrier against the outside world and are specialized for the process of mucociliary clearance. The alveoli are lined by type 1 and 2 alveolar epithelial cells, called AEC1 and AEC2, respectively, hereafter. These cells are also specialized for barrier function and the extremely thin

AEC1s share a basement membrane with the surrounding network of pulmonary capillaries to

facilitate the diffusion of gases between the atmosphere and the circulation. This general distribution of epithelial cell types is conserved between humans and model organisms such as rodents. However, there are notable differences [2]. For example, the transition from a pseudostratified to columnar epithelium occurs more proximally in rodents, so only the trachea and mainstem bronchi are lined with a pseudostratified epithelium. Nearly all intralobar airways in mice are lined with a simple columnar or cuboidal epithelium with few, if any, basal cells. In mice, the abrupt transition from a conducting airway to the alveoli it supplies is known as a bronchioalveolar duct junction. In humans, terminal bronchioles give rise to respiratory bronchioles from which many alveolar ducts terminate ultimately in alveoli [3].

2.3 Stem cell populations in the lung

Unlike some other organs, the lung is relatively quiescent under steady state conditions [4]. Relatively infrequent progenitor cell divisions maintain the respiratory epithelium. For this reason it is common to experimentally induce cell turnover in order to study stem cell behaviors and clonal dynamics in the lung [5, 6]. As a result, relatively little is known about cell lineage relationships and stem cell niches under state conditions. Moreover, because assays for human lung stem cells are only just gaining popularity, our understanding of lung maintenance and repair is primarily based on studies from model organisms. Here, we discuss recent advances toward the identification of stem cell populations in the lung and their putative niche components, highlighting species differences and experimental design where appropriate.

It is generally accepted that under steady state conditions and in response to mild injury, distinct epithelial stem cell populations maintain and repair each of the lung regions described above (reviewed in [1, 7]). Basal cells of the pseudostratified conducting airway epithelium characteristically express the transcription factor Trp63, cytokeratin 5, podoplanin, NGFR and, variably, cytokeratin 14 [2, 8]. Early studies showed that basal cells purified from donor rats are capable of generating a pseudostratified epithelium

comprised of basal, ciliated and secretory cells when seeded into a denuded trachea grafted subcutaneously in a host [9]. This suggested that basal cells, as a population, are capable of self-renewal and differentiation. More recently, in vivo genetic lineage tracing studies in mice and humans have shown that basal cells are capable of long-term self-renewal and the generation of secretory and ciliated cells [8, 10, 11].

Finally, individual p63+ basal cells from either mouse or human lungs can be cultured in Matrigel to generate multicellular tracheospheres (or bronchospheres) that are made up of basal cells and Krt8+ luminal cells (including secretory and ciliated cells) [8, 12]. Emerging data suggest that basal cells are heterogeneous, at both the transcriptional and functional levels [6, 13]. The degree to which this heterogeneity is intrinsic or a function of microenvironmental cues is not known.

Secretory Club cells (previously known as Clara cells, [14]), characterized by apical protrusions packed with secreted proteins including SCGB1A1, are also found in the conducting airways. In simple columnar and cuboid epithelia where basal cells are rare or absent, evidence from lineage tracing in mice suggests that Club cells are capable of long-term self-renewal and the generation of ciliated and mucous-producing goblet cells under steady state conditions and in response to injury [15, 16]. Club cells of human airways proliferate under steady state conditions [17], but the extent of their capacity for self-renewal and differentiation is not known.

In the alveoli, AEC2s are the primary source of surfactant-associated protein C (Sftpc), a component of the layer of surfactant that reduces surface tension to prevent alveolar collapse. Over 40 years ago, it was reported that AEC2 proliferate in response to injury in rodents, suggestive of a role in repair [18, 19]. More recently, genetic lineage tracing experiments have provided support for a model in which AEC2s are capable of long-term self-renewal and the generation of AEC1 in both alveolar regeneration and under steady state conditions [20– 22]. AEC2s purified from human lungs and cultured on plastic or in 3D with fibroblasts have the ability to proliferate and give rise to cells with some characteristics of AEC1 [20, 23]. These data

suggest that AEC2s also function as a stem cell population in human lungs.

Recent data suggest that there are exceptions to the compartmentalization of lung epithelial cell lineage relationships described above. In the trachea, cells expressing Scgb1a1 are capable of “ de-differentiating” into basal cells following depletion of basal cells using SO₂ or genetic ablation with diphtheria toxin [16, 24]. Lineage tracing studies have also shown that Scgb1a1+ cells, perhaps airway Club cells, can give rise to alveolar lineages following severe injury with bleomycin [20, 22, 25, 26]. The bronchio-alveolar junction harbors a putative progenitor called the bronchioalveolar stem cell or BASC that can give rise to both airway and alveolar lineages in vitro and under some injury conditions [27]. To date, no human counterpart of this cell type has been identified and its contribution to maintenance and repair in vivo awaits genetic lineage tracing. Following very severe lung injury in mice caused by infection with a murinized version of the pandemic H1N1 strain of influenza, “pods” of cells expressing the airway markers p63 and Krt5 are observed in the alveolar region [28]. The origin and differentiation potential of these pods in vivo is not clear [28– 31].

Finally, in the alveoli at least a subset of AEC1, long thought to be post-mitotic, appear to be able to generate AEC2 under regenerative conditions [32]. Because these data were obtained in mouse models of injury/repair, their relevance to human lung maintenance and repair are not clear.

2.4 Putative niche components

Considerable progress has been made toward identifying the signals that regulate lung epithelial stem cell selfrenewal and differentiation. These include Notch, Hippo/Yap, ROS/Nrf2, EGF, FGF, c-myb, and cytokines including IL-4, -13 and -6 [13, 29, 33–40]. Neighboring epithelial cells, stromal cells (including fibroblasts, smooth muscle cells, and endothelium) and immune cells all represent potential sources for these factors. Here, we discuss some data to support each of these as components of the lung epithelial stem cell niche.

2.4.1 Niche of the pseudostratified airway epithelium with basal cells

Basal cells of the surface epithelium that lines the airways are capable of long-term self-renewal and differentiation [8]. However, a population of label retaining basal cells is localized to the submucosal glands of the large airways [41, 42]. These cells are protected from inhaled noxious gases, particulates and microorganisms, therefore representing a reserve to repopulate the airways following extreme injury. Their location near the basal lamina preferentially exposes basal cells to factors secreted by the underlying stromal cells. A recent report showed that basal cell differentiation into ciliated cells is enhanced by IL-6/Stat3 signaling [38]. Following injury of luminal cells by inhalation of SO₂, surviving basal cells self-renew and differentiate into ciliated and secretory cells to repopulate the epithelium. During this regenerative response, subepithelial PDGFRA⁺ fibroblasts upregulate the expression of IL-6, presumably directing the differentiation of basal cells [38] and Fig 1. Another study investigated subepithelial endothelial cells as a potential niche component of isolated human airway basal cells [43]. Transcriptional profiling data and in vitro assays support a model in which airway basal cells express VEGF that activates MAPK in endothelial cells via VEGFR2. The endothelial cells, in turn, support the growth of basal cells [43] and Fig 1. Whether changes in this axis are altered in disease or during repair is not known, but could represent a new therapeutic approach for the management of airway disease. Importantly, basal cells are capable of forming tracheospheres in Matrigel with growth factors independent of supporting cells types, although addition of lung fibroblasts and endothelium can enhance colony forming efficiency [8, 12, 38, 40].

Several lines of evidence suggest that neighboring epithelial cells are components of the lung epithelial stem cell niche. For example, secretory cells (but not basal cells) divide to repopulate the airway epithelium following the depletion of ciliated cells; however, basal cells repopulate the epithelium following depletion of secretory and ciliated cells of the trachea [8, 16, 44]. Together, these data suggest that surviving epithelial cells communicate the degree and kind of injury to stem cells so that an appropriate regenerative response is mounted. The

molecular mediators of this feedback loop are not known. A recent report provided evidence that this signaling is bidirectional. Basal cells supply a Notch signal to their daughter secretory cells. In the absence of this maintenance signal, secretory cells terminally differentiate to generate ciliated cells [45].

2.4.2 Niche of the mouse intralobar airways and alveoli Airways

Clusters of neuroepithelial cells, known as neuroepithelial bodies (NEBs), represent another putative niche within the airway epithelium Fig 1. A population of injury resistant “variant” Club cells localizes to these clusters and repopulates the airway epithelium following depletion of Club cells by administration of the polycyclic aromatic hydrocarbon naphthalene [46–48]. There is evidence that calcium signaling in Club cells is induced by the secretion of ATP from NEBs [49]. How this and other NEB-derived signals affect club cell survival, quiescence, proliferation, and differentiation is not known. During embryonic development, the specification of Club cell precursors is dependent on Notch signaling from the NEBs [50]. Several studies have reported a role for FGF10 secreted by parabronchial smooth muscle cells or resident mesenchymal stromal cells in the activation of epithelial stem cells, including Club cells [40, 51, 52] and Fig 1.

2.4.3 Most distal terminal airways

The diversity of cell types and complex 3D organization of the terminal airways and alveoli complicate the characterization of the epithelial stem cell niche in these regions in vivo. One way of overcoming this problem is to exploit in vitro assays. Genetic and pharmacological manipulation of candidate pathways as co-culture experiments allow for the efficient identification of niche components, signaling cascades, and cell:cell interactions that would be tedious in mice. However, the interpretation of this type of experiment must be cautious, as isolation can change cellular phenotypes and culture conditions, including growth factors and

substrate, profoundly affect cellular behaviors. The growth and differentiation of BASCs in vitro requires the presence of fibroblast feeder cells or lung endothelial cells, implicating these cells as niche components [27, 53] and Fig 1. Co-culturing BASCs with Tsp1 null endothelial cells significantly reduced the differentiation of BASCs toward alveolar lineages. This study went on to provide data to support a model in which Bmp4, expressed in epithelial cells, induces calcineurin/NFATc1 signaling and Tsp1 expression in nearby endothelial cells. Endothelial Tsp1, in turn, stimulates the alveolar differentiation of BASCs [53]. Mice homozygous for a null allele of Tsp1 showed impaired regeneration following treatment with bleomycin, suggesting that this pathway is active in vivo.

2.4.4 The alveoli

Most models used to study cell lineage relationships in the distal lung induce significant acute lung injury and disrupt the intricate cell-cell interactions of the alveoli. One very promising approach to interrogate the alveolar niche is to study compensatory regeneration following partial pneumonectomy (PNX), the removal of one or more lung lobes. This is a well-established model of adult alveologenesis that stimulates activation and proliferation of alveolar niche components without inducing acute lung injury [54, 55]. In this model, AEC2s are the major proliferating epithelial cell type [56]. Recent studies in the mouse identified a subset of PDGFRA⁺ fibroblasts in the alveolar niche that increase in number and differentiate into myofibroblasts post-PNX [57]. Blocking PDGFRA⁺ fibroblast function or differentiation through FGFR2 inhibition or targeting the PPAR γ pathway impaired alveolar septation and compensatory growth post-PNX. Therefore, similar to their function in embryonic lung development, PDGFRA⁺ fibroblasts are essential niche cells during PNX-mediated lung regeneration [58, 59] and Fig 1. In vitro co-culture of mouse or human AEC2s with lung fibroblasts generated clonal and proliferating “alveolar-spheres,” consisting of an internal layer of cells with AEC1 morphology and marker expression, and an external layer of surfactant-

producing AEC2- like cells indicative of self-renewal and differentiation [20]. Importantly, AEC2s were unable to form spheres or survive unless fibroblasts were intimately associated with them, further implicating fibroblasts as a critical support cell for AEC2 [20, 40]. Pharmacologic manipulation of the FGF pathway in these cocultures suggests that this pathway promotes the differentiation of alveolar lineages from lung epithelial stem cells at the expense of airway lineages [40].

Beyond potential trophic factors derived from fibroblasts, these cells are also a source of extracellular matrix that modulates alveolar stretch and recoil. Data from a number of systems, including the lung, have shown that biomechanical forces are potent modulators of stem cell behaviors. This will be important to consider for the improvement of biomimetic and bioengineered lung replacements [60, 61].

The heterogeneity of fibroblasts and the cell lineage relationships amongst stromal cells of the lung are exceptionally poorly understood. There is evidence that alveolar epithelial cells communicate with the surrounding endothelium. During branching morphogenesis, distal lung endoderm stimulates development of the capillary plexus, which, in turn, stimulates endodermal proliferation and alveolar septation [62].

During lung regeneration following partial PNx, inhibition of either VEGFR2+ or FGFR1+ signaling in pulmonary capillary endothelial cells (PCECs) impaired proliferation of both BASCs and AEC2s [63] and Fig 1. This group found that PCECs secrete matrix metalloproteinase 14, which activates EGF-like growth factors sequestered in the surrounding matrix. This subsequently stimulates AEC2 proliferation by activating EGFR. Importantly, restoring EGF signaling in animals with defective vasculature rescued defects in lung regeneration following PNx. This suggests that the regenerative effect of vasculature is more than simple perfusion. Recently, they showed that upstream stromal-cell-derived factor-1 (SDF-1, also known as CXCL12) secreted from platelets primes endothelial cell production of MMP14 during PNx-induced alveologenesis [64].

Numerous immune cell types populate the alveolus and lie in close proximity to AEC2s. Myeloid cells of the lung, including alveolar macrophages and neutrophils, promote alveologenesis during development and protect the epithelium throughout life by clearing proteinaceous debris from airway lumens, battling pathogens that escape the mucociliary escalator, and modulating the inflammatory milieu [65– 69]. In the mouse model of bleomycin-induced lung fibrosis, macrophage depletion with clodronate during fibrotic stages of the model ameliorated the phenotype, while depletion of these cells during the recovery stage of the injury made it worse [70]. This effect was attributed to loss of alternatively activated M2 macrophages during recovery, but the molecular mechanisms by which these cells promote repair in the lung are not currently known. In compensatory growth following PNX, alveolar macrophages proliferate and upregulate proangiogenic and matrix remodeling genes [71]. Researchers also identified an increase in CD11b + myeloid cells in regenerating lung tissue post-PNX and provided some evidence that CD18-deficient mice, which suffer impaired leukocyte trafficking, have impaired generation of new lung tissue post-PNX [72] and Fig 1. Our own unpublished data show that macrophage number peaks together with epithelial proliferation and that depletion of macrophages impairs the proliferation of AEC2 post-PNX. These studies are beginning to probe how immune cells affect alveolar epithelial stem cells, but the identities of specific immune cell populations and their regenerative niche signals remain largely unknown.

2.5 Conclusion

As our understanding of progenitor populations within the lung epithelium improves, we can begin elucidating the signals that regulate epithelial stem cell behavior. Animal model systems have enabled controlled studies of both progressive and acute lung injury where relevant regenerative and maladaptive mechanisms can be probed and manipulated. Furthermore, in vitro model systems have allowed reconstitution of human epithelial progenitor niches to facilitate testing of mechanistic hypotheses. We have highlighted some important niches for

several lung epithelial progenitors. Further elucidation of lung stem cell niches and the signals with which they regulate progenitor cell behaviors have the potential to lead to improved targeted therapies to prevent or reverse pathological remodeling in lung injury and disease.

References:

1. Hogan BL, Barkauskas CE, Chapman HA, Epstein JA, Jain R, Hsia CC, et al. Repair and regeneration of the respiratory system: complexity, plasticity, and mechanisms of lung stem cell function. *Cell Stem Cell*. 2014;15(2):123–38.
2. Rock JR, Randell SH, Hogan BL. Airway basal stem cells: a perspective on their roles in epithelial homeostasis and remodeling. *Dis Model Mech*. 2010;3(9-10):545–56.
3. Opbroek AA, Verberne CJ, Dubbeldam JA, Dykman JH. The proximal border of the human respiratory unit, as shown by scanning and transmission electron microscopy and light microscopical cytochemistry. *Anat Rec*. 1991;229(3):339–54.
4. Kauffman SL. Cell proliferation in the mammalian lung. *Int Rev Exp Pathol*. 1980;22:131–91.
5. Giangreco A, Arwert EN, Rosewell IR, Snyder J, Watt FM, Stripp BR. Stem cells are dispensable for lung homeostasis but restore airways after injury. *Proc Natl Acad Sci U S A*. 2009;106(23):9286–91.
6. Watson JK, Rulands S, Wilkinson AC, Wuidart A, Ousset M, Van Keymeulen A, et al. Clonal Dynamics Reveal Two Distinct Populations of Basal Cells in Slow-Turnover Airway Epithelium. *Cell Reports*. 2015;12(1):90–101.
7. Rock JR, Hogan BL. Epithelial progenitor cells in lung development, maintenance, repair, and disease. *Annu Rev Cell Dev Biol*. 2011;27:493–512.
8. Rock JR, Onaitis MW, Rawlins EL, Lu Y, Clark CP, Xue Y, et al. Basal cells as stem cells of the mouse trachea and human airway epithelium. *Proc Natl Acad Sci U S A*. 2009;106(31):12771–5.
9. Randell SH, Comment CE, Ramaekers FC, Nettekheim P. Properties of rat tracheal epithelial cells separated based on expression of cell surface alpha-galactosyl end groups. *Am J Respir Cell Mol Biol*. 1991;4(6):544–54.
10. Hong KU, Reynolds SD, Watkins S, Fuchs E, Stripp BR. Basal cells are a multipotent progenitor capable of renewing the bronchial epithelium. *Am J Pathol*. 2004;164(2):577–88.

11. Teixeira VH, Nadarajan P, Graham TA, Pipinikas CP, Brown JM, Falzon M, et al. Stochastic homeostasis in human airway epithelium is achieved by neutral competition of basal cell progenitors. *eLife*. 2013;2:e00966.
12. Hegab AE, Ha VL, Darmawan DO, Gilbert JL, Ooi AT, Attiga YS, et al. Isolation and in vitro characterization of basal and submucosal gland duct stem/progenitor cells from human proximal airways. *Stem Cells Transl Med*. 2012;1(10):719–24.
13. Pardo-Saganta A, Law BM, Tata PR, Villoria J, Saez B, Mou H, et al. Injury induces direct lineage segregation of functionally distinct airway basal stem/progenitor cell subpopulations. *Cell Stem Cell*. 2015;16(2):184–97.
14. Winkelmann A, Noack T. The Clara cell: a “Third Reich eponym”? *Eur Respir J*. 2010;36(4):722–7.
15. Chen G, Korfhagen TR, Xu Y, Kitzmiller J, Wert SE, Maeda Y, et al. SPDEF is required for mouse pulmonary goblet cell differentiation and regulates a network of genes associated with mucus production. *J Clin Invest*. 2009;119(10):2914–24.
16. Rawlins EL, Okubo T, Xue Y, Brass DM, Auten RL, Hasegawa H, et al. The role of Scgb1a1+ Clara cells in the long-term maintenance and repair of lung airway, but not alveolar, epithelium. *Cell Stem Cell*. 2009;4(6):525–34.
17. Boers JE, Ambergen AW, Thunnissen FB. Number and proliferation of clara cells in normal human airway epithelium. *Am J Respir Crit Care Med*. 1999;159(5 Pt 1):1585–91.
18. Evans MJ, Cabral LJ, Stephens RJ, Freeman G. Transformation of alveolar type 2 cells to type 1 cells following exposure to NO₂. *Exp Mol Pathol*. 1975;22(1):142–50.
19. Adamson IY, Bowden DH. The type 2 cell as progenitor of alveolar epithelial regeneration. A cytodynamic study in mice after exposure to oxygen. *Lab Invest; a journal of technical methods and pathology*. 1974;30(1):35–42.
20. Barkauskas CE, Cronic MJ, Rackley CR, Bowie EJ, Keene DR, Stripp BR, et al. Type 2 alveolar cells are stem cells in adult lung. *J Clin Invest*. 2013;123(7):3025–36.

21. Desai TJ, Brownfield DG, Krasnow MA. Alveolar progenitor and stem cells in lung development, renewal and cancer. *Nature*. 2014;507(7491):190–4.
22. Rock JR, Barkauskas CE, Crouce MJ, Xue Y, Harris JR, Liang J, et al. Multiple stromal populations contribute to pulmonary fibrosis without evidence for epithelial to mesenchymal transition. *Proc Natl Acad Sci U S A*. 2011;108(52):E1475–83.
23. Gonzalez RF, Dobbs LG. Isolation and culture of alveolar epithelial Type I and Type II cells from rat lungs. *Methods Mol Biol*. 2013;945:145–59.
24. Tata PR, Mou H, Pardo-Saganta A, Zhao R, Prabhu M, Law BM, et al. Dedifferentiation of committed epithelial cells into stem cells in vivo. *Nature*. 2013;503(7475):218–23.
25. Tropea KA, Leder E, Aslam M, Lau AN, Raiser DM, Lee JH, et al. Bronchioalveolar stem cells increase after mesenchymal stromal cell treatment in a mouse model of bronchopulmonary dysplasia. *Am J Physiol Lung Cell Mol Physiol*. 2012;302(9):L829–37.
26. Zheng D, Limmon GV, Yin L, Leung NH, Yu H, Chow VT, et al. Regeneration of alveolar type I and II cells from Scgb1a1-expressing cells following severe pulmonary damage induced by bleomycin and influenza. *PLoS One*. 2012;7(10):e48451.
27. Kim CF, Jackson EL, Woolfenden AE, Lawrence S, Babar I, Vogel S, et al. Identification of bronchioalveolar stem cells in normal lung and lung cancer. *Cell*. 2005;121(6):823–35.
28. Kumar PA, Hu Y, Yamamoto Y, Hoe NB, Wei TS, Mu D, et al. Distal airway stem cells yield alveoli in vitro and during lung regeneration following H1N1 influenza infection. *Cell*. 2011;147(3):525–38.
29. Vaughan AE, Brumwell AN, Xi Y, Gotts JE, Brownfield DG, Treutlein B, et al. Lineage-negative progenitors mobilize to regenerate lung epithelium after major injury. *Nature*. 2015;517(7536):621–5.
30. Zheng D, Yin L, Chen J. Evidence for Scgb1a1(+) cells in the generation of p63(+) cells in the damaged lung parenchyma. *Am J Respir Cell Mol Biol*. 2014;50(3):595–604.
31. Zuo W, Zhang T, Wu DZ, Guan SP, Liew AA, Yamamoto Y, et al. p63(+)Krt5(+) distal airway

stem cells are essential for lung regeneration. *Nature*. 2015;517(7536):616–20.

32. Jain R, Barkauskas CE, Takeda N, Bowie EJ, Aghajanian H, Wang Q, et al. Plasticity of Hopx(+) type I alveolar cells to regenerate type II cells in the lung. *Nat Commun*. 2015;6:6727.

33. Danahay H, Pessotti AD, Coote J, Montgomery BE, Xia D, Wilson A, et al. Notch2 is required for inflammatory cytokine-driven goblet cell metaplasia in the lung. *Cell Reports*. 2015;10(2):239–52.

34. Lange AW, Sridharan A, Xu Y, Stripp BR, Perl AK, Whitsett JA. Hippo/Yap signaling controls epithelial progenitor cell proliferation and differentiation in the embryonic and adult lung. *J Mol Cell Biol*. 2015;7(1):35–47.

35. Paul MK, Bisht B, Darmawan DO, Chiou R, Ha VL, Wallace WD, et al. Dynamic changes in intracellular ROS levels regulate airway basal stem cell homeostasis through Nrf2-dependent Notch signaling. *Cell Stem Cell*. 2014;15(2):199–214.

36. Rock JR, Gao X, Xue Y, Randell SH, Kong YY, Hogan BL. Notch dependent differentiation of adult airway basal stem cells. *Cell Stem Cell*. 2011;8(6):639–48.

37. Shaykhiev R, Zuo WL, Chao I, Fukui T, Witover B, Brekman A, et al. EGF shifts human airway basal cell fate toward a smoking-associated airway epithelial phenotype. *Proc Natl Acad Sci U S A*. 2013;110(29):12102–7.

38. Tadokoro T, Wang Y, Barak LS, Bai Y, Randell SH, Hogan BL. IL-6/STAT3 promotes regeneration of airway ciliated cells from basal stem cells. *Proc Natl Acad Sci U S A*. 2014;111(35):E3641–9.

39. Zhu Z, Homer RJ, Wang Z, Chen Q, Geba GP, Wang J, et al. Pulmonary expression of interleukin-13 causes inflammation, mucus hypersecretion, subepithelial fibrosis, physiologic abnormalities, and eotaxin production. *J Clin Invest*. 1999;103(6):779–88.

40. Hegab AE, Arai D, Gao J, Kuroda A, Yasuda H, Ishii M, et al. Mimicking the niche of lung epithelial stem cells and characterization of several effectors of their in vitro behavior. *Stem Cell Res*. 2015;15(1):109–21.

41. Borthwick DW, Shahbazian M, Krantz QT, Dorin JR, Randell SH. Evidence for stem-cell niches in the tracheal epithelium. *Am J Respir Cell Mol Biol.* 2001;24(6):662–70.
42. Lynch TJ, Engelhardt JF. Progenitor cells in proximal airway epithelial development and regeneration. *J Cell Biochem.* 2014;115(10):1637–45.
43. Curradi G, Walters MS, Ding BS, Rafii S, Hackett NR, Crystal RG. Airway basal cell vascular endothelial growth factor-mediated cross-talk regulates endothelial cell-dependent growth support of human airway basal cells. *Cell Mol Life Sci.* 2012;69(13):2217–31.
44. Evans MJ, Shami SG, Cabral-Anderson LJ, Dekker NP. Role of nonciliated cells in renewal of the bronchial epithelium of rats exposed to NO₂. *Am J Pathol.* 1986;123(1):126–33.
45. Pardo-Saganta A, Tata PR, Law BM, Saez B, Chow R, Prabhu M, et al. Parent stem cells can serve as niches for their daughter cells. *Nature.* 2015;523(7562):597–601.
46. Giangreco A, Reynolds SD, Stripp BR. Terminal bronchioles harbor a unique airway stem cell population that localizes to the bronchoalveolar duct junction. *Am J Pathol.* 2002;161(1):173–82.
47. Hong KU, Reynolds SD, Giangreco A, Hurley CM, Stripp BR. Clara cell secretory protein-expressing cells of the airway neuroepithelial body microenvironment include a label-retaining subset and are critical for epithelial renewal after progenitor cell depletion. *Am J Respir Cell Mol Biol.* 2001;24(6):671–81.
48. Reynolds SD, Hong KU, Giangreco A, Mango GW, Guron C, Morimoto Y, et al. Conditional clara cell ablation reveals a self-renewing progenitor function of pulmonary neuroendocrine cells. *Am J Physiol Lung Cell Mol Physiol.* 2000;278(6):L1256–63.
49. De Proost I, Pintelon I, Wilkinson WJ, Goethals S, Brouns I, Van Nassauw L, et al. Purinergic signaling in the pulmonary neuroepithelial body microenvironment unraveled by live cell imaging. *FASEB J.* 2009;23(4):1153–60.
50. Guha A, Vasconcelos M, Cai Y, Yoneda M, Hinds A, Qian J, et al. Neuroepithelial body microenvironment is a niche for a distinct subset of Clara-like precursors in the developing

airways. *Proc Natl Acad Sci U S A*. 2012;109(31):12592–7.

51. Volckaert T, Dill E, Campbell A, Tiozzo C, Majka S, Bellusci S, et al. Parabronchial smooth muscle constitutes an airway epithelial stem cell niche in the mouse lung after injury. *J Clin Invest*. 2011;121(11):4409–19.

52. McQualter JL, McCarty RC, Van der Velden J, O'Donoghue RJ, Asselin-Labat ML, Bozinovski S, et al. TGF-beta signaling in stromal cells acts upstream of FGF-10 to regulate epithelial stem cell growth in the adult lung. *Stem Cell Res*. 2013;11(3):1222–33.

53. Lee JH, Bhang DH, Beede A, Huang TL, Stripp BR, Bloch KD, et al. Lung stem cell differentiation in mice directed by endothelial cells via a BMP4-NFATc1-thrombospondin-1 axis. *Cell*. 2014;156(3):440–55.

54. Brown LM, Rannels SR, Rannels DE. Implications of post-pneumonectomy compensatory lung growth in pulmonary physiology and disease. *Respir Res*. 2001;2(6):340–7.

55. Hoffman AM, Shifren A, Mazan MR, Gruntman AM, Lascola KM, Nolen-Walston RD, et al. Matrix modulation of compensatory lung regrowth and progenitor cell proliferation in mice. *Am J Physiol Lung Cell Mol Physiol*. 2010;298(2):L158–68.

56. Nolen-Walston RD, Kim CF, Mazan MR, Ingenito EP, Gruntman AM, Tsai L, et al. Cellular kinetics and modeling of bronchioalveolar stem cell response during lung regeneration. *Am J Physiol Lung Cell Mol Physiol*. 2008;294(6):L1158–65.

57. Chen L, Acciani T, Le Cras T, Lutzko C, Perl AK. Dynamic regulation of platelet-derived growth factor receptor alpha expression in alveolar fibroblasts during realveolarization. *Am J Respir Cell Mol Biol*. 2012;47(4):517–27.

58. Bostrom H, Willetts K, Pekny M, Leveen P, Lindahl P, Hedstrand H, et al. PDGF-A signaling is a critical event in lung alveolar myofibroblast development and alveogenesis. *Cell*. 1996;85(6):863–73.

59. Lindahl P, Karlsson L, Hellstrom M, Gebre-Medhin S, Willetts K, Heath JK, et al. Alveogenesis failure in PDGF-A-deficient mice is coupled to lack of distal spreading of alveolar

- smooth muscle cell progenitors during lung development. *Development*. 1997;124(20):3943–53.
60. Ott HC, Clippinger B, Conrad C, Schuetz C, Pomerantseva I, Ikonomou L, et al. Regeneration and orthotopic transplantation of a bioartificial lung. *Nat. Med.* 2010;16(8):927–33.
61. Petersen TH, Calle EA, Zhao L, Lee EJ, Gui L, Raredon MB, et al. Tissue-engineered lungs for in vivo implantation. *Science*. 2010;329(5991):538–41.
62. Yamamoto H, Yun EJ, Gerber HP, Ferrara N, Whitsett JA, Vu TH. Epithelial vascular cross talk mediated by VEGF-A and HGF signaling directs primary septae formation during distal lung morphogenesis. *Dev Biol*. 2007;308(1):44–53.
63. Ding BS, Nolan DJ, Guo P, Babazadeh AO, Cao Z, Rosenwaks Z, et al. Endothelial-derived angiocrine signals induce and sustain regenerative lung alveolarization. *Cell*. 2011;147(3):539–53.
64. Rafii S, Cao Z, Lis R, Siempos II, Chavez D, Shido K, et al. Platelet-derived SDF-1 primes the pulmonary capillary vascular niche to drive lung alveolar regeneration. *Nat Cell Biol*. 2015;17(2):123–36.
65. Herold S, Mayer K, Lohmeyer J. Acute lung injury: how macrophages orchestrate resolution of inflammation and tissue repair. *Front Immunol*. 2011;2:65.
66. Shibata Y, Berclaz PY, Chroneos ZC, Yoshida M, Whitsett JA, Trapnell BC. GM-CSF regulates alveolar macrophage differentiation and innate immunity in the lung through PU.1. *Immunity*. 2001;15(4):557–67.
67. Li MO, Sarkisian MR, Mehal WZ, Rakic P, Flavell RA. Phosphatidylserine receptor is required for clearance of apoptotic cells. *Science*. 2003;302(5650):1560–3.
68. Savill JS, Wyllie AH, Henson JE, Walport MJ, Henson PM, Haslett C. Macrophage phagocytosis of aging neutrophils in inflammation. Programmed cell death in the neutrophil leads to its recognition by macrophages. *J Clin Invest*. 1989;83(3):865–75.
69. Blackwell TS, Hipps AN, Yamamoto Y, Han W, Barham WJ, Ostrowski MC, et al. NF-

kappaB signaling in fetal lung macrophages disrupts airway morphogenesis. *J Immunol.* 2011;187(5):2740–7.

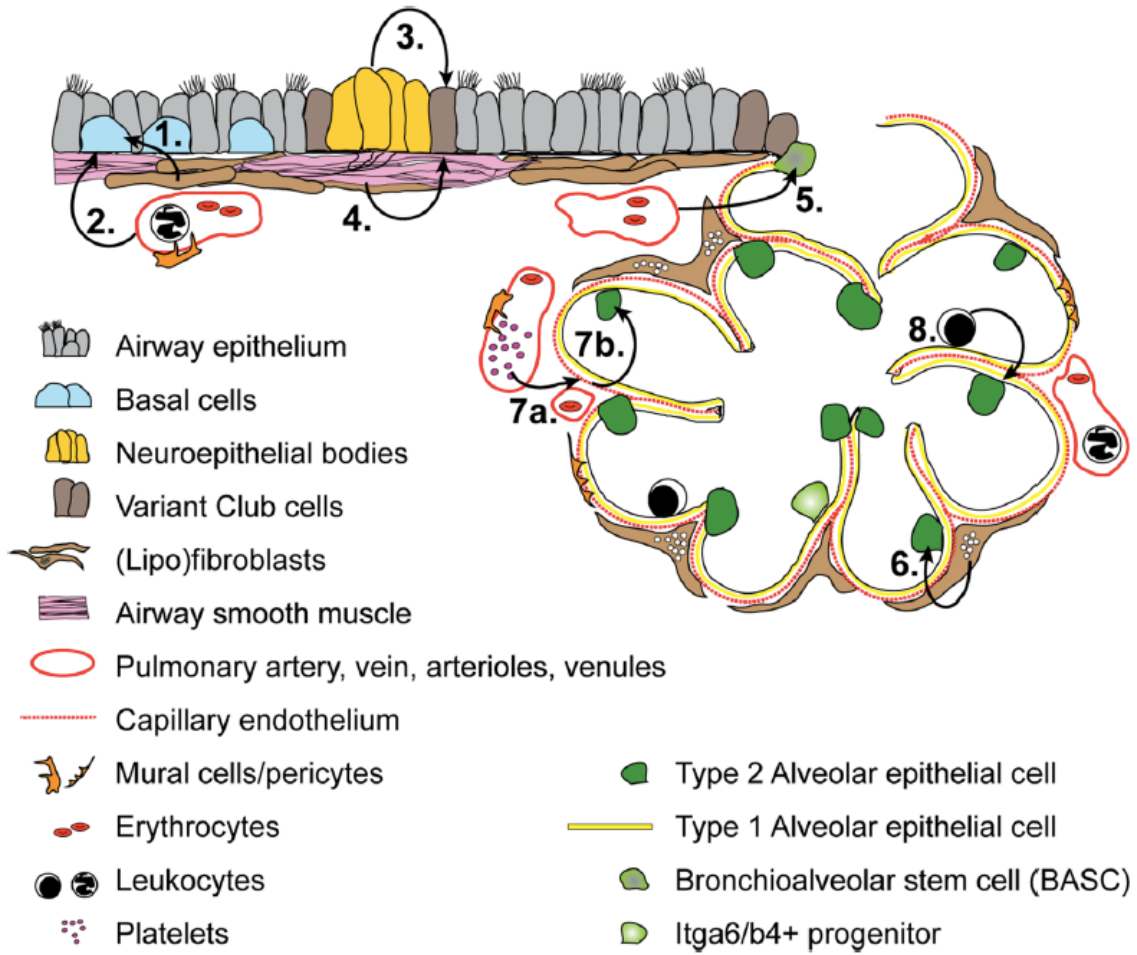
70. Gibbons MA, MacKinnon AC, Ramachandran P, Dhaliwal K, Duffin R, Phythian-Adams AT, et al. Ly6Chi monocytes direct alternatively activated profibrotic macrophage regulation of lung fibrosis. *Am J Respir Crit Care Med.* 2011;184(5):569–81.

71. Chamoto K, Gibney BC, Ackermann M, Lee GS, Lin M, Kondering MA, et al. Alveolar macrophage dynamics in murine lung regeneration. *J Cell Physiol.* 2012;227(9):3208–15.

72. Chamoto K, Gibney BC, Lee GS, Ackermann M, Kondering MA, Tsuda A, et al. Migration of CD11b + accessory cells during murine lung regeneration. *Stem Cell Res.* 2013;10(3):267–77.

Figure 1. Selected putative niche-stem cell interactions in lung repair/regeneration. (1)

Fibroblasts upregulate the expression of IL-6 following injury of the airway epithelium to promote ciliated cell differentiation from basal stem cells in mice [38]. **(2)** Human airway basal stem cells secrete VEGF to simulate endothelial cells that, in turn, support basal stem cells [43]. **(3)** Variant Club cells are found adjacent to neuroepithelial bodies and repopulate simple columnar airway epithelia following injury in mice [46–48]. **(4)** Parabronchial smooth muscle cells secrete FGF10 following airway injury to promote the activation of variant Club cells in mice [51]. **(5)** BASCs secrete Bmp4 to activate calcineurin/NFAT-c1 signaling in endothelial cells that, in turn, secrete Tsp1 to promote alveolar differentiation of BASCs in mice [53]. **(6)** (Lipo)fibroblasts are required for the growth of mouse and human AEC2 in vitro [20]. Evidence suggests that these cells give rise to myofibroblasts that are critical for compensatory lung growth following pneumonectomy [57]. **(7a)**. Platelet derived SDF-1 promotes the production of MMP14 in endothelial cells following pneumonectomy in mice [64]. **(7b)** MMP14 activates EGF-like growth factors sequestered in the matrix to promote the activation of AEC2s [63]. **(8)** Myeloid cells are critical for the resolution of bleomycin-induced pulmonary fibrosis in mice [70]. The proliferation of AEC2 and compensatory growth following pneumonectomy is impaired in mice with insufficient numbers of myeloid cells in the lung ([72] and our unpublished data).



Chapter 3

Recruited monocytes and type-2 cytokines promote lung regeneration

3.1 Introduction

The past few decades have brought many discoveries about the identities and behaviors of epithelial stem cells in the lung (Hogan et al., 2014; Kotton and Morrisey, 2014; Rock and Hogan, 2011). These data have intensified efforts toward stimulating the regeneration of the human lung from endogenous progenitors to ameliorate declining function associated with aging and progressive end stage disease. However, the realization of this goal requires a more complete knowledge of the molecular and cellular events mediating lung homeostasis, pathological remodeling and regeneration.

In many mammalian species, partial pneumonectomy (PNX), the surgical removal of one or more lung lobes, stimulates compensatory growth in the remaining lobes that restores alveolar surface area and lung diffusing capacity (Buhain and Brody, 1973; Dane et al., 2013; Fehrenbach et al., 2008; Ravikumar et al., 2013; Voswinckel et al., 2004). This compensatory growth requires the coordinated proliferation and rearrangement of numerous epithelial and stromal cell types, including type 2 alveolar epithelial cells (AEC2s), an alveolar epithelial stem cell population capable of self-renewal and differentiation into type 1 alveolar epithelial cells (AEC1s) (Barkauskas et al., 2013; Brody et al., 1978; Desai et al., 2014; Ding et al., 2011; Hoffman et al., 2010; Li et al., 2013; Nolen-Walston et al., 2008; Rock et al., 2011a). Recent efforts have elucidated some components of the regenerative AEC2 niche, but the roles of recruited and resident lung macrophages during adult alveologenesis post-PNX remain unclear (Chamoto et al., 2012, 2013; Chen et al., 2012; Ding et al., 2011; Rafii et al., 2015).

Tissue macrophages in different organ systems are heterogeneous with respect to origin, marker expression, and functions. Recent work has helped to delineate these parameters for macrophages in the lung (Tan and Krasnow, 2016). Three main subpopulations of lung macrophages have been characterized by their ontogeny, mode of maintenance, and location within the lung tissue. Two of these, “primitive” interstitial macrophages and alveolar macrophages, are initially derived from hematopoietic progenitors arising from the yolk sac and

fetal liver, respectively. The third population of “definitive” interstitial macrophages is derived from circulating bone marrow-derived monocytes and gradually replaces the “primitive” interstitial macrophages over time. Recent data suggest that lung macrophages are maintained independently by self-renewal under steady-state conditions (Guilliams et al., 2013; Hashimoto et al., 2013; Hoeffel and Ginhoux, 2015; Hoeffel et al., 2015; Jakubzick et al., 2013; Perdiguero et al., 2015; Schulz et al., 2012; Suzuki et al., 2014; Yona et al., 2013). In fact, bone marrow-derived and circulating monocytes replenish and supplement resident macrophages only after severe tissue macrophage depletion and during some inflammatory/regenerative states (Hashimoto et al., 2013; Yona et al., 2013), often through a mechanism involving the chemokine receptor CCR2 (Willenborg et al., 2012; Lee et al., 2015; Nishiyama et al., 2015; Ramachandran et al., 2012). Both resident and recruited macrophages are capable of proliferation at their sites of action (Davies et al., 2013).

Mounting evidence supports a model in which macrophages play essential roles in the regeneration of organs including limbs, intestines, liver, kidney, and heart (Aurora and Olson, 2014; Aurora et al., 2014; Boulter et al., 2012; Dutta et al., 2015; Epelman et al., 2014; Gibbons et al., 2011; Godwin et al., 2013; Lin et al., 2010; Pull et al., 2005; Ramachandran et al., 2012). However, while their roles in lung host defense are relatively well established (Aggarwal et al., 2014; Herold et al., 2011), including how epithelial-macrophage crosstalk regulates lung immunity (Westphalen et al., 2014), little is known about how macrophages might modulate lung regeneration, including adult alveologenesis. The pathology of bleomycin-induced lung fibrosis in mice was worsened when inflammatory monocytes were adoptively transferred during the fibrotic stage, but also when macrophages were depleted during the recovery stage (Gibbons et al., 2011), suggesting that optimal tissue regeneration requires specific macrophage subtypes and dynamics. Changes in the leukocyte population, including increased numbers of alveolar macrophages, have been reported in the context of PNX-induced lung regeneration (Chamoto et al., 2012, 2013). Consistent with current models of macrophage dynamics, parabiosis

experiments demonstrated that the observed increase in alveolar macrophages post-PNX arises by local proliferation rather than recruitment from circulation (Chamoto et al., 2012), but whether these cells affect lung regeneration was not addressed. This same group showed that Cd11b is required for optimal regeneration (Chamoto et al., 2013). However, the nonspecific expression of Cd11b by a number of leukocyte subpopulations, both interstitial and in the airspace, leaves many unanswered questions regarding the mechanisms by which resident and recruited cells promote lung regeneration.

Once macrophages arrive at their site of action, they are polarized along a molecular and functional spectrum by microenvironmental cues (Martinez and Gordon, 2014; Murray et al., 2014). Generally speaking, classically activated macrophages (M1) are associated with inflammatory conditions, while “alternatively activated” macrophages (M2) have been implicated in wound repair and tissue regeneration (Aurora and Olson, 2014; Aurora et al., 2014; Gibbons et al., 2011; Gordon and Martinez, 2010). Cytokines associated with type 2 immunity, such as IL-4 and IL-13 signaling through IL4-R α heterodimers, can induce M2 macrophage polarization and variably activate transcription of *Arg1*, *Fizz1*, *Ym1 (Chil3)*, and *Mrc1* (Stein et al., 1992); however, M2 macrophages are best defined functionally. For example, M2 macrophages may dampen inflammation through IL-10 secretion, secrete growth factors that directly affect stem cell behavior, or remodel matrix to reverse fibrosis (De’Broski et al., 2004; Ruffell et al., 2009; Shiraishi et al., 2016). M2-polarized macrophages may arise from either tissue resident or monocyte-derived macrophages (Arnold et al., 2007; Egawa et al., 2013; Shechter et al., 2013). The polarization state of macrophages in the regenerating lung following PNX has not been reported.

Here, we use flow cytometry, immunofluorescence, and both population level and single cell RNA sequencing to characterize the dynamics of macrophage subpopulations following PNX. Myeloid cells in the regenerating lung were most abundant at the peak of AEC2 stem cell proliferation. We use genetic loss of function, adoptive transfer and bone marrow chimeras in

mice to demonstrate that recruited CCR2 monocytes and type-2 cytokine signaling are critical components of the regenerative niche required for lung regeneration following PNx. Our in vivo and in vitro data suggest that monocytes and macrophages stimulate AEC2 progenitor cell behaviors. Finally, we provide evidence that ILC2s are a source of IL13 in the regenerating lung. These data establish important roles for two myeloid lineages in promoting regenerative alveologenesis.

3.2 Results

3.2.1 Increased numbers of macrophages in regenerating lung tissue post-PNX

To examine myeloid cell abundance and distribution in the lung following PNx, we performed immunofluorescence staining and flow cytometry. Analysis of lungs from *Csf1r-GFP* reporter mice, in which macrophages, monocytes and some dendritic cells express green fluorescent protein (GFP) (Rae et al., 2007), showed a peak in the number of GFP+ cells at 7d post-PNX and a return to steady state by 14d (Figure 1A). These cells were localized throughout the pulmonary tissue, in close proximity to AEC2s, and at the periphery of the lung where the majority of neo-alveologenesis is thought to occur (Figure S1) (Konerding et al., 2012). As a percent of all live cells, CSF1R-GFP+, F4/80+ lung macrophages were significantly increased at 7d post-PNX (18.6% +/- 2.8% of total cells) compared to 7d post-sham littermate controls (14.4% +/- 2.1%) (Figure 2B). These data are consistent with a previous report demonstrating an increase in lung macrophages after PNx (Chamoto et al., 2012). Flow cytometry showed that as a percent of all hematopoietic cells (CD45+), both interstitial macrophages/circulating monocytes (F4/80+, CD11b+) and alveolar macrophages (F4/80+, CD11c+) were significantly increased at 7d after PNx (29.1% +/- 3.2%; 15.4% +/- 2.1%) compared to sham surgery (19.9% +/- 2.7%; 9.6% +/- 1.6%) (Figures 1C, 1D, 1E, and 1F). We also observed a transient increase in neutrophils (CD45+, CD11b+, Ly6G+) 4d after PNx, but

this subsided by 7d after PNX when macrophage numbers and epithelial proliferation peaked (Figure S1).

To define the macrophage populations in the lung post-PNX at the molecular level, we isolated all resident and recruited macrophages (CD45+, CSF1R-GFP+, F4/80+, Ly6G-) by FACS 7d post-PNX. Negative selection for Ly6G eliminated contamination by neutrophils that can aberrantly express GFP in *Csf1r-GFP* reporter mice (Sasmono et al., 2007). We performed single cell RNA sequencing of 68 individual cells. Unsupervised hierarchical clustering revealed subpopulations of cells (Figure 1G, x-axis) defined by distinct but partially overlapping transcriptional profiles (Figures 1G and 1H). These included CCR2+;Ly6c+ recruited monocytes (orange) and CD206+;Chil3+ “M2-like” macrophages (red). We performed additional single cell RNA sequencing on macrophages from sham operated mice to allow comparison of macrophage subpopulations in response to PNX. Expression of markers of monocytes (CCR2) and M2-like macrophages (CD206 and Arg1) expression was significantly higher in macrophages 7d post-PNX compared to sham (Figure S1).

3.2.2 CCR2-dependent recruitment of monocytes into the regenerating lung tissue post-PNX

Because a subset of lung macrophages post-PNX was characterized by the expression of CCR2, we hypothesized that a CCL2-CCR2 recruitment axis drives the accumulation of macrophages during regeneration. Increased levels of CCL2 protein have been reported in lungs following PNX (Chamoto et al., 2012, 2013a; Chen et al., 2012; Ding et al., 2011; Rafii et al., 2015), with increased *Ccl2* transcription in AEC2 7d post-PNX (Chamoto et al., 2013a) and PDGFRA+ lung fibroblasts 4d post-PNX (data not shown). We detected a 4.2-fold increase in CCL2 protein in whole lung lysate 7d post-PNX compared to sham operated control (Figures 2A and S2). To assess the recruitment of CCL2-responsive cells, we used *Ccr2-RFP^{Tm2.1^{flc}}* mice in which red fluorescent protein (RFP) is knocked into the *Ccr2* locus to mark inflammatory

monocytes, further functioning as a null allele of CCR2. Immunofluorescence stains of lungs from *Ccr2*^{RFP/+} mice showed increased numbers of CCR2+ cells throughout the lung tissue, with concentrations around large vessels, a likely site of entry from circulation into the pulmonary tissue, and at the periphery of the regenerating lung lobes (Figures 2B and S2). We crossed the *Ccr2-RFP*^{tm2.1lf} allele to mice carrying *Sftpc-CreER*; *Rosa-fGFP* alleles and administered 3 doses of tamoxifen (250 mg/kg) to adult animals, resulting in the expression of GFP in AEC2 and RFP in CCR2+ monocytes. Analysis of lungs confirmed increased numbers of CCR2+ cells 7d post-PNX compared to sham operated animals and demonstrated that these cells were frequently in close proximity to lineage labeled AEC2s (Figure S2). Flow cytometry showed a significant increase in recruited monocytes (CCR2-RFP+, CD11b+) at 7d post-PNX (18.5% +/- 5.6% of live, CD45+ cells) compared to unoperated littermate controls (10.9% +/- 2.7%) (Figures 2B, 2C, and 2D). This suggested that circulating monocytes are recruited into regenerating lung tissue by CCL2. However, we also noticed a significant increase in CCR2+ monocytes 7d post-sham (17.1% +/- 3.6%), suggesting that monocyte mobilization into lung tissue is a response to thoracic surgery. Of note, sham operations similar to those performed here stimulate proliferation in the lung pleura, possibly a conserved function of recruited monocytes (Brody et al., 1978). Another population of non-inflammatory monocytes expresses CX3CR1 (Geissmann et al., 2003) and has also been implicated in tissue regeneration (Arnold et al., 2007). However, using *Cx3Cr1*^{tm1Litt} reporter mice, we did not detect an increase in *Cx3cr1*+ monocytes post-PNX (Figure S2). Thus, the major monocyte population post-PNX is defined by expression of CCR2.

To determine whether CCR2 is required for the increase in macrophages and monocytes post-PNX, we performed PNx in two CCR2-deficient mouse strains: *Ccr2*^{RFP/RFP} mice (described above) and *Ccr2*^{tm1Mae} null mice (hereafter *Ccr2*^{-/-}). Lung tissue from *Ccr2*^{RFP/RFP} mice contained fewer CCR2-RFP+, CD11b+ cells 7d post-PNX compared to *Ccr2*^{RFP/+} controls (Figure 2 B,E). Flow cytometry on lungs of *Ccr2*^{-/-} mice showed a significant decrease in

interstitial macrophages/recruited monocytes (F4/80+, CD11b+) 7d post-PNX (18.1% +/- 1.9% of total CD45+ cells) compared to their wild type littermate controls (25.3% +/- 1.0%) (Figure 2G). In contrast, the number of alveolar macrophages (F4/80+, CD11c+) 7d post-PNX was unaffected by CCR2-deficiency (15.5% +/- 5.3% of total CD45+ cells) compared to wild type littermate controls (15.2% +/- 2.4%) (Figure 2H). This is consistent with data demonstrating that circulating monocytes rarely contribute to lung resident alveolar macrophages, as these cells are capable of self-renewal (Jakubzick et al., 2013; Suzuki et al., 2014).

Previous work has shown that local proliferation is an additional mechanism by which macrophage numbers increase post-PNX (Chamoto et al. 2012). We performed short-term EdU pulse labeling and confirmed an increase in the proliferation of CSF1R-GFP+ macrophages immediately after PNx that peaked at 4d post-PNX, and subsided by 7d post-PNX (Figure S2). Closer examination of these proliferating macrophages revealed localization in alveolar airspaces and a rounded morphology - characteristics of alveolar macrophages. Together, our data suggest that both local proliferation of lung macrophages and CCR2-dependent recruitment of monocytes contribute to the increased number CSF1R-GFP+ lung macrophages in the lung post-PNX. Because previous studies have focused on airspace macrophages (Chamoto et al., 2012, 2013a), but recruited CCR2+ monocytes have not been studied in the context of PNx-induced lung regeneration, we sought to determine their potential role in compensatory lung growth through disruption of the CCL2-CCR2 axis.

3.2.3 CCR2+ monocytes promote lung regeneration post-PNX

After PNx, all of the remaining right lobes grow, but the response is most profound in the accessory lobe (Konerding et al., 2012). Whole mount images show that the right accessory lobes of *Ccr2*^{-/-} mice are smaller than littermate controls 21d after PNx, when lung regeneration is complete (Figure 3A). The generation of new alveoli post-PNX in wild type mice is associated with a 48% increase in the dry weight of the remaining right lobes compared to those of

unoperated mice (Figure 3B). In contrast, PNX only induced a 23% increase in dry weight in *Ccr2*^{-/-} mice, suggesting a significant impairment of lung regeneration (Figure 3B). To determine if this impairment was permanent or reflected a delay in regeneration, we measured lung dry weights at 35d post-PNX. *CCR2*^{-/-} lungs were significantly smaller than wild type littermate control lungs (Figure S3). Since AEC2s are the most proliferative epithelial progenitor cells post-PNX (Nolen-Walston et al., 2008), we hypothesized that reduced AEC2 proliferation contributes to the regenerative defect in *CCR2*^{-/-} mice. Indeed, flow cytometry showed a significant reduction in EdU incorporation in AEC2 in *CCR2*^{-/-} mice 7d post-PNX (5.4% +/- 1.3%) compared to wild type littermate controls (7.4% +/- 1.6%) (Figures 3C and 3D). As new alveoli are formed post-PNX, AEC2 are the major source of new AEC1 (Jain et al., 2015). To determine whether *CCR2*-deficiency affects the differentiation of AEC2 into AEC1, we generated *Ccr2*^{+/+} and *Ccr2*^{-/-} mice that also carry *Sftpc-CreER* and *Rosa-tomato* alleles for lineage tracing experiments. We administered 3 doses of tamoxifen (250 mg/kg) to adult animals, resulting in the heritable expression of RFP in AEC2 (Barkauskas et al., 2013; Rock et al., 2011a). Two weeks later we performed PNX and analyzed tissue sections for lineage traced AEC1s (RFP+, RAGE+) 21d post-PNX, looking specifically at the periphery of accessory lobes (Figure 3E). Quantification revealed that *Ccr2*^{-/-} mice had significantly fewer lineage traced AEC1s (9.1% +/- 2.9%) compared to wild type littermate controls (43.7 % +/- 11.4%) (Figure 3F). Together, these data suggest that the *CCR2*-dependent recruitment of myeloid cells is critical for lung regeneration post-PNX, at least partly through the direct or indirect modulation of AEC2 behaviors.

3.2.4 Bone marrow-derived CCR2+ monocytes are sufficient to support lung regeneration

We next performed adoptive transfer experiments to further demonstrate that the impaired lung regeneration in *Ccr2*^{-/-} mice is attributable to decreased recruitment of monocytes and monocyte-derived macrophages. Bone marrow-derived monocytes express high levels of *CCR2* protein, and when stimulated, this receptor promotes monocytes to enter the circulation

and regenerating tissues (Gordon and Taylor, 2005). Flow cytometry revealed that approximately 10% of all bone marrow cells are CCR2⁺, CD11b⁺ monocytes (Figure S4). We isolated whole bone marrow from *Csf1r-GFP* mice and injected 1×10^7 cells via tail vein into *Ccr2*^{-/-} mice that were either unoperated or 6d post-PNX. We timed this adoptive transfer to coincide with the increased CCL2 and peak influx of recruited monocytes we observed in wild type animals post-PNX (Figure 1). Flow cytometry 24 hours later revealed CSF1R-GFP⁺ cells in the lungs of recipients, with significantly more accumulating in PNX lungs (1.7% +/- 0.3%) compared to unoperated controls (0.5% +/- 0.1%) (Figure S4). To determine how CCR2 signaling affects monocyte accumulation in regenerating lungs, we injected 1×10^7 whole bone marrow cells from wild type *Csf1r-GFP* or *Ccr2*^{-/-}; *Csf1r-GFP* mice into *Ccr2*^{-/-} mice 6d post-PNX. The next day, we dosed mice with 2 ug APC-CD45 by retro-orbital injection to specifically label cells in the pulmonary vasculature that had not extravasated into the interstitial tissue or airspace. Five minutes later, the mice were sacrificed and lungs were dissociated and incubated with FITC-CD45 to label all leukocytes, regardless of localization. Flow cytometry showed the proportion of CSF1R-GFP⁺, FITC-CD45⁺ cells that was APC-CD45 negative (interstitial and airspace cells) in recipients of *Ccr2*^{+/+} donor bone marrow was nearly 2-fold higher than this population in the lungs of recipients of *Ccr2*^{-/-} donor bone marrow cells (Figure S4). This suggests that CCR2 plays an active role in the extravasation and retention of adoptively transferred bone marrow in regenerating lungs. Furthermore, analysis of *Ccr2*^{-/-} recipients of *Ccr2*^{+/+}; *Csf1r-GFP*⁺ donor bone marrow demonstrated that adoptively transferred cells persist until at least 14d post-PNX (Figure S4). Next we sought to determine whether *Ccr2*^{+/+} bone marrow-derived cells were sufficient to rescue the defect in lung regeneration in *Ccr2*^{-/-} mice. We delivered 1×10^7 whole bone marrow cells from *Ccr2*^{+/+} littermate controls to *Ccr2*^{-/-} mice by tail vein injection 4d and 7d post-PNX (Figure 4A). *Ccr2*^{-/-} recipients of wild type bone marrow had significantly increased lung dry weights (46% increase from unoperated) compared to *Ccr2*^{-/-} mice that had not been injected (23% increased from unoperated) or recipients of *Ccr2*^{-/-} bone

marrow (28% increase from unoperated) (Figure 4B). Importantly, the regenerated lung mass of *Ccr2*^{-/-} mice receiving *Ccr2*^{-/-} bone marrow was not statistically different from uninjected *Ccr2*^{-/-} mice. Furthermore, adoptive transfer of *Ccr2*^{+/+} bone marrow cells into *Ccr2*^{-/-} mice increased the number of lineage traced AEC1s at 21d post-PNX (27.2% +/- 0.08%) compared to uninjected *Ccr2*^{-/-} mice (9.1% +/- 2.9%) (Figure S4). Together, these data suggest that CCR2 plays an active role in the recruitment of monocytes and macrophages into lungs post-PNX where they promote regeneration.

3.2.5 Macrophages support alveolar stem cells in culture

To better understand how macrophages might regulate AEC2 behavior, we modified a co-culture organoid system AEC2s are sorted and cultured in a mixture of Matrigel and supplemented growth medium (Barkauskas et al., 2013). Cultured alone under these conditions, AEC2s rarely form colonies. However, the addition of PDGFRA⁺ fibroblasts, a putative component of the alveolar stem cell niche, greatly enhances the ability of AEC2 to form three-dimensional organoids called “alveolospheres” (Barkauskas et al., 2013). We isolated RFP⁺ lineage labeled AEC2s and CD45⁺;F4/80⁺ macrophages by FACS and co-cultured them in varying ratios without the addition of fibroblasts or endothelial cells (Figures 4D and S5). As expected, AEC2 alone rarely formed colonies (colony forming efficiency, CFE < 0.1%), but the addition of macrophages had a dose-dependent effect on the formation of organoids that we call pneumospheres (CFE = 1.61% +/- 0.51%) (Figures 4E and 4F). Pneumospheres had clear lumens and contained both lineage labeled RFP epithelial cells and F4/80⁺ macrophages (Figure 4G). Macrophages persisted in co-cultures with AEC2-derived pneumospheres at least 14d, but also survived when cultured alone (Figure S4). Partial overlap of the AEC2 marker SPC and AEC1 marker RAGE suggests that these cultured AEC2s may be reverted to a bipotential state *in vitro* (Treutlein et al., 2014)(Figure S4). Importantly, AEC2 co-cultured in a 1:1 ratio with splenic macrophages formed far fewer spheres (CFE = 0.20% +/- 0.6%) compared

to lung macrophages at the same ratio (CFE = 1.38% +/- 0.22%) (Figures 4F and S4). To determine whether bone marrow-derived macrophages (BMDMs) can also support AEC2-pneumospheres, we derived macrophages using an established protocol whereby whole bone marrow is cultured with MCSF-enriched media for at least 7d. BMDM cultured in a 1:1 ratio with AEC2s also promoted sphere formation (CFE = 1.01% +/- 0.10) (Figure S4). We conclude that lung macrophages can support formation of organoids from AEC2s and might directly promote AEC2 survival and proliferation.

3.2.6 Matrix-remodeling and M2-like macrophage gene signature in regenerating lungs

Our single cell RNA sequencing data suggested that a subset of the accumulating macrophages in post-PNX lungs express markers of M2-polarization (Figures 1G and 1H). To further understand how these cells might contribute to the regenerative process, we performed population level RNA sequencing on macrophages sorted from lungs 7d after PNx and sham operation (Figure 4C). These data confirmed robust expression of markers associated with M2-like macrophages, including Arginase1 (up 2.3 fold), Retnla/Fizz1 (up 2.9 fold), and Chil3/Ym1 (up 1.5 fold) in macrophages 7d post-PNX compared to sham controls. We also observed increased expression of genes associated with extracellular matrix and matrix remodeling including matrix metalloproteinases-2, 3, 12, 14, and 19 and collagens-1a1, 1a2, 3a1, 5a1, and 14a1. Macrophages from the lungs of pneumonectomized mice expressed lower levels of inflammatory cytokines TNF α , IL-1 β , and IL-6, further suggesting an anti-inflammatory M2-like phenotype. Using qPCR, we confirmed that the expression of Arginase1 is increased in CD45 $^{+}$;F4/80 $^{+}$ macrophages isolated from the lungs of mice 7d after PNx compared to sham operation (Figure 5S).

3.2.7 Decreased M2 macrophages and lung regeneration in IL-4R α -deficient mice

Because M2-like macrophages are present during alveolar formation during post-natal lung development (Jones and Williams, 2013; Saluzzo et al., 2017) modulate tissue inflammation (Gibbons et al., 2011, Herbert et al., 2004), and promote progenitor cell activity in muscle and heart (Ruffel et al., 2009, Shiraishi et al., 2016), we hypothesized that this subset of macrophages promotes post-PNX alveologensis. To investigate M2 macrophages in this regenerative process, we performed PNx in *Arg1^{Tm1Lky}/J* mice (hereafter YARG), in which yellow fluorescent protein is knocked into the *Arginase-1* locus (Van Dyken and Locksley, 2013; Reese et al., 2007). Flow cytometry and immunofluorescence show that there are few YARG⁺;F4/80⁺ M2-like macrophages in sham operated controls (0.4% +/- 0.1%). However, the number of these cells increases more than 2-fold post-PNX, with a peak at 4d post-PNX (1.4% +/- 0.4%) (Figures 5A, 5B, and 5C). Consistent with previous reports showing that M2-like macrophages proliferate in “Th2-type” microenvironments (Jenkins et al., 2011), EdU pulse experiments revealed that some YARG⁺ M2-like macrophages proliferate 4d and 7d post-PNX (Figure S5).

IL4RA is a shared receptor subunit for both IL4 and IL13, cytokines that promote the polarization of M2-like macrophages. Consistent with a role for M2-like macrophages in lung regeneration, both *Il4ra* and a co-receptor *Il13ra1* were expressed at significantly higher levels in macrophages 7d post-PNX compared to sham controls (Figure S1). To determine whether loss of IL4/13 signaling would negatively impact lung regeneration in vivo, we utilized *Il4ra^{tm1Sz}* mice, which lack a functional IL4RA. By crossing the YARG reporter allele onto the *Il4ra^{-/-}* background, we confirmed that *Il4ra^{-/-}* mice had significantly fewer M2-like macrophages 4d post-PNX (1.1% +/- 0.4%) compared to wild type littermate controls (2.2% +/- 0.4%) (Figures 5D-F). Moreover, *Il4ra^{-/-}* mice showed impaired compensatory growth by lung mass 14d post-PNX compared to wild type littermate controls (Figure 5G). Finally, when AEC2 were lineage traced as described above in *Il4ra^{-/-}* mice, there were fewer lineage traced AEC1 21d post-PNX (13.4% +/- 4.5%) compared to wild type controls (39.7% +/- 6.3%) (Figure 5S).

We performed bone marrow chimera experiments to confirm that the lung regeneration defect in *Il4ra*^{-/-} mice is attributable to loss of IL4/13 signaling in leukocytes and not another cell type (Figure 5J). Wild type CD45.1 mice were lethally irradiated at 6 weeks of age and transplanted with bone marrow from CD45.2 wild type or *Il4ra*^{-/-} mice. After 10 weeks to allow for hematopoietic reconstitution, we performed PNX. At the time of surgery, resected left lobes were dissociated for flow cytometric assessment of hematopoietic reconstitution from donor-derived cells. Lung monocytes were ~99% donor-derived and alveolar macrophages were ~97% donor-derived in all irradiated animals (Figure S5). Mice reconstituted with *Il4ra*^{-/-} bone marrow had impaired lung regeneration assessed by dry weight 14d post-PNX compared to littermate controls reconstituted with wild type bone marrow (Figure 5K). These data demonstrate that IL4RA signaling is required within the hematopoietic compartment for optimal lung regeneration.

Our single cell RNA sequencing revealed a subset of myeloid cells that expresses markers of both monocytes and M2-like macrophages, raising the possibility that CCR2+ monocytes could be a source of M2-like macrophages. We observed CCR2-RFP+ and CCR2-RFP- YARG+ M2-like macrophages in tissue sections of lungs from YARG;*Ccr2*^{RFP/+} mice 7d post-PNX (Figure 5H). However, these alleles are transcriptional reporters rather than heritable marks for lineage tracing, so we cannot draw conclusions about lineage relationships between monocytes and M2-like macrophages.

We sought to determine whether CCR2+ monocytes influence the generation of M2-like macrophages post-PNX, regardless of their origin. Immunofluorescence stains of lungs from YARG;*Ccr2*^{RFP/RFP} mice showed the presence of YARG+, F4/80+ M2-like macrophages 7d post-PNX (Figure S5), but flow cytometry revealed that *Ccr2*^{RFP/RFP} mice had significantly fewer YARG+, F4/80+ M2-like macrophages (91,000 +/- 22,000 cells, 1.1% +/- 0.2% of CD45+ cells) compared to wild type mice (158,000 +/- 26,000 cells, 1.9% +/- 0.5%) 4d post-PNX (Figures 5I and 5S). Based on these data and the fact that loss of CCR2 did not affect Arg1 expression in

macrophages (Figure 5S), we conclude that CCR2⁺ recruited monocytes are not an essential source of M2-like macrophages post-PNX. However, we note that the absence of CCR2⁺ monocytes leads less efficient generation of M2-like macrophages.

3.2.8 Innate lymphoid cells are a source of IL13 in regenerating lungs

Macrophage polarization towards an M2-like phenotype can be induced by IL4 and IL13 in the microenvironment. Sources of these cytokines include CD4 helper T cells, basophils, and eosinophils (DeNardo et al., 2009; Egawa et al., 2013; Herbert et al., 2004; Loke et al., 2007; Wu et al., 2011). To determine whether helper T cells may play a role in PNX-induced lung regeneration, either directly or indirectly by regulating macrophage activity, we performed PNX in *Rag1^{Tm1Mom}* null mice that lack all functional T and B cells. There was no difference in lung mass 14d post-PNX between *Rag1^{-/-}* mice and wild type littermate controls (Figure S6). Furthermore, we did not detect an increase in IL4-expressing basophils, ILC2s, CD4⁺ T cells, nor NKT cells in the lungs of KN2 mice, a high-fidelity reporter for IL4 (Mohrs et al., 2005; Sullivan et al., 2011) (data not shown). Combined, these data implicate IL13 as the important type-2 cytokine in regenerating lungs.

Type 2 innate lymphoid cells (ILC2s) have been shown to be a major producer of IL13 that polarizes lung macrophages toward an M2-like phenotype in certain inflammatory models (Van Dyken et al., 2014; Molofsky et al., 2013). We utilized Red5 mice in which RFP is knocked into the *Ii5* locus as a highly specific marker for ILC2s (Nussbaum et al., 2013). Immunofluorescent stains demonstrated that ILC2s were present post-PNX near small conducting airways (central) and at the periphery of the lung (Figure 6A). Additionally, we performed flow cytometry to quantify ILC2s based on cell surface markers (Lin⁻Thy1⁺ST2⁺ cells) and by reporter activity (Lin⁻Red5⁺ cells) and found that the proportion and absolute numbers of ILC2s was significantly increased 7d post-PNX (1.46% +/- 0.21%; 39,300 +/- 17,200) compared to sham-operated mice (0.64% +/- 0.33%; 23,700 +/- 9,200) (Figure 6B,C). Similar to steady

state lungs, almost all Red5+ cells in the lung post-PNX were ILC2s (Figure S6C) (Nussbaum et al., 2013). Lastly, to determine if ILC2s are a source of IL13 post-PNX, we FACS purified ILC2s 4d post-PNX or sham for qRT-PCR analysis. ILC2s 4d post-PNX had a significant increase in IL5 and IL13 transcripts, but not in IL4 transcripts, compared to sham operated controls (Figure 6S). We analyzed lungs of Smart13 reporter mice, in which a modified human CD4 is knocked into the *Il13* locus (Liang et al., 2012), to evaluate IL13 expression in vivo. There was a significant increase in the proportion of ILC2s (Lin⁻Thy1⁺ST2⁺ cells) that were Smart13⁺ by flow cytometry 4d post-PNX when compared to sham-operated littermate controls (Figure 6D,E). Finally, using Ki67-based flow, we found a significant increase in proliferating ILC2s 7d post-PNX compared to sham-operated littermate controls (Figure 6S). Together, these data demonstrate an expansion of ILC2s post-PNX and implicate ILC2s as a source of IL13 during lung regeneration post-PNX.

3.3 Discussion:

3.3.1 Single cell RNA sequencing reveals macrophage heterogeneity

When studied in the context of repair/regeneration, macrophages are usually categorized as classically or alternatively activated based on the expression of a panel of markers. Here, we took the unbiased approach of single cell sequencing to determine the extent of heterogeneity amongst myeloid cells in the regenerating lung. As expected, and consistent with data from other regeneration models, our single cell transcriptional profiling revealed a population of cells that expressed markers of M2-like macrophages post-PNX. In addition, this unbiased approach led us to the unexpected discovery that CCR2⁺ Ly6c⁺ inflammatory monocytes constitute a component of the myeloid compartment in the regenerating lung following PNx. These data do not exclude the possibility of additional myeloid subsets at other stages during regeneration or subsets that were below the detection threshold of our analysis.

3.3.2 CCR2+ monocytes and interstitial macrophages are required for optimal regeneration post-PNX

The chemokine receptor CCR2 has been well characterized as a mode of egress for monocytes from the bone marrow (Gordon and Taylor, 2005). Recent evidence suggests that bone marrow derived and circulating monocytes rarely contribute to resident macrophage populations during adult homeostasis, but replace macrophages following their depletion or during inflammation (Gordon and Taylor, 2005; Hashimoto et al., 2013; Yona et al., 2013). In many contexts, such as adult myocardial infarction, pulmonary fibrosis, and influenza infection, CCR2+ monocytes prolong and exacerbate injury (Gibbons et al., 2011; Herold et al., 2008; Nahrendorf et al., 2007). However, recruitment of CCR2+ monocytes is essential for tissue regeneration in other contexts, including the resolution liver fibrosis and regeneration of the heart and skin (Aurora et al., 2014; Gibbons et al., 2011; Ramachandran et al., 2012; Willenborg et al., 2012).

Previous data have demonstrated a requirement for a broadly defined CD18+ leukocyte population in lung regeneration post-PNX (Chamoto et al., 2013a). Our data demonstrate that bone marrow-derived CCR2+ monocytes enter the lung through a CCL2-CCR2 axis. CCR2 deficiency impairs accumulation of interstitial monocytes and macrophages, but not alveolar macrophages, in the lung post-PNX. CCR2-deficient mice have impaired capacity for compensatory lung growth following PNx, unequivocally demonstrating for the first time a requirement for recruited monocytes in lung regeneration. We show that the adoptive transfer of wild type, but not CCR2-deficient, bone marrow was able to rescue the regeneration defect in CCR2-deficient mice.

Our bone marrow chimera experiments demonstrate that *Il4ra* is required specifically on leukocytes for the optimal regeneration. Although not conclusive, these data are consistent with

a role for M2-like macrophages in lung regeneration post-PNX. Interestingly, human peripheral blood monocytes show M2-like polarization in response to CCL2 (Roca et al, 2009). Consistent with this, we observed fewer M2-like macrophages in the lungs of pneumonectomized CCR2-deficient mice compared to controls. However, M2-like macrophages were not completely absent in the lungs of CCR2-deficient mice. Together, our data suggest that recruited monocytes promote the generation of M2-like macrophages in the regenerating lung, either as a direct source or through modulation of the microenvironment. Future lineage tracing experiments are required to determine the relative contributions of recruited and resident cells to the M2-like macrophage population.

3.3.3 Macrophages are a component of the regenerative AEC2 niche

We show that the number of myeloid cells in the regenerating lung peaks at the time of maximal AEC2 proliferation. Consistent with these cells constituting a component of the regenerative niche, we frequently observed CSF1R-GFP⁺ cells and CCR2⁺ monocytes adjacent to AEC2 stem cells during regeneration. Indeed, resident lung macrophages and bone marrow-derived macrophages were able to support the growth of AEC2-derived pneumospheres *in vitro*, suggesting a direct interaction between these populations. These *in vitro* data and our analysis of AEC2 stem cell behaviors *in vivo* are consistent with a model in which macrophages and monocytes promote the proliferation and differentiation of AEC2 (Figure 6F). Our transcriptional profiling of macrophages also revealed a number of mechanisms by which myeloid cells might indirectly promote lung regeneration post-PNX. These include the secretion of pro-angiogenic factors and matrix remodeling enzymes (including MMP14), both of which have been shown to promote lung regeneration post-PNX (Chamoto et al., 2013a; Ding et al., 2011).

Our data implicate ILC2s as a source of IL-13 in a sterile model of lung regeneration. This cytokine could promote the polarization of M2-like macrophages and modulate their

biochemical functions, including anti-inflammation, collagen synthesis and remodeling of the extracellular matrix (Chiaramonte et al., 1999; Knipper et al., 2015; Madala et al., 2010; Martinez et al., 2009 Pellicoro et al., 2012; Pouladi et al., 2004; Zheng et al., 2000). Alternatively or in addition, IL-13 could directly influence other cell types including lung epithelium (Kuperman et al., 2002). Further studies will characterize the ontogeny, activation and functions of M2-like macrophages and ILC2s in lung homeostasis and repair.

There is at least one report of adult alveologenesi in humans over a period of 15 years following lung reduction surgery (Butler et al., 2012). Our data further support the development of macrophage-based therapies to enhance the efficiency and kinetics of this regenerative capacity as a therapeutic approach for lung disease. This will require a deeper understanding of the manner in which monocytes, macrophages and other populations – including epithelial stem cells - interact in the context of the healthy, diseased and regenerating lung.

3.4 Methods and Materials

EXPERIMENTAL MODEL AND SUBJECT DETAILS

Mice

All mice were bred and maintained in a specific-pathogen-free barrier facility. Tg(Csf1r-EGFP)1Hume/J (also referred to as *Csf1r-GFP*) mice, *CCR2^{tm1Mae}* (also referred to as *Ccr2^{-/-}*) mice, *Ccr2^{tm2.1fc}* (also referred to as *Ccr2^{RFP/+}*) mice, and *Cx3Cr1^{tm1Litt}* (also referred to as *Cx3cr1^{GFP/+}*) mice were used for macrophage and monocyte studies (Kuziel et al., 1997; Jung et al., 2000; Saederup et al., 2010; Sasmono et al., 2003) *Ccr2^{-/-}* (pure-bred BALB/c strain) and *Ccr2^{RFP/RFP}* (pure-bred C57Bl/6 strain) mice were used to assess the contribution of CCR2+ cells in PNx-induced lung regeneration. Mice containing *Sftpc-CreER* and *Rosa-dtomato* alleles for lineage tracing AEC2s were backcrossed to *Ccr2^{tm1Mae}* BALB/c mice for at least 5 generations. *Arg1^{tm1Lky/J}* (also referred to as YARG) mice were used to assess M2-like

polarization of macrophages and *I4ra*^{tm1Sz} mice were used to test a requirement for M2-like macrophages in PNX-induced lung regeneration (Noben-Trauth et al., 1997; Reese et al., 2007). *Rag1*^{tm1Mom} were used to assess the requirement for lymphoid cells in PNX-induced lung regeneration (Mombaerts et al., 1992). B6-Ly5.1/Cr were obtained from Charles River Laboratories International, Inc. and used to distinguish host vs. donor-derived hematopoietic cells in bone marrow chimera experiments. *I5*^{tm1.1(Cre)Lky} (also referred to as Red5) mice were used to assess the contribution of ILC2s in PNX-induced lung regeneration (Nussbaum et al., 2013). *IL13*^{tm2.1Lky} (also referred to as Smart13) mice were used to measure IL-13 protein production from ILC2s (Liang et al., 2012). All studies were approved by University of California, San Francisco (UCSF) Institutional Animal Care and Use Committees (IACUC).

METHOD DETAILS

Pneumonectomy procedure

Prior to surgery, adult mice (8-12 weeks old) were weighed, given Buprenex (0.3 mg/mL, Reckitt Benckiser, catalog #NDC 12496-0757-5) at 20g/kg, and shaved at the surgical site on the left lateral side. Mice were anesthetized with 2% isoflurane and intubated for ventilation using a Harvard mini-vent ventilator. Mice were anesthetized and ventilated throughout the pneumonectomy procedure with 200 μ L of stroke volume at 200 strokes per minute. The surgical site was sterilized with ethanol and beta-iodine and then a 2 cm long incision was made on the left lateral side of the skin. Left-sided thoracotomy was performed with a 1 cm long incision at the 5th intercostal space to expose the left lung lobe underneath. The ribs were spread by retraction and the left pulmonary vasculature and mainstem bronchus were ligated with a titanium clip. The left lobe was resected, and the ribs and skin closed. An angiocath port was inserted to evacuate the void space and reestablish negative intrathoracic pressure. Sham control surgeries were performed as thoracotomy procedure without lung removal. After closure, topical analgesics were applied at the surgical sites (Lidocaine, 5 mg/mL, Phoenix, catalog

#NDC 57319-533-05; Bupivacaine, 2.5 mg/mL, Hospira, catalog #NDC 0409-1159-01). Anesthesia was discontinued and mice remained intubated until autonomous breathing recovered. Mice were placed on a warming pad and monitored until awake. A second Buprenex dose was given 4-6 hours later and monitored to ensure that a full recovery was made.

Tissue harvest and fixation

Mice were euthanized by CO₂ exposure until respiration ceased. Mice were dissected to expose the diaphragm, which was cut to cause pneumothorax. To perfuse the pulmonary vasculature, the descending aorta was cut and a 21 gauge needle was inserted into the right ventricle to flush at least 20 mL of cold PBS until lungs had blanched. The trachea was exposed and a small incision was made at the pharyngeal cartilage to allow inflation with cold 4% paraformaldehyde. Lungs were inflated to 20 cm H₂O pressure and fixed *in situ* for 10 minutes. Lungs were then removed *en bloc* and then submerged 4% paraformaldehyde for 1 hour at 4°C. Individual lung lobes were separated and then washed three times for 15 minutes in cold PBS. In preparation for embedding, lungs were submerged in 30% sucrose for 24 hours, then moved to a 50:50 mixture of 30% sucrose/O.C.T medium (Optimal Cutting Temperature Medium, Tempura) for 24 hours, and then finally embedded in 100% O.C.T. medium and immediately frozen on dry ice and stored at -20°C.

Immunostaining for histology

Tissue blocks were sectioned at 12-13 μm and were left to dry on a slide warmer overnight. Wax slides were dewaxed and rehydrated. Tissue sections were permeabilized with 0.5% TritonX-100 in PBS for 5 minutes. Tissue sections were blocked in 5% donkey serum (Sigma, catalog #D9663-10ML), 5% goat serum (Sigma, catalog #G9023-10ML), 3% bovine serum albumin (Fisher, catalog #BP1600-100) and 0.1% TritonX-100 for 1 hour at room temperature. Primary antibodies were diluted in block at concentrations listed in the Key Resources Table

and incubated overnight at 4°C. All fluorophore-conjugated secondary antibodies were diluted in block at 1:500. EdU staining was performed according to manufacturer recommendations (Invitrogen, see Proliferation Studies). DAPI nuclear staining was performed according to manufacturer recommendations. Tissue sections were washed 5x with PBS for 15 minutes after/between antibody incubations. Images of sections were captured on a Zeiss Imager M2 AxioCam MRm microscope. For pneumonectomy studies, imaging was focused exclusively on the accessory lobe for all mice. For quantification of cells, at least 10 randomly selected images were counted per animal. Images were processed with ImageJ/FIJI (version 2.0.0, NIH).

Lung dissociation for flow cytometry and FACS

Mice were sacrificed as described in the tissue harvest protocol. After perfusion, lungs were inflated intratracheally with 1 mL of protease solution containing Collagenase Type I (Gibco, catalog #17100-017, used at 450 U/mL), Elastase (Worthington Biochemical Corporation, catalog #LS002279, used at 4 U/mL;), Dispase (BD Biosciences, catalog #354235, used at 5 U/mL;) and DNaseI (Roche, catalog #10104159001, used at 0.33 U/mL) solubilized in DMEM/F12. The lungs were resected *en bloc*, separated into individual lobes and cut into small pieces (<2 mm²) by scalpel blade. Diced tissues were incubated in 4-5 mL protease solution for 30 minutes at 37 °C with frequent agitation until completely dissociated into single cells. Cells were washed with serum media made from 10% FBS in DMEM/F12. Cells were incubated with 2 mL of red blood cell lysis buffer (Biolegend, catalog #420301-BL) for 4 minutes at room temperature and the washed with serum media. Cells were filtered through a 40-µm strainer, centrifuged, and resuspended in flow cytometry/FACS buffer (5% FBS in HANKS buffer or HBSS, modified without Ca²⁺ or Mg²⁺). Flow cytometry was performed on a BD LSR II and sorting was performed on a BD FACSAria II. Specifically for ILC2 flow cytometry, lungs were dissociated with GentleMACS protocol “m_lung_01_01” (Miltenyi Biotec), digested for 30 minutes with Liberase TM (Roche, catalog #05401119001) & DNase I (Sigma-Aldrich), further

homogenized using gentleMACS protocol “m_lung_01_02,” and treated with Pharm Lyse (BD Biosciences). Data was analyzed with FACS Diva (BD Biosciences) and FlowJo (version 10.1r5, FLOWJO LLC).

Immunostaining for flow cytometry & FACS

Single isolated cells were kept on ice and stained in flow cytometry/FACS buffer (5% FBS in HANKS buffer or HBSS, modified without Ca^{2+} or Mg^{2+}). Cells were blocked with CD16/CD32 Fc receptor block (BD Biosciences, catalog #553142) at 1:100 for 20 minutes and washed. Fluorophore-conjugated antibodies were used according to the Key Resources Table and cells were stained for 30 minutes - 1 hour. For live cell staining and sorting, a cell viability dye was added before sample acquisition (Sytox Blue at 1:1000, Life Tech, catalog #S34857 or DAPI at 1:2000 of 1 mg/mL). For intracellular flow cytometry (detection of SPC, Gata-3, or Ki67), cells were prepped using a cell fixation and permeabilization kit (Invitrogen, catalog #GAS003). EDU-based proliferation was assessed using the Click-iT® EdU Alexa Fluor® 647 Imaging Kit (Invitrogen, catalog #C10340) as per the manufacturer's instructions. Flow cytometry was performed on a BD LSR II or BD LSRFortessa DUAL and cell sorting was performed on BD FACSAria II or Sony SH800S Cell Sorter. Compensation was performed with single antibody/channel controls using a AbC Anti-Mouse Bead kit (Molecular Probes, catalog #A10344). Gating controls for each channel were established with samples containing all the staining antibodies except the antibody in that channel (fluorescence minus one). To determine gating controls for reporter gene expression, mice lacking the reporter or protein were used. Data were analyzed with FACS Diva (BD Biosciences) and FlowJo (v10.1r5, FLOWJO LLC).

Intravascular CD45 Labeling

To label immune cells in the pulmonary vasculature, we injected mice with CD45 bound to high molecular weight fluorophore by intravenous route shortly before sacrifice. 2 µg of CD45-APC

(10 μ L, Biolegend, cat# 103112) were diluted in 100 μ L of sterile saline and loaded into a 28.5 gauge insulin syringe. Mice were put in a sealed container containing a cotton ball soaked in isofluorane and monitored closely. When breathing slowed, mice were removed from the container. Gentle pressure was applied around the peri-orbital area to induce eye protrusion. The syringe needle was inserted in the retro-orbital space and contents injected. Mice were allowed to regain consciousness and were sacrificed by CO₂ asphyxiation 5 minutes later.

Dry weight lyophilization

Murine lungs were perfused as previously described, isolated into individual lobes, and flash frozen in liquid N₂ immediately after harvest. Lobes were placed into microcentrifuge tubes and transferred to a freeze/dry flask attached to a Labconco Freeze Dry System. Lung lobes were lyophilized for twenty-four hours and immediately weighed. Lung lobe weights were normalized to mouse height (anus to snout).

Proliferation studies

For assessing cell proliferation *in vivo*, EdU (Thermo Fisher Scientific, Catalog #E10415) was resuspended at 5 mg/mL in sterile PBS and administered to mice by intraperitoneal injection at 50 mg of EdU per kg of mouse weight. For flow cytometry, EdU incorporation was detected using the Click-iT EdU Alexa Fluor 647 Imaging Kit (Invitrogen, catalog #C10340). For tissue histology, EdU incorporation was detected using the Click-iT *Plus* EdU Alexa Fluor 647 Imaging Kit (Invitrogen, catalog #C10640). To assess AEC2 proliferation by flow cytometry, EDU was given twenty-four hours prior to sacrifice. To assess local macrophage proliferation, EdU was given 3.5 hours prior to sacrifice.

Lineage labeling

Tamoxifen (Sigma-Aldrich, catalog #T5648) was dissolved in corn oil and administered to mice via intraperitoneal injection at 0.25 mg of Tamoxifen per kg of mouse weight. Three full doses of TMX were given to each animal at eight weeks every other day. To provide a tamoxifen “wash-out” period, we waited at least 14 days after the last tamoxifen dose before any study intervention.

Adoptive transfer of bone marrow cells

Mice were sacrificed by CO₂ asphyxiation. Long bones (femur and humerus) were isolated and flushed with 10% FBS in DMEM to clear bone marrow cells. Bone marrow cells were filtered through a 40 µm strainer and resuspended in sterile saline for injection. Cells were manually counted using a Fisher Scientific Hemacytometer (catalog #0267110) and a Zeiss Primo Vert Inverted Microscope. 10 million bone marrow cells were resuspended in 200 µL of sterile saline for intravenous lateral tail vein injection. Prior to injection, mouse tails were sterilized and gently warmed.

Generation of bone-marrow derived macrophages

Bone marrow cells were isolated as described in adoptive transfer protocol, and plated on non-tissue treated petri dishes with macrophage-differentiation media. This media contained 10% F.B.S, 1x penicillin/streptomycin, and 10% MCSF-enriched media harvested from MCSF secreting-3T3 fibroblasts. Bone marrow-derived macrophages were cultured for at least 7 days, with media changes every 3-4 days, until use in co-culture 3D-organoid *in vitro* pneumosphere assay.

Pneumosphere *in vitro* assay

FACS sorted cells were plated in the upper chamber of 0.4 µm transwells nestled in 24-well plates and grown in a 5% CO₂, 37 °C incubator. Cells were seeded in 75 µL of growth factor

reduced Matrigel (BD Biosciences, catalog #356230) and 75 μ L of pneumosphere media to form a cell-mixture plug. This plug was pipetted at the bottom of the transwell and 1000-900 μ L of pneumosphere media was placed in the lower chamber. Pneumosphere media contained 10% F.B.S. (Hyclone, catalog #SH30071), 1x Insulin-Transferrin-Selenium (Gibco Life Tech, Catalog #41400-045), 1x penicillin/streptomycin, EGF 20 ng/mL (R&D Systems, catalog #2028-EG-200), FGF2 25 ng/mL (Gibco Life Tech, catalog #PMG0033), KGF 10 ng/mL (Gibco Life Tech, catalog #PHG0094), HGF 10 ng/mL (Gibco Life Tech, #PHG0254) in DMEM / F12 + GlutaMAX (Gibco Life Tech, catalog #10565-018). Pneumosphere media was changed every two-three days after plating. Pneumospheres were counted on day 14 by bright-field microscopy.

Bone marrow chimeras

At 6 weeks of age, co-housed littermate Ly5.1 (CD45.1) B6 mice were lethally irradiated with 2 doses of 550 rads separated by 4 hours, followed by a whole bone marrow transplant several hours later. Bone marrow was harvested from wild type or *Il4ra*-deficient mice, counted, and divided amongst the recipient mice. Bone marrow was re-suspended in sterile saline and injected by intravenous tail vein route. Animals were carefully monitored over the next 10 weeks to allow turn-over and reconstitution of lung myeloid and bone marrow-derived monocytes.

Protein Cytokine Array

Tissues were harvested as above, except lungs were not fixed. Whole accessory lobes were isolated and weighed *ex vivo*. Accessory lobes were then flash frozen in liquid nitrogen and pulverized with a chilled glass dounce. RIPA lysis and extraction buffer (ThermoFischer Scientific, catalog #89900) containing Complete, Mini protease inhibitor cocktail (Roche, catalog #11-836-153-001) was added to each sample at 1 mL of solution per 60 mg of tissue. Tissue were further homogenized by dounce and then briefly sonicated. Samples were then centrifuged

at 14,000g for 15 minutes and supernatants were isolated. A standardized Bradford assay was performed to measure lysate protein concentration (Protein Assay Dye Reagent Concentrate, Biorad, catalog #500-0006; Bio-Rad SmartSpec Plus Spectrophotometer, catalog #170-2525). Purified protein lysates (200 µg) were applied to the Proteome Profiler Mouse Cytokine Array Kit, Panel A (R&D Systems, catalog #ARY006). The chemiluminescence reaction was measured with a ChemiDoc XRS+ System (Biorad). Densitometry quantitation was performed in FIJI/ImageJ (NIH).

qRT-PCR

Single cells isolated by FACS were lysed using the QIAshredder (Qiagen, catalog #79654) or immediately sorted into RLT buffer. RNA was purified using the RNeasy Plus Micro Kit (Qiagen, catalogue #74034). RNA quantity and quality was measured using a Nanodrop (Thermo Scientific). cDNA was made using the SuperScript IV VILO cDNA Mastermix Kit (Invitrogen, catalog #11756050). qRT-PCR was performed using the SYBR GreenER qPCR Supermix Universal Kit (Invitrogen, catalog #11762100). Reactions were run in triplicate on a ViiA7 Real-Time PCR System (Thermo Fischer). Expression levels were measured using the $2^{-\Delta\Delta CT}$ method in which $n \geq 3$ PNX mice were compared to $n \geq 3$ sham mice and normalized to house-keeping genes.

RNA sequencing

For bulk population level RNA sequencing, RNA was obtained as described in qRT-PCR methods. Quality control was performed with an Agilent RNA 600 Pico Kit (catalog #5067-1513) using an Agilent 2100 Bioanalyzer (Agilent Technologies). Purified RNA was submitted to the UCSF Genomics Core for high throughput RNA sequencing. The library was prepared with TruSeq Stranded mRNA and sequencing was done on an Illumina HiSeq 4000 with 50 bp single-end reads. Sequencing yielded ~230 million reads with an average read depth of 28.7

million reads/sample. Reads were then aligned to the mouse genome (Ensemble Mouse GRCm38.78) using STAR_2.3.2a. Those that mapped uniquely to known mRNAs were used to assess differential expression.

For single cell RNA sequencing, lung macrophages were isolated by FACS. Fluidigm C1 and C1 integrated fluidics circuits (IFCs) were used to capture live cells, lyse, convert polyA+RNA into full length cDNA, amplify cDNA and generate cDNA according to their detailed protocol (“Using C1 to Generate Single-Cell cDNA Libraries for mRNA Sequencing”, Fluidigm, PN 100-7168). 88 single CD45+, CSF1R-GFP+, F4/80+, Ly6G- cells were captured on a C1 Single-Cell DNA seq IFC, 5-10 μ m (Fluidigm, catalog #100-5759) using the C1 Single-Cell Reagent Kit for mRNA Seq (Fluidigm, catalog #100-6201). Library preparation for sequencing was performed following the modified Illumina Nextera XT DNA library preparation protocol using the Nextera XT DNA Library Preparation Kit (Illumina, Catalog #FC-131-1096). The concentration of cDNA was determined using the Quant-iT™ PicoGreen® dsDNA Assay Kit (Life Technologies, catalog #P7589). Sequencing was performed by Elim BioPharm (Oakland, CA) on one lane of an Illumina HiSeq2500 Flow cell in rapid mode with 50bp paired end reads. De-multiplexed files were created using CASAVA 1.8 (Illumina).

Reads were aligned and mapped using Tophat (v2.1.0) and Bowtie2 (v2.2.6) and Cufflinks (v2.2.1) software (Kim et al., 2013; Trapnell et al., 2012) 141 million reads were aligned with an average of 1.66 million reads per cell per end. All of the accepted hits in bam files output from cufflinks were processed using Picard tools: FixMateInformation (<http://broadinstitute.github.io/picard/>). Counts were compiled using HTSeq-count (Anders et al., 2015; <http://www-huber.embl.de/users/anders/HTSeq/doc/count.html>) and aligned with UCSC mm10 mouse assembly. All of the gene counts for each cell were compiled into a single file. Filtering was then performed to remove any cell that did not have at least a 50% alignment rate. Genes that did not have a least one read aligned in at least 3 cells were removed.

Fluidigm's R package Singular was used to generate an unbiased hierarchical clustering heat map.

During revisions, we performed additional single cell RNA sequencing on macrophages harvested 7 days after sham surgery to compare with our initial dataset of PNx-macrophages. These cells and their RNA were isolated as before, but the downstream analysis differed as follows:

Sequencing was performed by UCSF Genomics Core on one lane of an Illumina HiSeq2500 Flow cell in rapid mode with 100bp paired end reads. De-multiplexed files were created using CASAVA 1.8 (Illumina). Each sample was filtered using Trimmomatic v0.36 (Bolger et al., 2014; <http://www.usadellab.org/cms/?page=trimmomatic>) with the settings LEADING:3 TRAILING:3 SLIDINGWINDOW:4:15 MINLEN:70 and only paired matches were kept. Counts were compiled with RSEM aligner (v1.3.0, Li and Dewey, 2011) and aligned with genome Ensembl GRC m38 release 87. The gene count matrix was then created by running the rsem command "rsem-generate-data-matrix" on all of the genes.results files for each cell.

QUANTIFICATION AND STATISTICAL ANALYSIS

Statistical parameters, including the number of samples (n), descriptive statistics (mean and standard deviation), and significance are reported in the figures and figure legends. In general, at least n = 3 mice were used for each time point and for each intervention. For each metric analyzed, we performed an unpaired, two-tailed, Student's t test between treated and control groups. When quantifying cell numbers in histological sections, counters were blinded, microscopy fields randomly selected, and at least 10 images were scored per animal. GraphPad Software version 6.0 was used for all mathematical statistical analysis.

DATA AND SOFTWARE AVAILABILITY

Data Resources

The accession number for the RNA-seq data reported in this paper is NCBI GEO: GSE96104 (PNX) and GSE96105 (sham).

References:

- Aggarwal, N.R., King, L.S., and D'Alessio, F.R. (2014). Diverse macrophage populations mediate acute lung inflammation and resolution. *Am. J. Physiol. Lung Cell Mol. Physiol.* *306*, L709–25.
- Anders, S., Pyl, P.T., and Huber, W. (2015). HTSeq—a Python framework to work with high-throughput sequencing data. *Bioinformatics* *31*, 166–169.
- Arnold, L., Henry, A., Poron, F., Baba-Amer, Y., van Rooijen, N., Plonquet, A., Gherardi, R.K., and Chazaud, B. (2007). Inflammatory monocytes recruited after skeletal muscle injury switch into antiinflammatory macrophages to support myogenesis. *J. Exp. Med.* *204*, 1057–1069.
- Aurora, A., and Olson, E. (2014). Immune Modulation of Stem Cells and Regeneration. *Cell Stem Cell* *15*, 1425.
- Aurora, A.B., Porrello, E.R., Tan, W., Mahmoud, A.I., Hill, J.A., Bassel-Duby, R., Sadek, H.A., and Olson, E.N. (2014). Macrophages are required for neonatal heart regeneration. *J. Clin. Invest.* *124*, 1382–1392.
- Barkauskas, C.E., Crouse, M.J., Rackley, C.R., Bowie, E.J., Keene, D.R., Stripp, B.R., Randell, S.H., Noble, P.W., and Hogan, B.L. (2013). Type 2 alveolar cells are stem cells in adult lung. *J. Clin. Invest.* *123*, 3025–3036.
- Barner, M., Mohrs, M., Brombacher, F., and Kopf, M. (1998). Differences between IL-4R α -deficient and IL-4-deficient mice reveal a role for IL-13 in the regulation of Th2 responses. *Curr Biol* *8*, 669–672.
- Bolger AM, Lohse M & Usadel B (2014) Trimmomatic: a flexible trimmer for Illumina sequence data. *Bioinformatics* *30*, 2114–20
- Boulter, L., Govaere, O., Bird, T.G., Radulescu, S., Ramachandran, P., Pellicoro, A., Ridgway, R.A., Seo, S.S., Spee, B., Van Rooijen, N., et al. (2012). Macrophage-derived Wnt opposes Notch signaling to specify hepatic progenitor cell fate in chronic liver disease. *Nat. Med.* *18*, 572–579.

Butler, J.P., Loring, S.H., Patz, S., Tsuda, A., Yablonskiy, D.A., and Mentzer, S.J. (2012). Evidence for adult lung growth in humans. *N. Engl. J. Med.* *367*, 244–247.

Chamoto, K., Gibney, B.C., Ackermann, M., Lee, G.S., Lin, M., Konerding, M.A., Tsuda, A., and Mentzer, S.J. (2012). Alveolar macrophage dynamics in murine lung regeneration. *J. Cell. Physiol.* *227*, 3208–3215.

Chamoto, K., Gibney, B.C., Lee, G.S., Ackermann, M., Konerding, M.A., Tsuda, A., and Mentzer, S.J. (2013a). Migration of CD11b⁺ accessory cells during murine lung regeneration. *Stem Cell Res* *10*, 267–277.

Chamoto, K., Gibney, B.C., Ackermann, M., Lee, G.S., Konerding, M.A., Tsuda, A., and Mentzer, S.J. (2013b). Alveolar epithelial dynamics in postpneumectomy lung growth. *Anat Rec (Hoboken)* *296*, 495–503.

Chen, L., Acciani, T., Le Cras, T., Lutzko, C., and Perl, A.-K.T.K. (2012). Dynamic regulation of platelet-derived growth factor receptor α expression in alveolar fibroblasts during realveolarization. *Am. J. Respir. Cell Mol. Biol.* *47*, 517–527.

Dane, D.M., Yilmaz, C., Estrera, A.S., and Hsia, C.C. (2013). Separating in vivo mechanical stimuli for postpneumectomy compensation: physiological assessment. *J. Appl. Physiol.* *114*, 99–106.

Davies, L., Rosas, M., Jenkins, S., Liao, C.-T., Scurr, M., Brombacher, F., Fraser, D., Allen, J., Jones, S., Taylor, P., et al. (2013). Distinct bone marrow-derived and tissue-resident macrophage lineages proliferate at key stages during inflammation. *Nature Communications*.

De'Broski, RH, Hölscher, C, Mohrs, M, and Arendse, B (2004). Alternative macrophage activation is essential for survival during schistosomiasis and downmodulates T helper 1 responses and immunopathology. *Immunity*.

Desai, T.J., Brownfield, D.G., and Krasnow, M.A. (2014). Alveolar progenitor and stem cells in lung development, renewal and cancer. *Nature* *507*, 190–194.

Ding, B.-S.S., Nolan, D.J., Guo, P., Babazadeh, A.O., Cao, Z., Rosenwaks, Z., Crystal, R.G.,

Simons, M., Sato, T.N., Worgall, S., et al. (2011). Endothelial-derived angiocrine signals induce and sustain regenerative lung alveolarization. *Cell* *147*, 539–553.

Dutta, P., Sager, H.B., Stengel, K.R., Naxerova, K., Courties, G., Saez, B., Silberstein, L., Heidt, T., Sebas, M., Sun, Y., et al. (2015). Myocardial Infarction Activates CCR2(+) Hematopoietic Stem and Progenitor Cells. *Cell Stem Cell* *16*, 477–487.

Van Dyken, S.J., and Locksley, R.M. (2013). Interleukin-4- and interleukin-13-mediated alternatively activated macrophages: roles in homeostasis and disease. *Annu. Rev. Immunol.* *31*, 317–343.

Egawa, M., Mukai, K., Yoshikawa, S., Iki, M., Mukaida, N., Kawano, Y., Minegishi, Y., and Karasuyama, H. (2013). Inflammatory monocytes recruited to allergic skin acquire an anti-inflammatory M2 phenotype via basophil-derived interleukin-4. *Immunity* *38*, 570–580.

Epelman, S., Lavine, K.J., Beaudin, A.E., Sojka, D.K., Carrero, J.A., Calderon, B., Brija, T., Gautier, E.L., Ivanov, S., Satpathy, A.T., et al. (2014). Embryonic and adult-derived resident cardiac macrophages are maintained through distinct mechanisms at steady state and during inflammation. *Immunity* *40*, 91–104.

Fehrenbach, Voswinckel, Michl, Mehling, Fehrenbach, Seeger, and Nyengaard (2008). Neoalveolarisation contributes to compensatory lung growth following pneumonectomy in mice. *Eur Respir J* *31*, 515–522.

Geissmann, F., Jung, S., and Littman, D. (2003). Blood Monocytes Consist of Two Principal Subsets with Distinct Migratory Properties. *Immunity* *19*, 71–82.

Gibbons, M.A., MacKinnon, A.C., Ramachandran, P., Dhaliwal, K., Duffin, R., Phythian-Adams, A.T., van Rooijen, N., Haslett, C., Howie, S.E., Simpson, A.J., et al. (2011). Ly6Chi monocytes direct alternatively activated profibrotic macrophage regulation of lung fibrosis. *Am. J. Respir. Crit. Care Med.* *184*, 569–581.

Godwin, J.W., Pinto, A.R., and Rosenthal, N.A. (2013). Macrophages are required for adult salamander limb regeneration. *Proc. Natl. Acad. Sci. U.S.A.* *110*, 9415–9420.

Gordon, S., and Martinez, F. (2010). Alternative Activation of Macrophages: Mechanism and Functions. *Immunity* 32, 593–604.

Gordon, S., and Taylor, P. (2005). Monocyte and macrophage heterogeneity. *Nat Rev Immunol* 5, 953–964.

Guilliams, M., De Kleer, I., Henri, S., Post, S., Vanhoutte, L., De Prijck, S., Deswarte, K., Malissen, B., Hammad, H., and Lambrecht, B.N. (2013). Alveolar macrophages develop from fetal monocytes that differentiate into long-lived cells in the first week of life via GM-CSF. *J. Exp. Med.* 210, 1977–1992.

Hashimoto, D., Chow, A., Noizat, C., Teo, P., Beasley, M.B., Leboeuf, M., Becker, C.D., See, P., Price, J., Lucas, D., et al. (2013). Tissue-resident macrophages self-maintain locally throughout adult life with minimal contribution from circulating monocytes. *Immunity* 38, 792–804.

Herold, S., Steinmueller, M., von Wulffen, W., Cakarova, L., Pinto, R., Pleschka, S., Mack, M., Kuziel, W.A., Corazza, N., Brunner, T., et al. (2008). Lung epithelial apoptosis in influenza virus pneumonia: the role of macrophage-expressed TNF-related apoptosis-inducing ligand. *J. Exp. Med.* 205, 3065–3077.

Herold, S., Mayer, K., and Lohmeyer, J. (2011). Acute lung injury: how macrophages orchestrate resolution of inflammation and tissue repair. *Front Immunol* 2, 65.

Hoeffel, G., and Ginhoux, F. (2015). Ontogeny of Tissue-Resident Macrophages. *Front Immunol* 6, 486.

Hoeffel, G., Chen, J., Lavin, Y., Low, D., Almeida, F.F., See, P., Beaudin, A.E., Lum, J., Low, I., Forsberg, E.C., et al. (2015). C-Myb(+) erythro-myeloid progenitor-derived fetal monocytes give rise to adult tissue-resident macrophages. *Immunity* 42, 665–678.

Hoffman, A.M., Shifren, A., Mazan, M.R., Gruntman, A.M., Lascola, K.M., Nolen-Walston, R.D., Kim, C.F., Tsai, L., Pierce, R.A., Mecham, R.P., et al. (2010). Matrix modulation of compensatory lung regrowth and progenitor cell proliferation in mice. *Am. J. Physiol. Lung Cell*

Mol. Physiol. 298, L158–68.

Hogan, B.L., Barkauskas, C.E., Chapman, H.A., Epstein, J.A., Jain, R., Hsia, C.C., Niklason, L., Calle, E., Le, A., Randell, S.H., et al. (2014). Repair and regeneration of the respiratory system: complexity, plasticity, and mechanisms of lung stem cell function. *Cell Stem Cell* 15, 123–138.

Jain, R., Barkauskas, C.E., Takeda, N., Bowie, E.J., Aghajanian, H., Wang, Q., Padmanabhan, A., Manderfield, L.J., Gupta, M., Li, D., et al. (2015). Plasticity of Hopx(+) type I alveolar cells to regenerate type II cells in the lung. *Nat Commun* 6, 6727.

Jakubzick, C., Gautier, E.L., Gibbings, S.L., Sojka, D.K., Schlitzer, A., Johnson, T.E., Ivanov, S., Duan, Q., Bala, S., Condon, T., et al. (2013). Minimal differentiation of classical monocytes as they survey steady-state tissues and transport antigen to lymph nodes. *Immunity* 39, 599–610.

Jenkins, S.J., Ruckerl, D., Cook, P.C., Jones, L.H., Finkelman, F.D., van Rooijen, N., MacDonald, A.S., and Allen, J.E. (2011). Local macrophage proliferation, rather than recruitment from the blood, is a signature of TH2 inflammation. *Science* 332, 1284–1288.

Jung, S., Aliberti, J., Graemmel, P., Sunshine, M.J., Kreutzberg, G.W., Sher, A., and Littman, D.R. (2000). Analysis of fractalkine receptor CX(3)CR1 function by targeted deletion and green fluorescent protein reporter gene insertion. *Mol. Cell. Biol.* 20, 4106–4114.

Konerding, M.A., Gibney, B.C., Houdek, J.P., Chamoto, K., Ackermann, M., Lee, G.S., Lin, M., Tsuda, A., and Mentzer, S.J. (2012). Spatial dependence of alveolar angiogenesis in post-pneumonectomy lung growth. *Angiogenesis* 15, 23–32.

Kim, D., Pertea, G., Trapnell, C., Pimentel, H., Kelley, R., and Salzberg, S.L. (2013). TopHat2: accurate alignment of transcriptomes in the presence of insertions, deletions and gene fusions. *Genome Biol.* 14, R36.

Kotton, D.N., and Morrisey, E.E. (2014). Lung regeneration: mechanisms, applications and emerging stem cell populations. *Nat. Med.* 20, 822–832.

Knipper, J.A., Willenborg, S., Brinckmann, J., Bloch, W., Maaß, T., Wagener, R., Krieg, T., Sutherland, T., Munitz, A., Rothenberg, M.E., et al. (2015). Interleukin-4 Receptor α Signaling in

Myeloid Cells Controls Collagen Fibril Assembly in Skin Repair. *Immunity* 43, 803–816.

Kuziel, W.A., Morgan, S.J., Dawson, T.C., Griffin, S., Smithies, O., Ley, K., and Maeda, N. (1997). Severe reduction in leukocyte adhesion and monocyte extravasation in mice deficient in CC chemokine receptor 2. *Proc. Natl. Acad. Sci. U.S.A.* 94, 12053–12058.

Lee, Y.G., Jeong, J.J., Nyenhuis, S., Berdyshev, E., Chung, S., Ranjan, R., Karpurapu, M., Deng, J., Qian, F., Kelly, E.A., et al. (2015). Recruited alveolar macrophages, in response to airway epithelial-derived monocyte chemoattractant protein 1/CCl₂, regulate airway inflammation and remodeling in allergic asthma. *Am. J. Respir. Cell Mol. Biol.* 52, 772–784.

Li B & Dewey CN (2011) RSEM: accurate transcript quantification from RNA-Seq data with or without a reference genome. *BMC bioinformatics* 12, 323. Available at: <https://bmcbioinformatics.biomedcentral.com/articles/10.1186/1471-2105-12-323>.

Li, X., Rossen, N., Sinn, P., Hornick, A., Steines, B., Karp, P., Ernst, S., Adam, R., Moninger, T., Levasseur, D., et al. (2013). Integrin $\alpha 6\beta 4$ Identifies Human Distal Lung Epithelial Progenitor Cells with Potential as a Cell-Based Therapy for Cystic Fibrosis Lung Disease. *PLoS ONE*.

Lin, S.-L.L., Li, B., Rao, S., Yeo, E.-J.J., Hudson, T.E., Nowlin, B.T., Pei, H., Chen, L., Zheng, J.J., Carroll, T.J., et al. (2010). Macrophage Wnt7b is critical for kidney repair and regeneration. *Proc. Natl. Acad. Sci. U.S.A.* 107, 4194–4199.

Martinez, FO, and Gordon, S (2014). The M1 and M2 paradigm of macrophage activation: time for reassessment. *F1000Prime Rep*.

Mombaerts, P., Iacomini, J., Johnson, R.S., Herrup, K., Tonegawa, S., and Papaioannou, V.E. (1992). RAG-1-deficient mice have no mature B and T lymphocytes. *Cell* 68, 869–877.

Murray, P.J., Allen, J.E., Biswas, S.K., Fisher, E.A., Gilroy, D.W., Goerdts, S., Gordon, S., Hamilton, J.A., Ivashkiv, L.B., Lawrence, T., et al. (2014). Macrophage activation and polarization: nomenclature and experimental guidelines. *Immunity* 41, 14–20.

Nahrendorf, M., Swirski, F.K., Aikawa, E., Stangenberg, L., Wurdinger, T., Figueiredo, J.-L.L., Libby, P., Weissleder, R., and Pittet, M.J. (2007). The healing myocardium sequentially

mobilizes two monocyte subsets with divergent and complementary functions. *J. Exp. Med.* *204*, 3037–3047.

Nishiyama, K., Nakashima, H., Ikarashi, M., Kinoshita, M., Nakashima, M., Aosasa, S., Seki, S., and Yamamoto, J. (2015). Mouse CD11b+Kupffer Cells Recruited from Bone Marrow Accelerate Liver Regeneration after Partial Hepatectomy. *PLoS ONE* *10*, e0136774.

Noben-Trauth, N., Shultz, L.D., Brombacher, F., Urban, J.F., Gu, H., and Paul, W.E. (1997). An interleukin 4 (IL-4)-independent pathway for CD4+ T cell IL-4 production is revealed in IL-4 receptor-deficient mice. *Proc. Natl. Acad. Sci. U.S.A.* *94*, 10838–10843.

Nolen-Walston, R.D., Kim, C.F., Mazan, M.R., Ingenito, E.P., Gruntman, A.M., Tsai, L., Boston, R., Woolfenden, A.E., Jacks, T., and Hoffman, A.M. (2008). Cellular kinetics and modeling of bronchioalveolar stem cell response during lung regeneration. *Am. J. Physiol. Lung Cell Mol. Physiol.* *294*, L1158–65.

Perdiguer, E., Klapproth, K., Schulz, C., Busch, K., Azzoni, E., Crozet, L., Garner, H., Trouillet, C., de Bruijn, M., Geissmann, F., et al. (2015). Tissue-resident macrophages originate from yolk-sac-derived erythro-myeloid progenitors. *Nature* *518*.

Pull, S.L., Doherty, J.M., Mills, J.C., Gordon, J.I., and Stappenbeck, T.S. (2005). Activated macrophages are an adaptive element of the colonic epithelial progenitor niche necessary for regenerative responses to injury. *Proc. Natl. Acad. Sci. U.S.A.* *102*, 99–104.

Rae, F., Woods, K., Sasmono, T., Campanale, N., Taylor, D., Ovchinnikov, D.A., Grimmond, S.M., Hume, D.A., Ricardo, S.D., and Little, M.H. (2007). Characterisation and trophic functions of murine embryonic macrophages based upon the use of a Csf1r-EGFP transgene reporter. *Dev. Biol.* *308*, 232–246.

Rafii, S., Cao, Z., Lis, R., Siempos, I.I., Chavez, D., Shido, K., Rabbany, S.Y., and Ding, B.-S.S. (2015). Platelet-derived SDF-1 primes the pulmonary capillary vascular niche to drive lung alveolar regeneration. *Nat. Cell Biol.* *17*, 123–136.

Ramachandran, P., Pellicoro, A., Vernon, M.A., Boulter, L., Aucott, R.L., Ali, A., Hartland, S.N.,

Snowdon, V.K., Cappon, A., Gordon-Walker, T.T., et al. (2012). Differential Ly-6C expression identifies the recruited macrophage phenotype, which orchestrates the regression of murine liver fibrosis. *Proc. Natl. Acad. Sci. U.S.A.* *109*, E3186–95.

Ravikumar, P., Yilmaz, C., Bellotto, D.J., Dane, D.M., Estrera, A.S., and Hsia, C.C. (2013). Separating in vivo mechanical stimuli for postpneumonectomy compensation: imaging and ultrastructural assessment. *J. Appl. Physiol.* *114*, 961–970.

Reese, T.A., Liang, H.-E.E., Tager, A.M., Luster, A.D., Van Rooijen, N., Voehringer, D., and Locksley, R.M. (2007). Chitin induces accumulation in tissue of innate immune cells associated with allergy. *Nature* *447*, 92–96.

Rock, J.R., and Hogan, B.L. (2011). Epithelial progenitor cells in lung development, maintenance, repair, and disease. *Annu. Rev. Cell Dev. Biol.* *27*, 493–512.

Rock, JR, Barkauskas, CE, and Cronic, MJ (2011a). Multiple stromal populations contribute to pulmonary fibrosis without evidence for epithelial to mesenchymal transition. *Proceedings of the ...*

Rock, J.R., Barkauskas, C.E., Cronic, M.J., Xue, Y., Harris, J.R., Liang, J., Noble, P.W., and Hogan, B.L. (2011b). Multiple stromal populations contribute to pulmonary fibrosis without evidence for epithelial to mesenchymal transition. *Proc. Natl. Acad. Sci. U.S.A.* *108*, E1475–83.

Ruffell, D., Mourkioti, F., Gambardella, A., Kirstetter, P., Lopez, R., Rosenthal, N., and Nerlov, C. (2009). A CREB-C/EBP β cascade induces M2 macrophage-specific gene expression and promotes muscle injury repair. *Proceedings of the National Academy of Sciences* *106*, 17475–17480.

Saederup, N., Cardona, A.E., Croft, K., Mizutani, M., Coteleur, A.C., Tsou, C.-L.L., Ransohoff, R.M., and Charo, I.F. (2010). Selective chemokine receptor usage by central nervous system myeloid cells in CCR2-red fluorescent protein knock-in mice. *PLoS ONE* *5*, e13693.

Sano, F., Ueda, K., Murakami, J., Hayashi, M., Nishimoto, A., and Hamano, K. (2015). Enhanced tumor growth in the remaining lung after major lung resection. *Journal of Surgical*

Research.

Sasmono, R.T., Oceandy, D., Pollard, J.W., Tong, W., Pavli, P., Wainwright, B.J., Ostrowski, M.C., Himes, S.R., and Hume, D.A. (2003). A macrophage colony-stimulating factor receptor-green fluorescent protein transgene is expressed throughout the mononuclear phagocyte system of the mouse. *Blood* 101, 1155–1163.

Sasmono, R.T., Ehrnsperger, A., Cronau, S.L., Ravasi, T., Kandane, R., Hickey, M.J., Cook, A.D., Himes, S.R., Hamilton, J.A., and Hume, D.A. (2007). Mouse neutrophilic granulocytes express mRNA encoding the macrophage colony-stimulating factor receptor (CSF-1R) as well as many other macrophage-specific transcripts and can transdifferentiate into macrophages in vitro in response to CSF-1. *J. Leukoc. Biol.* 82, 111–123.

Schulz, C., Gomez Perdiguero, E., Chorro, L., Szabo-Rogers, H., Cagnard, N., Kierdorf, K., Prinz, M., Wu, B., Jacobsen, S.E., Pollard, J.W., et al. (2012). A lineage of myeloid cells independent of Myb and hematopoietic stem cells. *Science* 336, 86–90.

Shechter, R., Miller, O., Yovel, G., Rosenzweig, N., London, A., Ruckh, J., Kim, K.-W.W., Klein, E., Kalchenko, V., Bendel, P., et al. (2013). Recruitment of beneficial M2 macrophages to injured spinal cord is orchestrated by remote brain choroid plexus. *Immunity* 38, 555–569.

Shiraishi, M., Shintani, Y., Shintani, Y., Ishida, H., Saba, R., Yamaguchi, A., Adachi, H., Yashiro, K., and Suzuki, K. (2016). Alternatively activated macrophages determine repair of the infarcted adult murine heart. *J. Clin. Invest.*

Stein, M., Keshav, S., Harris, N., and Gordon, S. (1992). Interleukin 4 potently enhances murine macrophage mannose receptor activity: a marker of alternative immunologic macrophage activation. *J. Exp. Med.* 176, 287–292.

Suzuki, T., Arumugam, P., Sakagami, T., Lachmann, N., Chalk, C., Sallese, A., Abe, S., Trapnell, C., Carey, B., Moritz, T., et al. (2014). Pulmonary macrophage transplantation therapy. *Nature* 514, 450–454.

Tan, S.Y., and Krasnow, M.A. (2016). Developmental origin of lung macrophage diversity.

Development.

Trapnell, C., Roberts, A., Goff, L., Pertea, G., Kim, D., Kelley, D.R., Pimentel, H., Salzberg, S.L., Rinn, J.L., and Pachter, L. (2012). Differential gene and transcript expression analysis of RNA-seq experiments with TopHat and Cufflinks. *Nat Protoc* 7, 562–578.

Treutlein, B., Brownfield, D.G., Wu, A.R., Neff, N.F., Mantalas, G.L., Espinoza, F.H., Desai, T.J., Krasnow, M.A., and Quake, S.R. (2014). Reconstructing lineage hierarchies of the distal lung epithelium using single-cell RNA-seq. *Nature* 509, 371–375.

Voswinckel, M., Motejl, M., Fehrenbach, B., Wegmann, M., Mehling, A., Fehrenbach, B., and Seeger, T. (2004). Characterisation of post-pneumonectomy lung growth in adult mice. *Eur Respir J* 24, 524–532.

Westphalen, K., Gusarova, G.A., Islam, M.N., Subramanian, M., Cohen, T.S., Prince, A.S., and Bhattacharya, J. (2014). Sessile alveolar macrophages communicate with alveolar epithelium to modulate immunity. *Nature* 506, 503–506.

Willenborg, S., Lucas, T., van Loo, G., Knipper, J.A., Krieg, T., Haase, I., Brachvogel, B., Hammerschmidt, M., Nagy, A., Ferrara, N., et al. (2012). CCR2 recruits an inflammatory macrophage subpopulation critical for angiogenesis in tissue repair. *Blood* 120, 613–625.

Yona, S., Kim, K.-W.W., Wolf, Y., Mildner, A., Varol, D., Breker, M., Strauss-Ayali, D., Viukov, S., Guilliams, M., Misharin, A., et al. (2013). Fate mapping reveals origins and dynamics of monocytes and tissue macrophages under homeostasis. *Immunity* 38, 79–91.

Figure 1. Increased numbers of myeloid cells in the lungs of mice after PNX. (A) Immunofluorescent staining of sections of mouse lungs after PNX shows increased number of CSF1R-GFP+ cells (green, myeloid lineages) compared to unoperated animals. Scale bar = 100 um. **(B)** Flow cytometry of dissociated lungs shows increased numbers of CSF1R-GFP+, F4/80+ macrophages 7d post-PNX compared to sham operated animals. n=3 animals per group, data are represented as mean +/- SD. **(C)** Flow cytometry of dissociated lungs shows increased numbers of CD45+, F4/80+ CD11b interstitial macrophages and monocytes 7d post-PNX compared to sham operated animals. **(D)** Flow cytometry of dissociated lungs shows increased numbers of CD45+, F4/80+ CD11c alveolar macrophages and monocytes 7d post-PNX compared to sham operated animals. **(E,F)** Quantification of data in C and D, respectively. n≥3 animals for each group. Data are represented as mean +/- SD. **(G)** Hierarchical clustering of 68 CD45+, CSF1R-GFP+, F4/80+, Ly6G- macrophages isolated from mouse lungs 7d post-PNX. At least 6 cell groups (x-axis) were defined by expression of 4 gene groups (y-axis). **(H)** Subpopulations of lung macrophages post-PNX included those which expressed high levels of monocyte markers (orange bar) and those which expressed high levels of M2-like macrophage markers (red bar). See also Figure S1.

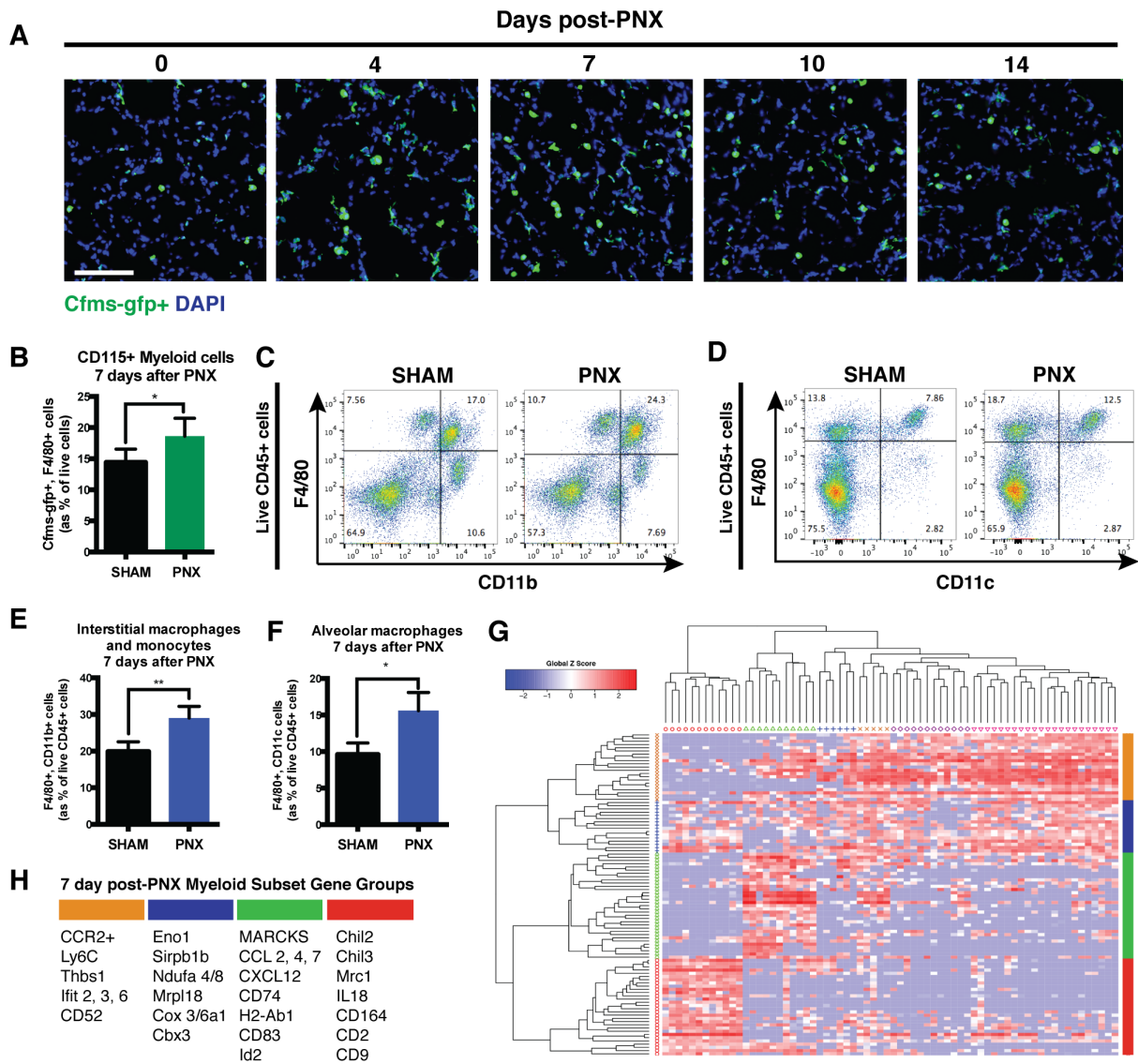


Figure 2. CCR2+ monocytes are recruited to the lung post-PNX. (A) A cytokine protein array shows that the chemokine CCL2 is upregulated in mouse lungs 7d post-PNX compared to sham operated animals. (B) Immunofluorescence on tissue sections from *Ccr2*^{RFP/+} transgenic reporter mice shows increased numbers of CCR2+ monocytes 7d post-PNX compared to sham operated mice. Scale bar = 100 um. (C) Flow cytometry of dissociated lungs from *Ccr2*^{RFP/+} mice shows increased numbers of CD45+, CD11b+, CCR2+ cells 7d post-PNX compared to unoperated littermate controls. (D) Quantification of flow cytometry data shows that both PNx and sham operation cause increased numbers of CCR2+ monocytes compared to unoperated littermate controls. Data are represented as mean +/- SD. (E) Immunofluorescence on lungs from *Ccr2*^{RFP/RFP} mice show decreased recruitment of RFP+ monocytes 7d post-PNX compared to heterozygous mice (see B above). Scale bar = 100 um. (F) Flow cytometry of dissociated lungs from *Ccr2*^{-/-} mice shows decreased numbers of CD45+, F4/80+, CD11b+ interstitial monocytes and macrophages 7d post-PNX compared to wild type littermate controls. n≥3 animals for each group. Data are represented as mean +/- SD. (G) Flow cytometry of dissociated lungs from *Ccr2*^{-/-} mice shows that the number of CD45+, F4/80+, CD11c+ alveolar macrophages 7d post-PNX is not different compared to wild type littermate controls. n≥3 animals for each group. Data are represented as mean +/- SD. See also Figure S2.

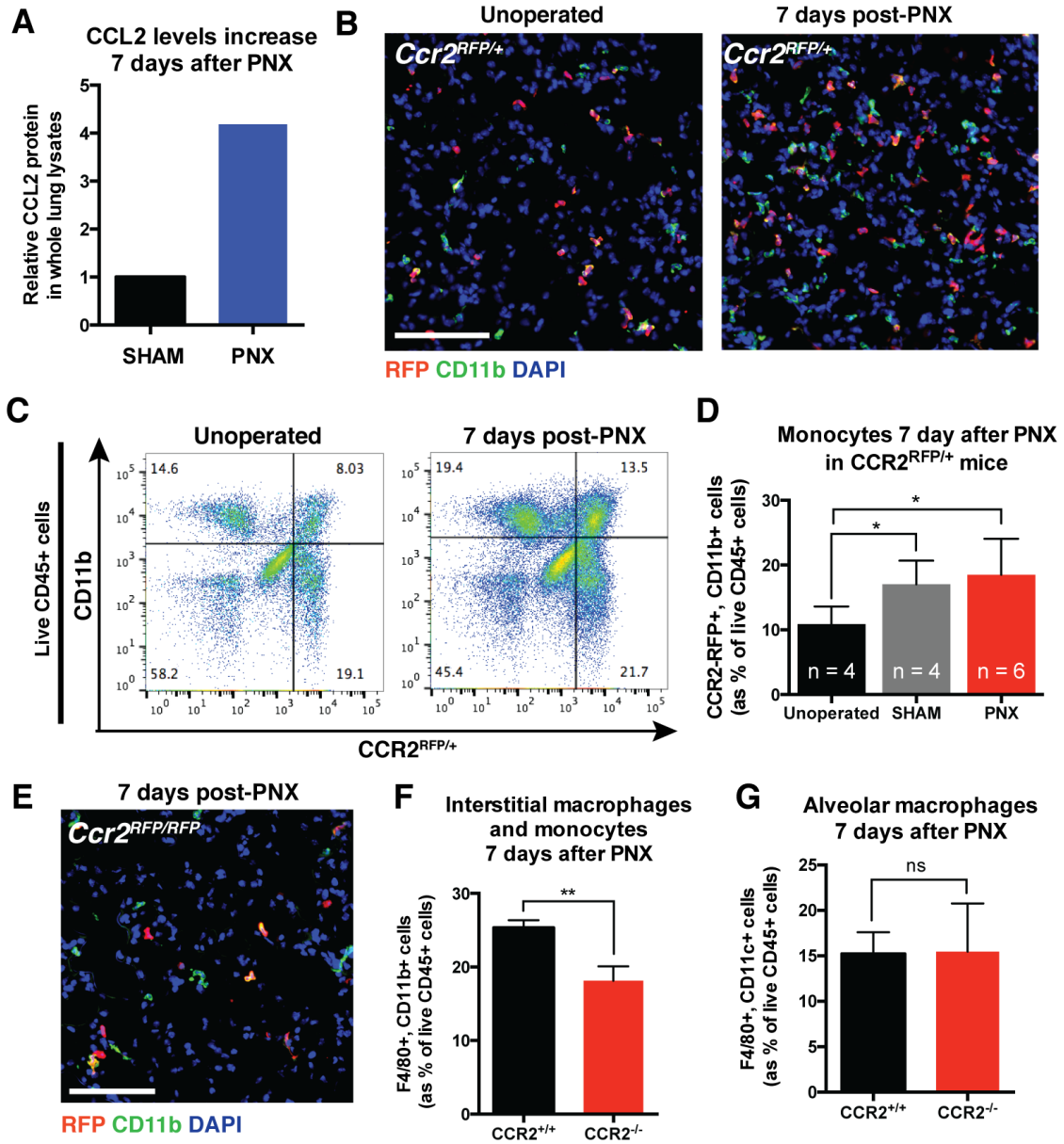


Figure 3. CCR2+ monocytes are required for lung regeneration post-PNX. (A) Whole mount images of right accessory lobes from mice 21d post-PNX show impaired regeneration in *Ccr2*^{-/-} mice compared to wild type littermate controls. Scale bar = 5000 um. (B) *Ccr2*^{-/-} mice show impaired lung regeneration assessed by dry weight of the remaining right lobes 14d post-PNX compared to wild type littermates. n≥3 mice per group. Data are represented as mean +/- SD. (C, D) Flow cytometry of dissociated lungs shows decreased incorporation of EdU in SPC+ AEC2 7d post-PNX in *Ccr2*^{-/-} mice compared to wild type littermate controls. EdU given 24 hours prior to sacrifice by intraperitoneal injection. n≥3 mice per group. Data are represented as mean +/- SD. (E,F) Immunofluorescence on sections of lungs from heterozygous *Sftpc-CreER;Rosa-dtomato* mice 21d post-PNX shows impaired differentiation of lineage labeled AEC2 (red) into AEC1 (RAGE, green) in *Ccr2*^{-/-} mice compared to wild type littermate controls. Mice were labeled with three tamoxifen doses and operated on 14 days after the last injection. Scale bar = 100 um. n≥3 mice per group. Data are represented as mean +/- SD. See also Figure S3.

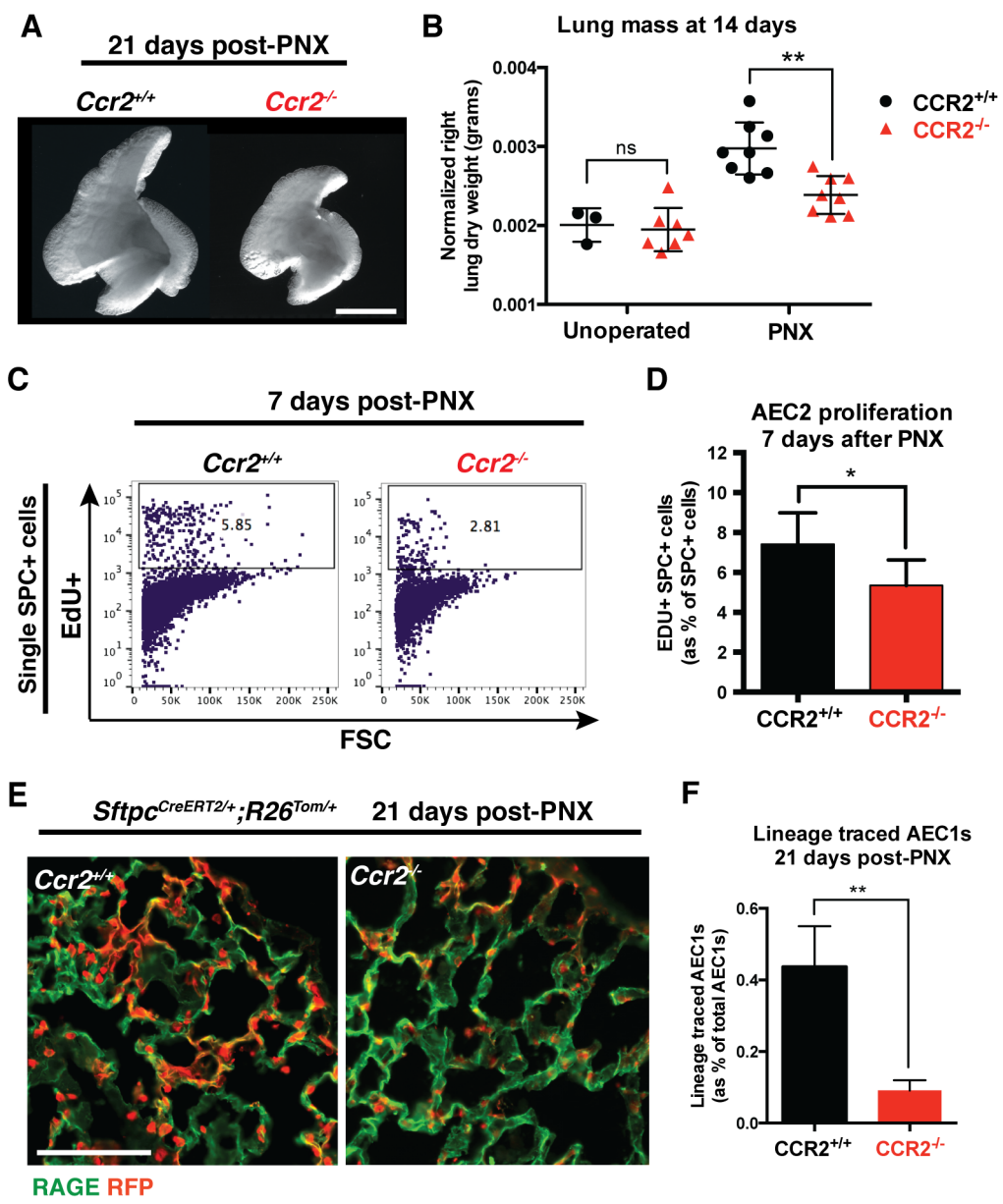


Figure 4. Macrophages are sufficient to support alveolar stem cells. (A) *Ccr2*^{-/-} mice were pneumonectomized and given whole bone marrow harvested from *Ccr2*^{+/+} or *Ccr2*^{-/-} mice 4 and 7 s later by intravenous (I.V.) lateral tail vein injection. Recipient mice were analyzed 14d post-PNX by lung dry weights. (B) Right lobe dry weights show that injection of cells from wild type bone marrow, but not bone marrow from *Ccr2*^{-/-} mice, rescues the lung regeneration defect in CCR2-deficient mice. n≥3 mice per group. Data are represented as mean +/- SD. * = p ≤ 0.05; ** = p ≤ 0.01; *** = p ≤ 0.001 (C) Heat map and selected genes from RNA sequencing of at least 200,000 pooled CD45+, F4/80+ macrophages isolated by FACS from wild type mice 7d post-PNX or sham operation. (D) Lineage labeled AEC2 were isolated by FACS from heterozygous *Sftpc-CreER;Rosa-dtomato* mice and cultured for 14 days in 3-dimensions in varying ratios with primary CD45+, CSF1R-GFP+, F4/80+ macrophages from wild type mice; all wells contained 10,000 AEC2s, and either no macrophages (A), 5,000 macrophages (B), 10,000 macrophages (C), or 20,000 macrophages (D). (E,F) Macrophages have a dose-dependent effect on the colony formation of lineage labeled AEC2 in co-culture. N≥5 co-cultures for each ratio. Data are represented as mean +/- SD. (G) Representative image of immunofluorescence on a histological section of a co-culture from condition D shows an F4/80+ macrophage in close association with a pneumosphere. Scale bar = 100 um. See also Figure S4.

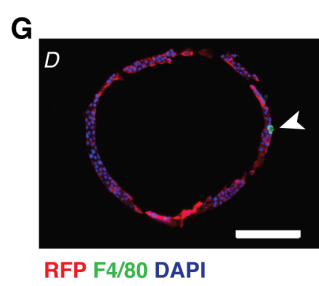
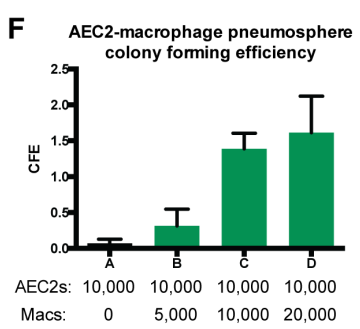
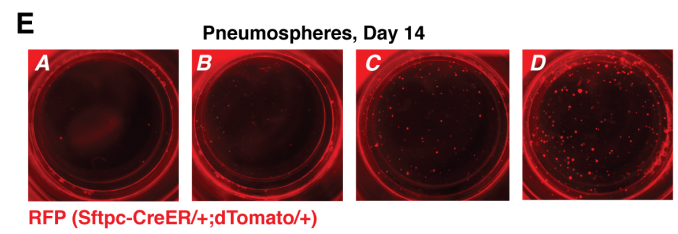
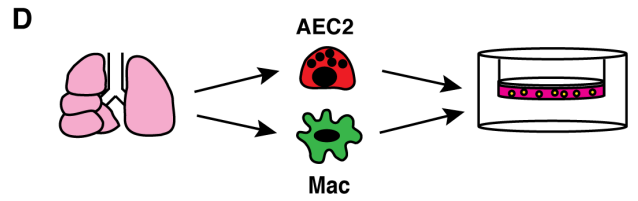
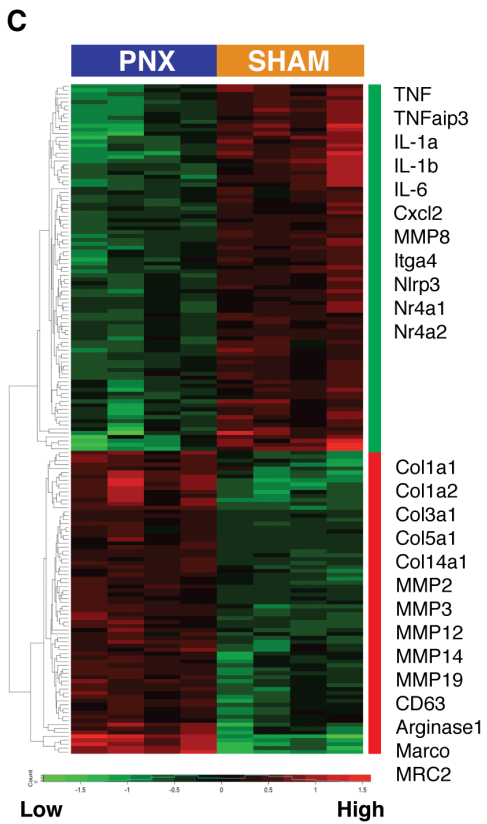
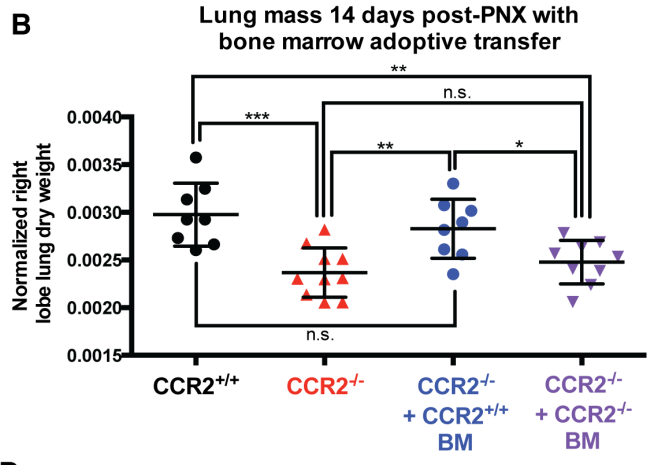
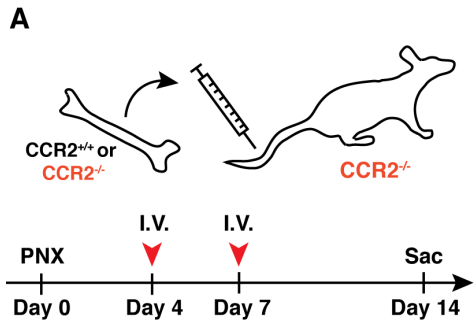


Figure 5. M2-like macrophages are required for lung regeneration. (A) Immunofluorescent stains on sections from lungs of Arginase-YFP (YARG) mice show increased numbers of YARG+, F4/80+ M2-like macrophages (arrowheads) 4 and 7d post-PNX compared to sham operation. Scale bar = 100 μ m. (B,C) Flow cytometry on dissociated lungs from YARG mice shows increased numbers of YARG+, F4/80+ M2-like macrophages 4 and 7d post-PNX compared to sham operated mice. (D-F) Immunofluorescence and flow cytometry on lungs from *I14ra*^{-/-} mice show rare YARG+; F4/80+ M2-like macrophages (arrowhead) 4d post-PNX compared to wild type YARG littermate controls (see A above). $n \geq 3$ mice for each group. Data are represented as mean \pm SD. (G) *I14ra*^{-/-} mice show impaired lung regeneration assessed by dry weight of the right accessory lobe 14d post-PNX. $n \geq 3$ mice for each group. Data are represented as mean \pm SD. ** = $p \leq 0.01$. (H) Immunofluorescence on sections of lungs from *Ccr2*^{RFP/+};YARG mice show YARG+ M2-like macrophages that are both CCR2-RFP+ (arrows) and CCR2-RFP- (arrowheads). Scale bar = 100 μ m. (I) Quantification of flow cytometry on dissociated lungs *Ccr2*^{RFP/RFP};YARG mice show decreased numbers of Yarg+, F4/80+ M2-like macrophages 4d post-PNX compared to wild type YARG controls. $n \geq 3$ mice for each group. (J) CD45.1 wild type mice were lethally irradiated and given bone marrow from either wild type or *I14ra*^{-/-} (CD45.2) mice by intravenous lateral tail vein injection to generate chimeric animals. 10 weeks were allowed for hematopoietic reconstitution and chimeras were analyzed by lung dry weights. (K) *I14ra*^{-/-} bone marrow chimeric mice show impaired lung regeneration assessed by dry weight of the right accessory lobe 14d post-PNX compared to wild type littermate controls. $n \geq 3$ mice for each group. Data are represented as mean \pm SD. * = $p \leq 0.05$. See also Figure S5.

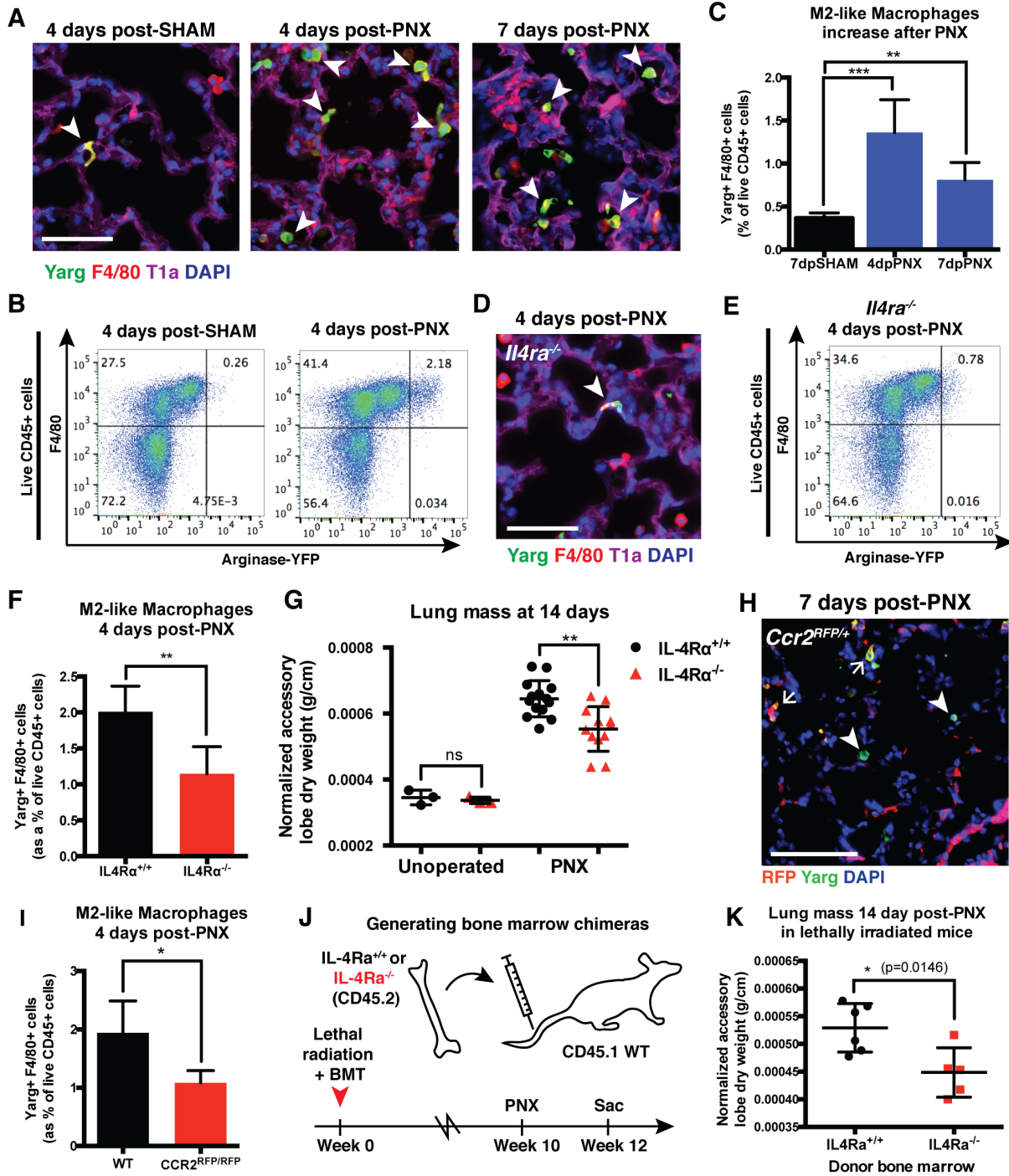


Figure 6. ILC2s accumulate and produce IL-13 post-PNX. (A) Immunofluorescent stains on sections from lungs of $IL5^{RFP/+}$ (Red5) mice show $IL5^+$ ILC2s at both small branching airways and in the alveolar spaces post-PNX Scale bar = 100 μ m. (B, C) Flow cytometry of dissociated lungs from $IL5^{RFP/+}$ mice shows increased numbers of $CD45^+Lin^-Thy1^+IL5^+$ ILC2s at 7d post-PNX compared to sham operated animals. (D,E) Flow cytometry of dissociated lungs from *Smart13* mice shows increased numbers of IL-13 producing ILC2s at 4d post-PNX compared to sham operated animals. $n \geq 3$ animals for each group. Data are represented as mean \pm SD. (F) Proposed schematic demonstrating the roles of CCR2⁺ monocytes, M2-like macrophages, and ILC2s in PNx-induced lung regeneration. See also Figure S6.

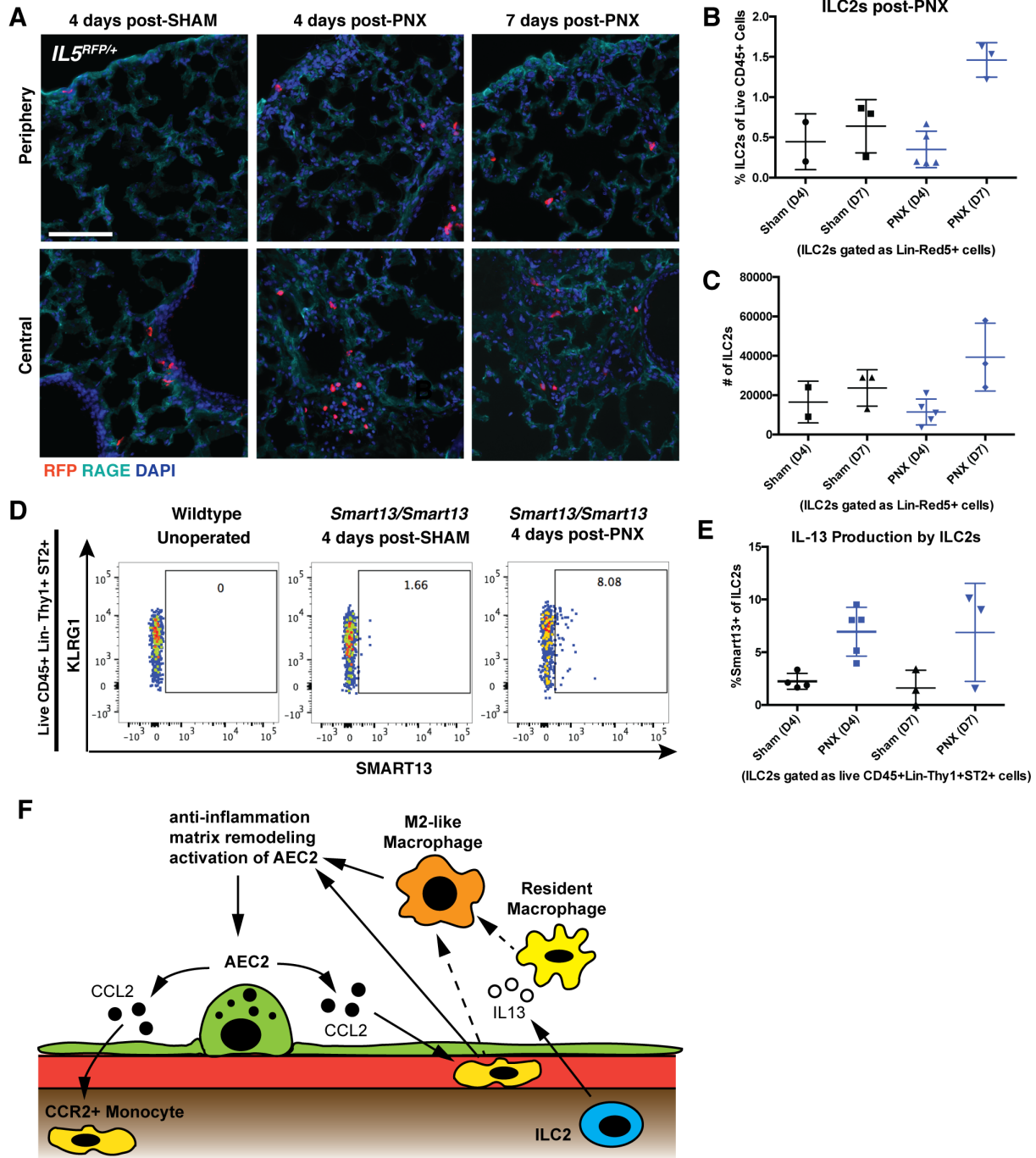


Figure S1. Related to Figure 1. CD115+ macrophages are the dominant myeloid population in regenerating lung tissue post-PNX. (A) Immunofluorescent stains of 7d post-PNX lungs from SPC-CreER;ROSA-Tomato;CSF1R-GFP mice show increased numbers of CD115+ (green) macrophages throughout the lung tissue, including at the tissue edge, compared to unoperated littermate controls. (B) A high magnification image of 7d post-PNX lungs from SPC-CreER;ROSA-Tomato;CSF1R-GFP mice shows many CD115+ (green) macrophages-AEC2s (red) interactions (arrowheads). (C) Immunofluorescence shows increased number of Ly6G+ (red) neutrophils in the lungs of mice 4d post-PNX, but not at 7d post-PNX, compared to unoperated littermate controls (D, E) Flow cytometry of dissociated cells from lungs of wild type mice shows that the number of CD45+, Ly6G+,CD11b+ neutrophils is not different 7d post-PNX compared to sham operated littermate controls. $n \geq 3$ mice for each group. Data are represented as mean \pm SD. (F) Average expression of selected genes from single cell RNA sequencing of CD45+, CSF1R-GFP+, F4/80+, Ly6G- macrophages sorted from lungs 7d post-PNX and sham.

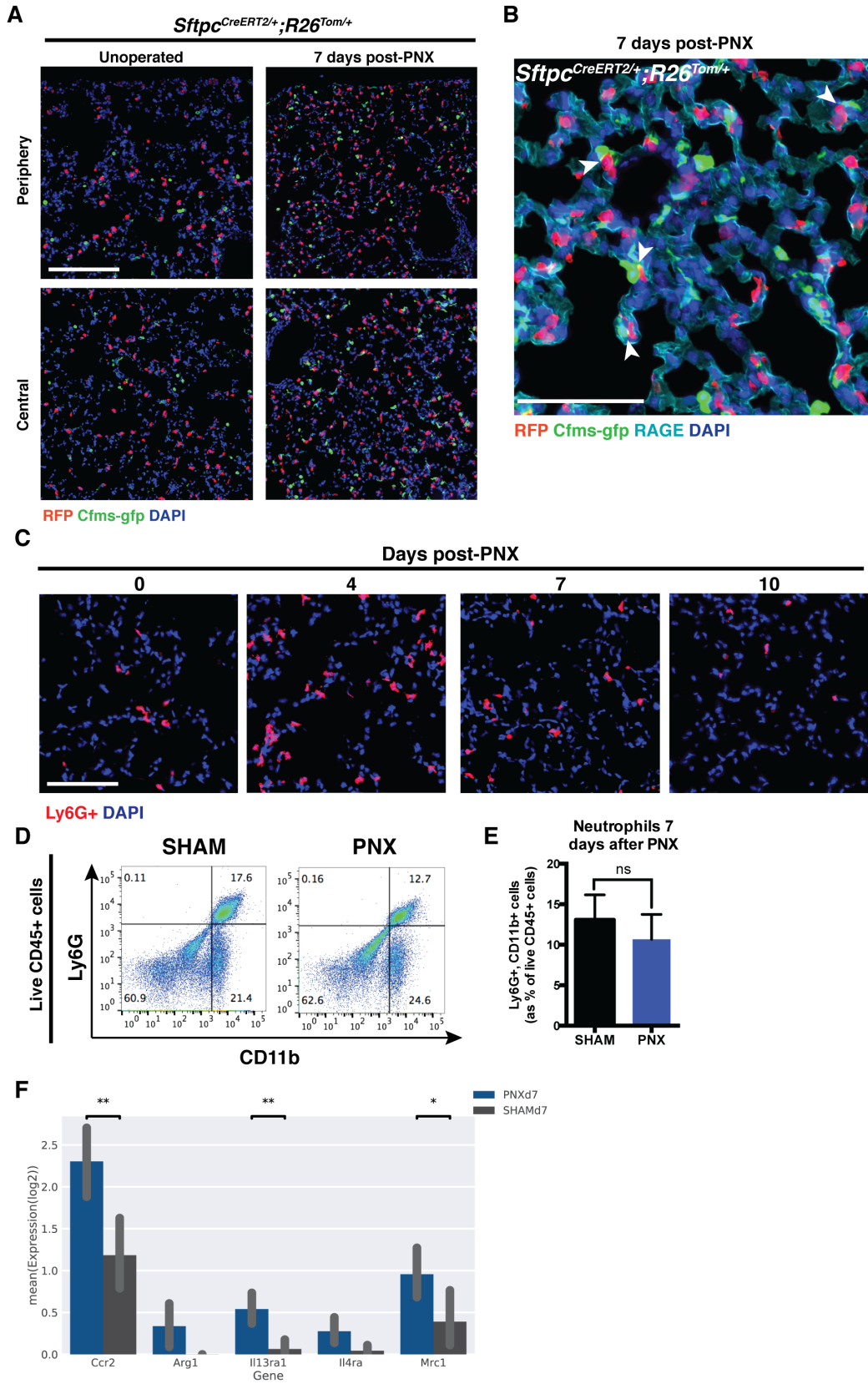


Figure S2. Related to Figure 2. CCR2⁺ monocytes are recruited and local macrophages proliferate post-PNX. (A) Raw blot images of cytokine array from whole lung lysates at 7d post-PNX compared to sham operated mice. (B) Quantification of cytokines by densitometry. (C) Immunofluorescence of CCR2-RFP mice shows CCR2⁺ cells accumulate around large vessels (arrowhead) and at the tissue edge (arrow). Scale bar = 200 μ m. (D) Immunofluorescent stains of 7d post-PNX lungs from heterozygous *Sftpc-CreER;Rosa-fGFP;Ccr2^{RFP/+}* mice show increased numbers of CCR2⁺ monocytes as well as increased CCR2⁺ (red) monocyte-AEC2s (green) interactions (arrowheads) compared to sham operated littermate controls. Scale bar = 100 μ m. (E) Representative images of sections from Cx3Cr1 reporter mice show that this population of macrophages does not increase post-PNX compared to unoperated mice. Scale bar = 200 μ m. (F,G) EdU was given to *Csf1r-GFP* mice by intraperitoneal injection 3.5 hours prior to sacrifice. Immunofluorescence analysis suggests that there is a transient increase in the number of proliferating CD115⁺ myeloid cells post-PNX. Of note, these cells have the distribution and morphology of alveolar macrophages rather than interstitial macrophages and monocytes. Scale bar = 100 μ m. $n \geq 3$ mice for each group. Data are represented as mean \pm SD.

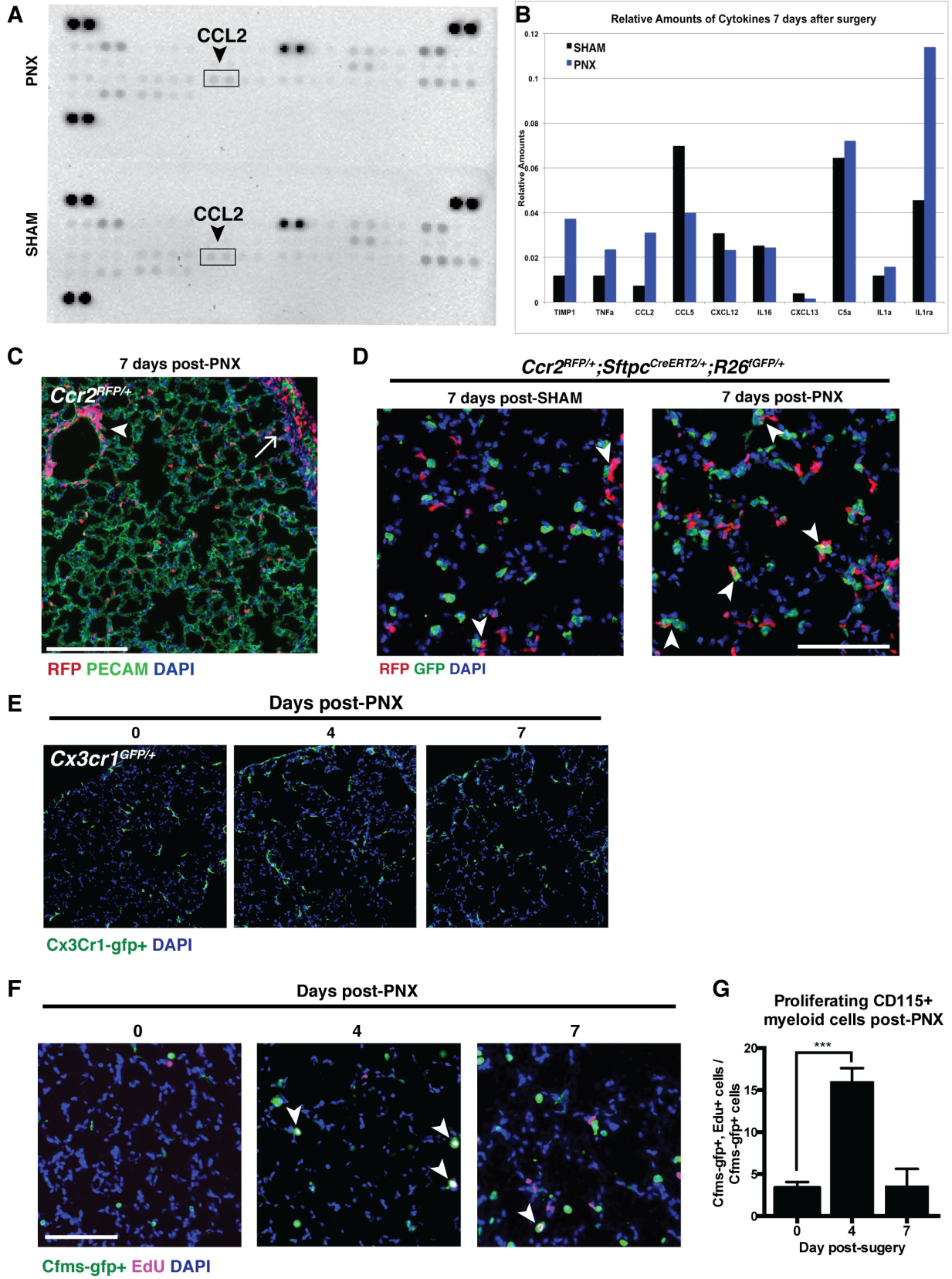


Figure S3. Related to Figure 3. Impaired lung regeneration in CCR2-deficient mice persists long-term. (A) *Ccr2*^{-/-} mice show impaired lung regeneration assessed by dry weight of the remaining accessory lobes 35d post-PNX compared to wild type littermate controls. n≥3 mice for each group. Data are represented as mean +/- SD.

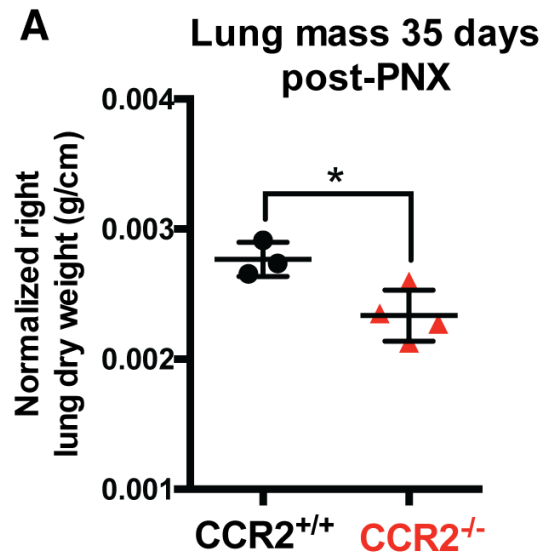


Figure S4. Related to Figure 4. Lung and bone marrow-derived macrophages support lung regeneration *in vivo* and *in vitro*. (A) Flow cytometry of cells isolated from the bone marrow of *Ccr2^{RFP/+}* transgenic reporter mice. Approximately 10% of bone marrow cells are CCR2+, CD11b+ monocytes. n=3 mice. (B,C) Evidence that adoptively transferred whole bone marrow cells populate the lung tissue post-PNX. 10x10⁶ whole bone marrow cells isolated from *Csf1r-GFP+* mice were injected by intravenous lateral tail vein injection into unoperated or 6d post-PNX *Ccr2^{-/-}* mice. 24 hours later, flow cytometry performed on dissociated lungs revealed rare GFP+ cells in lung tissue of both unoperated and PNX mice; however, the percentage of GFP+ cells was increased in the lungs of PNX mice compared to unoperated controls. n≥3 mice for each group. Data are represented as mean +/- SD. (D,E) Evidence that CCR2 plays an active role in recruiting adoptively transferred whole bone marrow cells to lung tissue post-PNX. 10x10⁶ whole bone marrow cells isolated from wild type *Csf1r-GFP+* or *Ccr2^{-/-}; Csf1r-GFP* mice were injected by intravenous lateral tail vein injection into 6d post-PNX *Ccr2^{-/-}* mice. 24 hours later, flow cytometry was performed on dissociated lungs to assess the localization of GFP+ cells. 5 minutes prior to sacrifice, mice were dosed with 2 ug APC-CD45 by retro-orbital injection to specifically label cells in the pulmonary vasculature. All lung cells were stained with APC-Cy7-CD45. The percentage of GFP+ cells within the lung tissue (APC-CD45-, APC-Cy7-CD45+) was almost 2-fold higher in animals given wild type bone compared to *Ccr2^{-/-}* bone marrow. n≥3 mice for each group. Data are represented as mean +/- SD. (F) Evidence that adoptively transferred whole bone marrow cells persist in lungs post-PNX. Immunofluorescent stain of lungs from *Ccr2^{-/-}* mice 14d post-PNX given intravenous lateral tail vein bone marrow injection from wild type *Csf1r-GFP+* mice at 4d and 7d post-PNX shows GFP+ cells in the host lung tissue. Cells were found both in the airways (arrowheads) and within the interstitium (arrows). Scale bar = 100 um. (G,H) Immunofluorescence on sections of lungs from heterozygous *Sftpc-CreER;Rosa-dtomato* mice 21d post-PNX shows increased differentiation of lineage labeled AEC2 (red) into AEC1 (RAGE, green) in *Ccr2^{-/-}* mice given wild type whole bone marrow at 4d

and 7d post-PNX compared to uninjected *Ccr2*^{-/-} controls. Mice were labeled with three tamoxifen doses and operated on 14 days after the last injection. Scale bar = 100 μ m. $n \geq 3$ mice per group. Data are represented as mean \pm SD. **(I)** Flow cytometry of cells isolated from the lungs of heterozygous *Sftpc-CreER;Rosa-dtomato* mice after three doses of tamoxifen given by intraperitoneal injection shows the gating strategy for single viable lineage labeled AEC2 (left). Flow cytometry of cells isolated from the lungs of wild type mice shows the gating strategy for the isolation of CD45⁺, F4/80⁺ macrophages (right). **(J)** Representative image of immunofluorescence on a histological section of a co-culture (condition C) shows expression of dual SPC and RAGE expression on many cells. Scale bar = 100 μ m. **(K)** Immunofluorescent image of transwell from d14 AEC-macrophage co-culture (Condition C) shows persistence of *Csf1r-GFP*⁺ macrophages in culture (arrowheads). Scale bar = 1000 μ m. **(L)** Higher magnification immunofluorescent image of transwell from d14 AEC-macrophage co-culture (Condition C) shows well-formed pneumospheres with lumens. Scale bar = 500 μ m. **(M)** Immunofluorescence image of transwell from 14d macrophage alone co-culture (Condition M) shows survival of macrophages without AEC2s. Scale bar = 1000 μ m. **(N)** Three-dimensional co-culture of CD45⁺, F4/80⁺ splenic macrophages with lineage labeled AEC2s in a 1:1 ratio (10,000 AEC2s, 10,000 macrophages) supported limited growth of pneumospheres. **(O,P)** Wild type bone marrow cells were grown in culture with MCSF-enriched media for 7 days to induce differentiation into macrophages. Three-dimensional co-culture of these cells in a 1:1 ratio with lineage labeled AEC2 (10,000 AEC2s, 10,000 macrophages) supported the growth of pneumospheres.

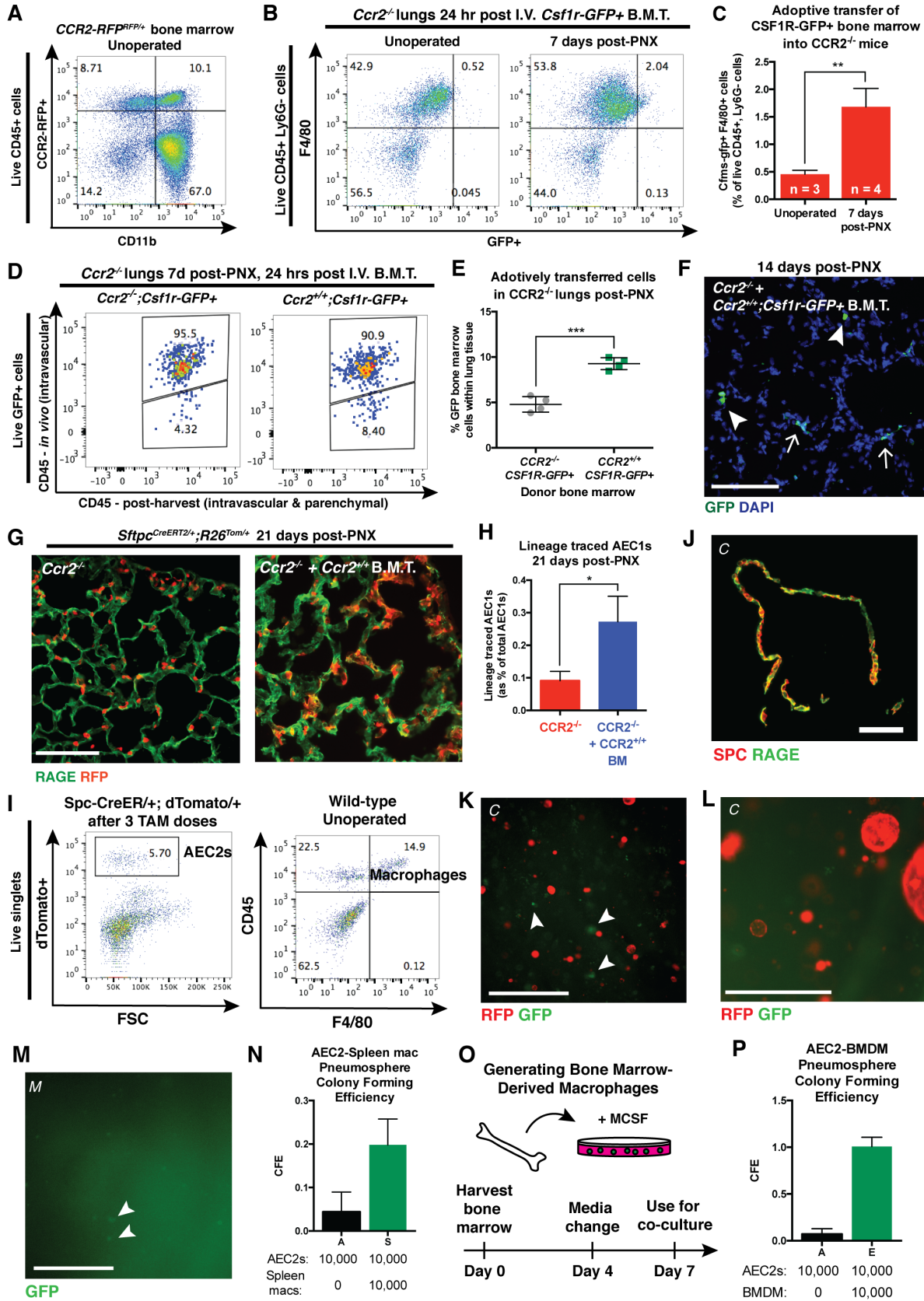


Figure S5. Related to Figure 5. CCR2-deficiency impairs the generation of IL4-dependent M2-like macrophages, which are required for lung regeneration and locally proliferate post-PNX. (A,B) Immunofluorescence on sections of lungs from heterozygous *Sftpc-CreER;Rosa-dtomato* mice 21d post-PNX shows impaired differentiation of lineage labeled AEC2 (RFP, red) into AEC1 (RAGE, green) in *Ii4ra*^{-/-} compared to wild type littermate controls. Mice were labeled with three tamoxifen doses and operated on 14 days after the last injection. Scale bar = 100 um. n≥3 mice per group. Data are represented as mean +/- SD. (C). Immunofluorescent stains of lungs from *Ccr2*^{RFP/RFP} mice reveal some YARG+, F4/80+ M2-like macrophages 7d post-PNX. Scale bar = 100 um. (D) qRT-PCR of RNA isolated from CD45+, F4/80+ lung macrophages from wild type and *Ccr2*^{-/-} mice shows no change in *Arg1* mRNA levels between macrophages from wild type and *Ccr2*^{-/-} mice 7d post-PNX. n=3 all groups. Data run in triplicate and represented as mean +/- SD. (E) Quantification of flow cytometry data shows decreased absolute numbers of YARG+, F4/80+ M2-like macrophages 4d post-PNX in *Ccr2*^{RFP/RFP} mice compared to wild type controls. n≥3 mice for each group. Data are represented as mean +/- SD. (F) EdU was given to wild type YARG mice by intraperitoneal injection 3.5 hours prior to sacrifice. Immunofluorescent stains of lungs show M2-like macrophages that are both locally proliferating (F4/80+, YARG+, EDU+, arrowhead) and not proliferating (F4/80+, YARG+, EDU-, arrow). Scale bar = 100 um. (G,H) Flow cytometry to determine host vs. donor origin of lung macrophage populations from excised left lung after PNx in irradiated mice 10 weeks after reconstitution with whole bone marrow from wild type or *Ii4ra*^{-/-} mice. Quantification shows interstitial macrophages/monocytes (F4/80+, CD11b+) were ~99% donor-derived while alveolar macrophages (CD11b-, F4/80+, CD11c+) were ~96.5% donor-derived. n≥3 mice for each group. Data are represented as mean +/- SD.

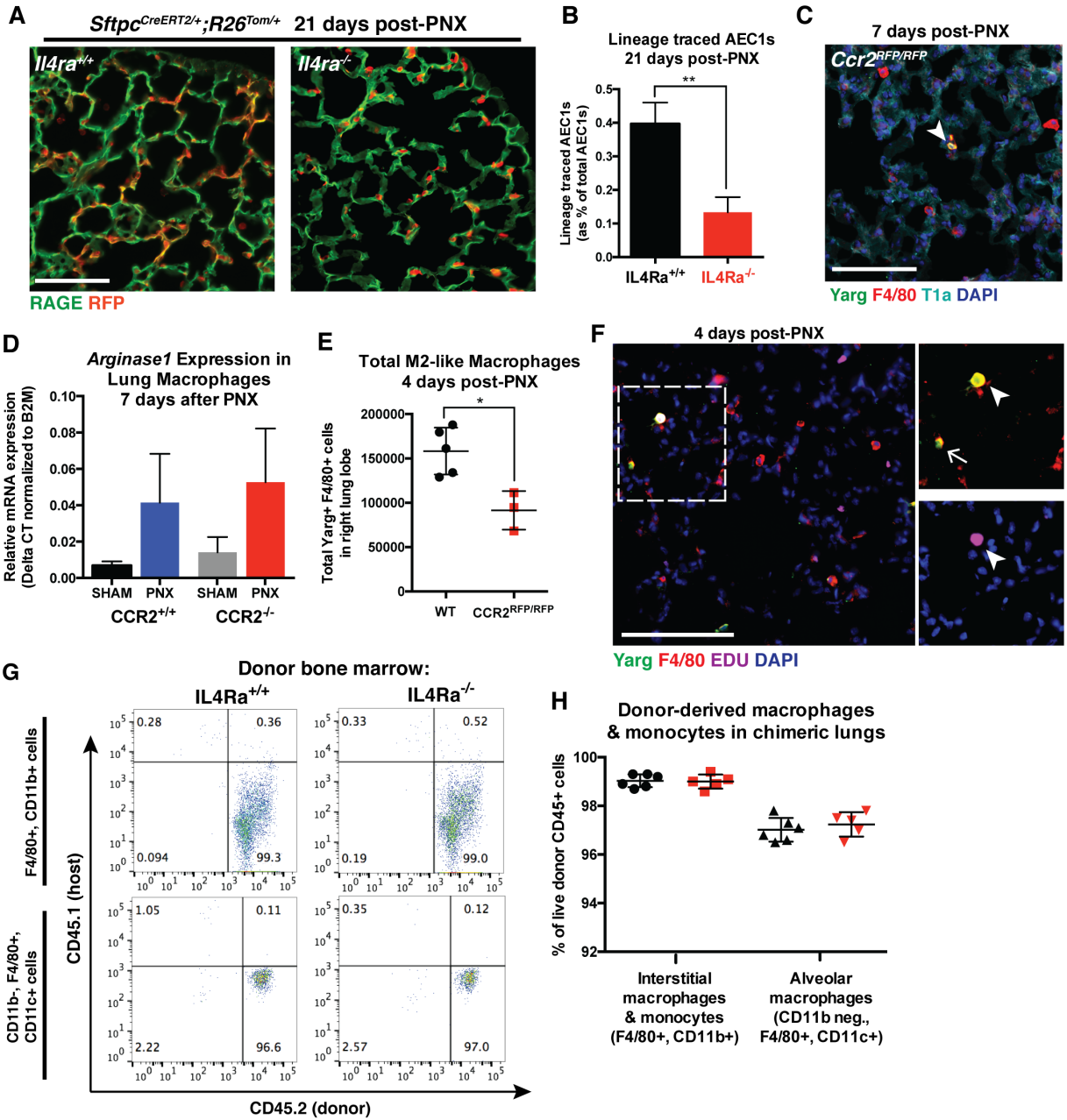
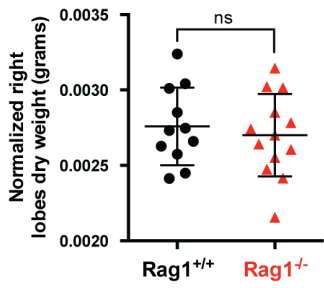
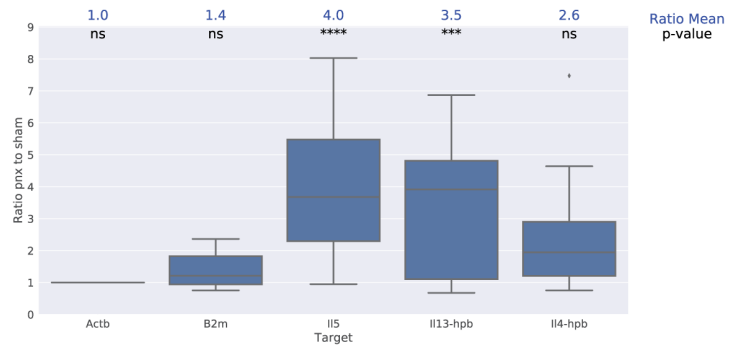


Figure S6: Related to Figure 6. ILC2s accumulate and produce IL-13 post-PNX. (A) *Rag1*^{-/-} mice do not show impaired lung regeneration assessed by dry weight of the remaining accessory lobes 14d post-PNX. n≥3 mice for each group. Data are represented as mean +/- SD. (B) qRT-PCR of RNA isolated from CD45+, Lin-, Thy1+, ST2+, IL5+ ILC2s in *IL5*^{RFP/+} mice shows significant fold change in gene expression of IL5 and IL13, but not IL4, 4d post-PNX compared to sham operated controls. n≥3 mice for each group. Data run in triplicate and represented as mean +/- SD. (C) Flow cytometry gating strategy for quantifying CD45+, Lin-, Thy1+, ST2+, IL5+ ILC2s in *IL5*^{RFP/+} mice post-PNX and sham. (D) Quantification of flow cytometry data reveals that IL5+ cells are predominately ILC2s and not CD4+ T cells post-PNX. n≥3 mice for each group. Data are represented as mean +/- SD. (E) Quantification of flow cytometry data reveals increased proliferation of ILC2s at 4d and 7d post-PNX compared to sham operated controls. n≥3 mice for each group. Data are represented as mean +/- SD.

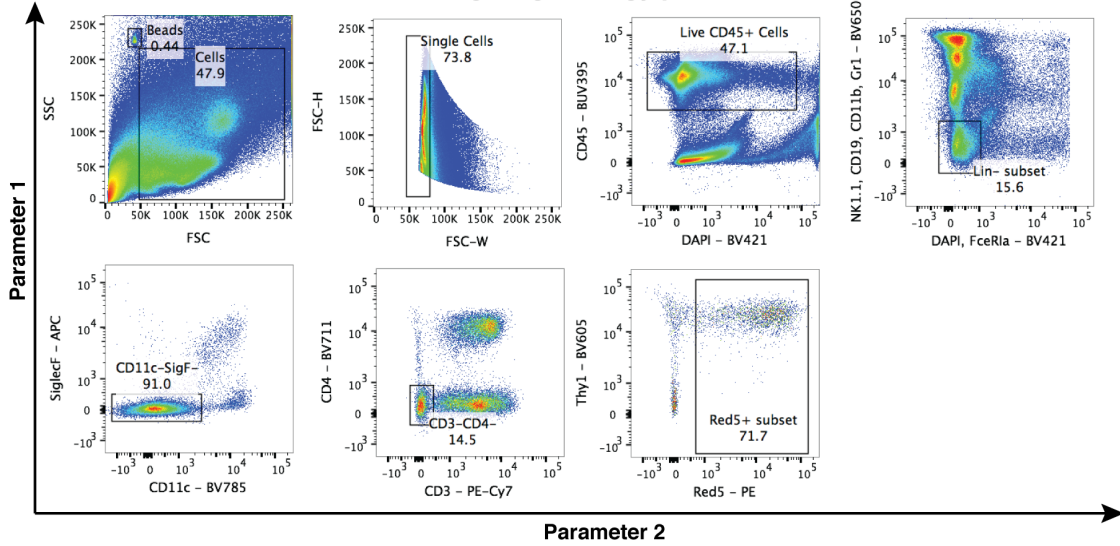
A Lung mass 14 days post-PNX in Rag1 null mice



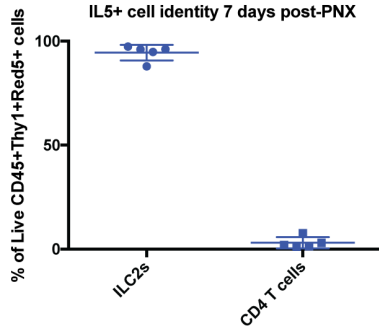
B mRNA fold change ILC2s 4 days post-PNX vs. SHAM



C ILC2 gating strategy post-PNX



D IL5+ cell identity 7 days post-PNX



E Proliferating ILC2s post-PNX

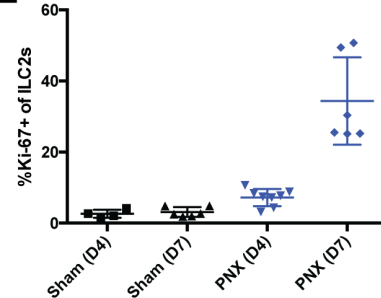


Table 1. KEY RESOURCES TABLE

REAGENT or RESOURCE	SOURCE	IDENTIFIER
Antibodies		
Rat monoclonal (clone M1/70) anti-mouse CD11b (purified, used at 1:150)	Biolegend	Cat#101201; RRID: AB_312784
Hamster monoclonal (clone N418) anti-mouse CD11c (purified, used at 1:150)	Biolegend	Cat#117301; RRID:AB_313770
Rat monoclonal (clone C1:A3-1) anti-mouse F4/80 (purified, used at 1:150)	Biorad/AbD Serotec	Cat#MCA497G; RRID:AB_872005
Hamster monoclonal (1A8) anti-mouse Ly6G (purified, used at 1:150)	Biolegend	Cat#127607; RRID:AB_1186104
Hamster monoclonal (30-F11) anti-mouse CD45 (purified, used at 1:200)	BD Bioscience	Cat#550539; RRID:AB_2174426
Rat monoclonal (clone MEC 13.3) anti-mouse PECAM (purified, used at 1:200)	BD Bioscience	Cat#550274; RRID:AB_393571
Rat monoclonal (clone 175410) anti-mouse RAGE (purified, used at 1:200)	R&D Systems	Cat#MAB1179; RRID:AB_2289349
Rabbit polyclonal anti-mouse PECAM (used at 1:250)	Millipore	Cat#AB3786; RRID:AB_91588
Hamster monoclonal (8.1.1) anti-mouse T1 α (used at 1:900)	Developmental Studies Hybridoma Bank, Univ. of Iowa	RRID: AB_531893
Chicken polyclonal anti-GFP (used at 1:500)	Aves	Cat#GFP-1020; RRID:AB_10000240
Rabbit polyclonal anti-RFP (used at 1:250)	Rockland	Cat#600-401-379; RRID:AB_2209751
Chicken polyclonal anti-RFP (used at 1:250)	Rockland	Cat#600-901-379; RRID:AB_10704808
Rat monoclonal (clone 30-F11) anti-CD45-Apc-Cy7 (used at 1:200)	Biolegend	Cat#103116; RRID:AB_312981
Rat monoclonal (M1/70) anti-CD11b-PerCP-Cy5 (used at 1:200)	Tonbo	Cat#65-0112 also OWL-A11257; RRID:AB_2621885
Rat monoclonal (N418) anti-CD11c-APC (used at 1:200)	Biolegend	Cat#117309; RRID:AB_313778
Rat monoclonal (BM8) anti-F4/80-PE (used at 1:200)	eBioscience	Cat#12-4801-82; RRID:AB_465923
Rat monoclonal (1A8) anti-Ly6G-PE-Cy7 (used at 1:400)	Biolegend	Cat#127617; RRID:AB_1877262
Goat anti-Chicken IgG (H+L) Secondary Antibody, Alexa Fluor 488 (used at 1:500)	Thermo Fisher Scientific	Cat#A-11039 also A11039; RRID:AB_142924
Donkey anti-Rabbit IgG (H+L) Secondary Antibody, Alexa Fluor 488 (used at 1:500)	Thermo Fisher Scientific	Cat#A-21206 also A21206; RRID:AB_2535792
Donkey anti-Rat IgG (H+L) Secondary Antibody, Alexa Fluor 488 (used at 1:500)	Thermo Fisher Scientific	Cat#A-21208 also A21208; RRID:AB_141709
Cy3-AffiniPure F(ab') ₂ Donkey anti-Chicken IgG (H+L) Secondary Antibody (used at 1:500)	Jackson ImmunoResearch Labs	Cat#703-166-155; RRID:AB_2340364

REAGENT or RESOURCE	SOURCE	IDENTIFIER
Donkey anti-Rabbit IgG (H+L) Secondary Antibody, Alexa Fluor 555 (used at 1:500)	Thermo Fisher Scientific	Cat#A-31572 also A31572; RRID:AB_162543
Goat anti-Rat IgG (H+L) Secondary Antibody, Alexa Fluor 555 (used at 1:500)	Thermo Fisher Scientific	Cat#A-21434 also A21434; RRID:AB_141733
Goat anti-Hamster IgG (H+L) Secondary Antibody, Alexa Fluor 647 (used at 1:500)	Thermo Fisher Scientific	Cat#A-21451; RRID:AB_2535868
Goat anti-Rat IgG (H+L) Secondary Antibody, Alexa Fluor 647 (used at 1:500)	Thermo Fisher Scientific	Cat#A-21247 also A21247; RRID:AB_141778
Rat monoclonal (clone 30-F11) anti-CD45-BUV395 (used at 1:100)	BD Biosciences	Cat# 564279
Rat monoclonal (clone 17A1) anti-CD3-PE-Cy7 (used at 1:100)	Biolegend	Cat# 100205; RRID:AB_312662
Rat monoclonal (clone RM4-5) anti-CD4-BV711 (used at 1:100)	Biolegend	Cat# 317439; RRID:AB_11219404
Rat monoclonal (clone 6D5) anti-CD19-BV650 (used at 1:100)	Biolegend	Cat#115541; RRID:AB_11204087
Rat monoclonal (clone PK136) anti-NK-1.1-BV650 (used at 1:100)	Biolegend	Cat#108735; RRID:AB_11147949
Rat monoclonal (clone RB6-8C5) anti-Ly6-G/Ly6-C-BV650 (used at 1:100)	Biolegend	Cat#108441; RRID:AB_2562401
Rat monoclonal (clone M1/70) anti-CD11b-BV650 (used at 1:100)	Biolegend	Cat#101239; RRID:AB_11125575
Rat monoclonal (clone N418) anti-CD11c-BV785 (used at 1:100)	Biolegend	Cat# 117335 RRID:AB_11219204
Rat monoclonal (clone E50-2440) anti-SiglecF-APC (used at 1:100)	BD Biosciences	Cat#562680
Rat monoclonal (PC61) anti-CD25-APC-Cy7 (used at 1:100)	Biolegend	Cat#102025; RRID:AB_830744
Rat monoclonal (53-2.1) anti-CD90.2-BV605 (used at 1:100)	Biolegend	Cat#140317; RRID:AB_11203724
Rat monoclonal (DJ8) anti-T1/ST2-PE (used at 1:100)	MD Biosciences	Cat#101001PE
Rat monoclonal (2F1) anti-KLRG1/MAFA-PerCP-eFluor710 (used at 1:100)	eBioscience	Cat#46-5893-80 also 46-5893; RRID:AB_10671072
Rat monoclonal (MAR-1) anti-FcεRIα Pacific Blue (used at 1:100)	Biolegend	Cat#134313; RRID:AB_10612933
Rat monoclonal (TAWJ) anti-Gata-3-eFluor660 (used at 1:20)	eBioscience	Cat#50-9966-41 also 50-9966; RRID:AB_10597909

REAGENT or RESOURCE	SOURCE	IDENTIFIER
Rat monoclonal (SolA15) anti-Ki67-FITC (used at 1:100)	eBioscience	Cat#11-5698-80; RRID:AB_11151689
Rat monoclonal (RPA-T4) anti-hCD4-APC (used at 1:100)	eBioscience	Cat#17-0049-41; RRID:AB_1272118
Rat monoclonal (A20) anti-hCD45.1-PE (used at 1:200)	Biolegend	Cat#110707; RRID:AB_313496
Rat monoclonal (104) anti-hCD45.2-APC (used at 1:200)	Biolegend	Cat#109813; RRID:AB_389210
CD16/CD32 Fc Receptor Block	BD Biosciences	Cat# 553142 RRID:AB_394657
Rat monoclonal (clone 30-F11) anti-CD45-Apc (used 2 ug/mouse for <i>in vivo</i> labeling)	Biolegend	Cat#103112
Bacterial and Virus Strains		
n/a		
Biological Samples		
n/a		
Chemicals, Peptides, and Recombinant Proteins		
Buprenex (0.3 mg/mL)	Reckitt Benckiser	Cat# NDC 12496-0757-5
Lidocaine (5 mg/mL)	Phoenix	Cat# NDC 57319-533-05
Bupivacaine (2.5 mg/mL)	Hospira	Cat# NDC 0409-1159-01
Donkey Serum	Sigma-Aldrich	Cat#D9663-10ML
Goat Serum	Sigma-Aldrich	Cat#G9023-10ML
Bovine Serum Albumin	Fisher	Cat#BP1600-100
Tamoxifen	Sigma-Aldrich	Cat#T5648
EdU (5-ethynyl-2'-deoxyuridine)	Thermo Fisher Scientific	Cat#E10415
Collagenase Type I (used at 450 U/mL)	Gibco Life Tech	Cat###17100-017
Elastase (used at 4 U/mL)	Worthington Biochemical Corporation	Cat###LS002279
Dispase (used at 5 U/mL)	BD Biosciences	Cat#354235
DNaseI (used at 0.33 U/mL)	Roche	Cat#10104159001
Red Blood Cell Lysis Buffer	Biolegend	Cat#420301-BL
Liberase TM	Roche	Cat#05401119001
Sytox Blue	Life Tech	Cat#S34857
AbC Anti-Mouse Bead kit	Molecular Probes	Cat#A10344
Fix and Perm Cell Permeabilization Kit	Thermo Fisher Scientific	Cat#GAS003
DMEM / F12 + GlutaMAX	Gibco Life Tech	Cat#10565-018
Matrigel (Growth Factor Reduced)	BD Biosciences	Cat#356230
Characterized Fetal Bovine Serum (used at 10%)	HyClone	Cat#SH30071
Insulin-Transferrin-Selenium (used at 1x)	Gibco Life Tech	Cat#41400-045
Epidermal Growth Factor (used at 20 ng/mL)	R&D Systems	Cat#2028-EG-200
Fibroblast Growth Factor 2 or Basic (used at 25 ng/mL)	Gibco Life Tech	Cat#PMG0033

REAGENT or RESOURCE	SOURCE	IDENTIFIER
Keratinocyte Growth Factor or Fibroblast Growth Factor 7 (used at 10 ng/mL)	Gibco Life Tech	Cat#PHG0094
Hepatocyte Growth Factor (used at 10 ng/mL)	Gibco Life Tech	Cat#PHG0254
RIPA Lysis and Extraction Buffer	Thermo Fisher Scientific	Cat#89900
Complete, Mini Protease Inhibitor Cocktail	Roche	Cat#11-836-153-001
Protein Assay Dye Reagent Concentrate	Bio-Rad	Cat#500-0006
Protector RNase Inhibitor	Roche	Cat#03-335-402-001
Critical Commercial Assays		
Click-iT EdU Alexa Fluor 647 Imaging Kit (for flow cytometry)	Invitrogen	Cat#C10340
Click-iT <i>Plus</i> EdU Alexa Fluor 647 Imaging Kit (for tissue histology)	Invitrogen	Cat#C10640
Proteome Profiler Mouse Cytokine Array Kit, Panel A	R&D Systems	Cat#ARY006
RNAeasy Plus Micro Kit	Qiagen	Cat#74034
SuperScript IV VILO Master Mix	Invitrogen Life Tech	Cat#11756050
SYBR GreenER qPCR Supermix Universal	Invitrogen Life Tech	Cat#1176202K
Agilent RNA 600 Pico Kit	Agilent Technologies	Cat#5067-1513
C1 Single-Cell Reagent Kit for mRNA Seq	Fluidigm	Cat#100-6201
Nextera XT DNA Library Preparation Kit	Illumina	Cat#FC-131-1096
Quant-iT™ PicoGreen® dsDNA Assay Kit	Thermo Fisher Scientific	Cat#P7589
Deposited Data		
Raw data files for RNA sequencing (PNX)	NCBI GEO	GEO: GSE96104
Raw data files for RNA sequencing (sham)	NCBI GEO	GEO: GSE96105
Experimental Models: Cell Lines		
n/a		
Experimental Models: Organisms/Strains		
Mouse: <i>Csf1r-GFP</i> : B6N.Cg-Tg(Csf1r-EGFP)1Hume/J	Jackson Laboratories	Stock No. 018549
Mouse: <i>Ccr2^{-/-} : CCR2^{tm1Mae}</i>		Kuziel et al., 1997
Mouse: <i>Ccr2^{RFP/+} : B6.129(Cg)-Ccr2^{tm2.1ffc}/J</i>	Jackson Laboratories	Stock No. 017586
Mouse: <i>Cx3cr1^{GFP/+} : B6.129P-Cx3cr1^{tm1Llt}/J</i>	Jackson Laboratories	Stock No. 005582
Mouse: <i>Sftpc-CreER</i> : <i>Sftpc^{tm1(Cre/ERT2)Bin}</i>	Jackson Laboratories	Stock No. 028054
Mouse: <i>Rosa-dTomato</i> : Gt(ROSA)26Sor ^{tm2(CAG-tdTomato)} Fawa		Rock et al., 2011
Mouse: <i>Rosa-fGFP</i> : Gt(ROSA)26Sor ^{tm1(CAG-EGFP)Bin}		Rawlins et al., 2009
Mouse: YARG : B6.129S4- <i>Arg1^{tm1Lky}/J</i>	Jackson Laboratories	Stock No. 015857
Mouse: <i>Il4ra^{-/-} : BALB/c-Il4ra^{tm1Sz}/J</i>	Jackson Laboratories	Stock No. 003514
Mouse: <i>Il5^{tm1.1(Cre)Lky}</i>		Nussbaum et al., 2013
Mouse: <i>IL13^{tm2.1Lky} : C.129S4(Cg)-Il13^{tm2.1Lky}/J</i>	Jackson Laboratories	Stock No. 018869

REAGENT or RESOURCE	SOURCE	IDENTIFIER
Mouse: CD45.1 : B6-Ly5.1/Cr	Charles River	Stock No. 564
Oligonucleotides		
Genotyping primers- See Supplemental Table 1	This paper	
qRT-PCR primers- See Supplemental Table 2	This paper	
Recombinant DNA		
n/a		
Software and Algorithms		
ImageJ	NIH	https://imagej.nih.gov/ij/
FlowJo (v10.1r5)	TreeStar Inc.	https://www.flowjo.com/
GraphPad Prism 6.0	GraphPad Software Inc.	http://www.graphpad.com/scientificsoftware/prism/
Tophat (v2.1.0)	Kim et al., 2013; Trapnell et al., 2012	
Bowtie2 (v2.2.8)	Kim et al., 2013; Trapnell et al., 2012	
Cufflinks (v2.2.1)	Kim et al., 2013; Trapnell et al., 2012	
Picard tools		http://broadinstitute.github.io/picard/
HTSeq-count	Anders et al., 2015	http://www-huber.embl.de/users/anders/HTSeq/doc/count.html
Trimmatic	Bolger et al., 2014	http://www.usadella.b.org/cms/?page=trimmomatic
RSEM	Li and Dewey, 2011	

Table S1. Primer sequences used for mouse genotyping.

Mouse/ Gene Name	Wildtype Forward Primer Sequence	Wildtype Reverse Primer Sequence	Mutant Forward Primer Sequence	Mutant Reverse Primer Sequence
CCR2 BALB/c	TGG GGA TAC TGC TTA AAT GGC GCA A	-	TTC CAT TGC TCA GCG GTG CT	TCA GAG ATG GCC AAG TTG AGC AGA
CCR2-RFP	TAA ACC TGG TCA CCA CAT GC	CTT GAT GAC GTC CTC GGA G		
CSF1R- GFP			ATG GTG AGC AAG GGC GAG GAG	CGA TGG GGG TGT TCT GCT GGT AGT
CX3CR1- GFP	CTC CCC CTG AAC CTG AAA C		CTC CCC CTG AAC CTG AAA C	CCC AGA CAC TCG TTG TCC TT
IL-4R α	GTA CAG CGC ACA TTG TTT TT	CTC GGC GCA CTG ACC ATC T	CCC TTC CTG GCC CTG AAT TT	CCC TTC CTG GCC CTG AAT TT
IL-5 (Red5)	TTCAGGACTCG CCTTTATTAGG TG	AGAGTGGGACAA GAGGACAGAACG		AGGATGATGACCA GGGTGTAGTTG
Rosa-CAG (Tomato; fGFP)	CAC TTG CTC TCC CAA AGT CG	TAG TCT AAC TCG CGA CAC TG	GTT ATG TAA CGC GGA ACT CC	
Smart13	CTG GCA GGG ACT TTT GGT AG	ATC TCC CTT CCT CCT CAA CC	AAT CCA ACA TCA AGG TTC TGC	
Spc-CreER	TGC TTC ACA GGG TCG GTA G	CAT TAC CTG GGG TAG GAC CA		ACA CCG GCC TTA TTC CAA G
YARG	AAC CAC CTA AGT GAC TGT GAA TGC G	TAC CTC TCT GGA TAC CTT TGC TTC C G	CGT GCT GCT GCC CGA CAA CCA CTA C	TGC TTT GCT GTG ATG CCC CAG ATG G

Table S2. Primer sequences used for quantitative RT-PCR analysis.

Gene name	Forward primer	Reverse primer
Actb	GGCTGTATTCCCCTCCATCG	CCAGTTGGTAACAATGCCATGT
B2M	TTCTGGTGCTTGTCTCACTGA	CAGTATGTTCCGGCTTCCCATTC
Arg1	GGAGCTGTCATTAGGGACATCA	CTCCAAGCCAAAGTCCTTAGAG
IL5	CTCTGTTGACAAGCAATGAGAGACG	TCTTCAGTATGTCTAGCCCCTG
IL4	GGTCTCAACCCCCAGCTAGT	GCCGATGATCTCTCTCAAGTGAT
IL13	CCTGGCTCTTGCTTGCCTT	GGTCTTGTGTGATGTTGCTCA

Chapter 4

Alveolar epithelial lung stem cells are vulnerable to exhaustion after repeated injury

4.1 Introduction:

The epithelial lining of the lung is exposed to a constant barrage of environmental insults from inhaled pollutants and infectious pathogens. These exposures can damage the specialized respiratory epithelium that facilitates efficient gas transport and exchange in the distal lung alveoli. Type 2 alveolar epithelial stem cells (AEC2) are stem cells that reside in the distal alveoli, able to maintain themselves through self-renewal and to differentiate into type 1 alveolar epithelial cells (AEC1s). While relatively quiescent at steady-state, AEC2s are imbued with facultative regenerative capacities such as restoring the epithelial lining after influenza infection (Kanegai et al., 2016) and spurring alveologenesis after pneumonectomy (Barkauskas et al., 2013). However, it is unknown to what degree AEC2s are required to maintain the lung epithelial barrier under steady-state conditions and to what extent AEC2s retain their regenerative capacities.

While the stem cells from other organs can be tested *in vivo* for long-term self-renewal or engraftment, these assays do not exist for lung AEC2s. In fact, serial transplantation of AEC2s has only been attempted *in vitro* (Jain et al., 2015) and AEC2 engraftment has only succeeded after severe epithelial clearing as in influenza infection (Vaughan et al., 2015; Zuo et al., 2015). These models do not test the normal demands of AEC2s *in vivo* and may not recapitulate human pathophysiology. To understand the extent to which AEC2s maintain the distal lung epithelium, we used a non-fibrosis stem-cell specific lung injury model (Barkauskas et al., 2013). Using this model we find that severe AEC2 depletion promotes proliferation of the AEC2 pool that gradually restores their numbers to steady-state levels. Lineage tracing studies of the surviving AEC2s suggest that no other distal lung epithelial progenitor contributes to AEC2 recovery. Although our model specifically kills AEC2s, we find that the surviving AEC2s differentiate into AEC1s. Finally, we provide evidence that repeated AEC2 depletion diminishes AEC2 recovery. Together, these data demonstrate that AEC2s are a self-sustaining stem cell population that is vulnerable to exhaust after repeated injury.

4.2 Results

4.2.1. Targeted AEC2 depletion results in significant AEC2 killing and eventual recovery

To specifically and genetically ablate AEC2s, we generated mice containing alleles for *Sftpc-CreER* (hereafter *Spc-CreER*); *Rosa26-loxp-stop-loxp-fGFP* (hereafter *Rosa-DTA*); and *Rosa26R-loxp-stop-loxp-diphtheria toxin A* (hereafter *Rosa-DTA*). Cre-mediated recombination results in two independent events: AEC2 death or lineage labeling with GFP. We induced dose-dependent AEC2 killing with intraperitoneal tamoxifen injections at 0.125 mg/kg separated by 48 hours. We then followed the behaviors of the surviving unlabeled (*SPC+GFP-*) and lineage labeled (*SPC+GFP+*) AEC2s (Figure 1A). Adult *Spc-CreER;Rosa-fGFP/DTA* mice and *Spc-CreER;Rosa-fGFP/+* littermate control mice sacrificed before tamoxifen injections had ~10% lineage labeled AEC2s (*SPC+fGFP+/SPC+* cells). This rate of tamoxifen-independent lineage labeling is comparable to other studies using *Spc-CreER* mice (Barkauskas et al., 2013). Three days after our tamoxifen regimen, lineage labeling of AEC2s had increased to ~70% in DTA-controls and ~90% in DTA+ mice (Figure 1B & 1D). A much smaller population of surviving AEC2s may account for the greater proportion of lineage labeled AEC2s in DTA+ mice. Our tamoxifen regimen eliminated ~75% of *SPC+* AEC2s by 3 days after the last injection (Figure 1C & 1E), although no gross morphological changes in lung physiology were noted. Thus, in our hands, this model seems to be an efficient system for directly killing AEC2s without any acute pathology.

We found that a large number of both lineage labeled and unlabeled AEC2s had returned by 3 weeks, with complete recovery by 2 months (Figure 1C, Figure 2A). Although we did not detect cell death in AEC1s by Caspase-3 staining (data not shown), we noticed a large number of newly formed AEC2-derived AEC1s during the recovery phase (Figure 2B). Since *SPC* protein expression may induce cell death, we reasoned that AEC1 formation is an adaptive response to epithelial repair after AEC2 depletion. In a murine-adapted model of H1N1 influenza

infection, significant epithelial damage and loss of AEC2s results in the formation of alveolar cysts or “pods” expressing Krt5 and Trp63 (Kumar et al., 2011). While the origin of these cells remains unknown (Vaughan et al., 2015), these studies suggest that severe depletion of lung epithelium, particularly resident stem cell populations, may drive aberrant repair mechanisms. However, we did not detect any Krt5+ pods in our model (Figure 2F).

To determine if a non-AEC2 distal lung epithelial progenitor contributes to the recovery of AEC2s after depletion, we quantified the numbers of lineage labeled and unlabeled AEC2s over time after AEC2 depletion. We hypothesized that if AEC2s are the sole source of new AEC2s during recovery, then the frequency of lineage labeled AEC2s should remain stable, or at least not decrease, over time. However, if another unlabeled epithelial progenitor is capable of replenishing the AEC2 pool during the recovery phase, the number of unlabeled AEC2s should increase over time. We found that the number of lineage labeled cells spiked during the killing phase, but then gradually increased over time (Figure 2C & D). To further address this point and to understand stem cell heterogeneity within the AEC2 pool, we assessed the proliferative capacity of both lineage labeled and unlabeled AEC2s using an *in vivo* EDU incorporation assay. We injected *Spc-CreER/+;Rosa-fGFP/DTA* mice and *Spc-CreER;Rosa-fGFP/+* littermate control mice, before and after tamoxifen injections, with 50 mg/kg of EDU by intraperitoneal injection 3.5 hours prior to sacrifice. We then quantified proliferating lineage labeled AEC2s (SPC+GFP+EDU+) and proliferating unlabeled AEC2s (SPC+GFP-EDU+). There was no difference in proliferation between these two AEC2s subsets at any time point before or after depletion. Furthermore, the greatest AEC2 proliferation occurred immediately after the killing phase in DTA+ mice (Figure 2E). These data suggest that AEC2s are a self-sustaining population with similar proliferative capacities.

4.2.2. Repeated AEC2 depletion inhibits AEC2 recovery

In order to understand how repetitive AEC2 injury affects lung homeostasis, we performed multiple rounds of tamoxifen injections in *Spc-CreER/+;Rosa-fGFP/DTA* mice. Each tamoxifen regimen was given as before (2 doses 48 hours apart), but repeated every 19-21 days (Figure 3A). After five rounds of tamoxifen, we assessed AEC2 depletion and recovery. After 5 rounds of tamoxifen, AEC2s were still ablated at 7d after the last tamoxifen injection. However, the ablation of AEC2 was less in mice given five rounds of tamoxifen compared to those given just one (Figure 3B & C). This result may be an artifact of continuous selection for AEC2s with lower CreER expression/activity or with *Rosa-DTA* loci recalcitrant to recombination. To assess AEC2 recovery, we quantified AEC2s at 21d after the last tamoxifen injection- the time at which most of the AEC2s have returned in DTA+ mice given just one round of tamoxifen (Figure 2A). Contrary to DTA+ mice given one round of tamoxifen, AEC2s numbers had not increased at 21d compared to 7d in DTA+ mice given five rounds of tamoxifen (Figure 3B & C). Despite repeated AEC2s killing and apparent lack of AEC2 recovery, we did not observe any fibrosis or other lung pathologies in DTA+ mice after five rounds of tamoxifen (data not shown).

To evaluate the dynamics of the AEC2 pool over time, we reassessed the ratios of lineage labeled and unlabeled AEC2s at 21d after the last tamoxifen injection. The ratio of labeled to unlabeled AEC2s was ~75:25 for DTA+ mice given one round of tamoxifen, and ~85:15 for DTA+ mice given five rounds of tamoxifen (Figure 3D). As before, these data suggest non-AEC2 epithelial progenitors do not contribute to restoring the AEC2 pool after depletion. Taken together, these data suggest that AEC2s comprise an independent distal lung epithelial stem cell population capable of robust proliferation and rapid re-epithelization following targeted injury. However, continuous AEC2 turnover may exhaust their long-term self-renewal capacity.

4.3 Discussion

AEC2s are abundant and facultative epithelial stem cells in the distal lung alveoli, but their ability for long-term stem cell potential has not been thoroughly investigated. Here, we demonstrate that after high frequency AEC2 killing, both lineage-labeled and non-lineage labeled AEC2s proliferate to restore AEC2 numbers. Since the proportion of unlabeled AEC2s does not increase over time, and both lineage-labeled and unlabeled AEC2s proliferate equally, we conclude that other epithelial progenitors do not significantly contribute to AEC2 recovery after depletion in our model.

After depletion AEC2 numbers increased steadily over time, recovering to ~75% of controls by 21 days, and reaching steady-state numbers by 2 months. Furthermore, through survival of lineage traced AEC2s, we observe that the remaining AEC2s generate significant numbers of newly formed AEC1s in as little as 2 weeks. Although we did not detect apoptosis specifically within the AEC1 population, we suspect that these AEC2-derived AEC1s develop as part of a repair mechanism to compensate for the loss of AEC2s after depletion.

In some contexts, severe AEC2 killing results in atypical epithelial repair mechanisms. For example, after infection with H1N1 influenza strain PR8, pods of Krt5+, Trp63+ cells appear in the distal lung alveoli. We were unable to find any of these pods in our AEC2 depletion model, suggesting that AEC2 killing alone does not drive the formation of distal lung Krt5+ pods. It must be noted that while influenza infection induces a robust immune response, we noted no increase in immune cell infiltrate after AEC2 depletion in our model. This difference in addition to the fact that influenza targets multiple epithelial progenitor populations beyond AEC2s may account for the emergence of Kr5+ pods.

To study the effects of repeated AEC2 killing on lung homeostasis, we modified our model by inducing AEC2 depletion at multiple repeated intervals after AEC2 recovery. Multiple rounds of depletion resulted in a ~50% loss of AEC2s compared to uninjected control mice and mice that had recovered from one round of depletion. However, multiple rounds of depletion resulted in less AEC2 killing than in mice exposed to one round (~75% loss of AEC2s),

suggesting that we are selecting for depletion-resistant AEC2s. During the recovery phase in mice exposed to multiple depletions, we continued to see newly formed AEC2s-derived AEC1s but we did not see an increase in AEC2s by 21d as in mice exposed to one depletion round.

We could not identify any fibrosis or other pathophysiology in our lung injury model, even after repeated AEC2s killing. The inability of AEC2s to recover at the later time points after multiple injury rounds could be due to a delayed recovery response and AEC2s may need more time to replenish steady-state levels. Alternatively, repeated AEC2 killing may have permanently altered the normal composition of the distal lung epithelium in favor of AEC1s over AEC2s. These findings raise the possibility that steady-state levels of AEC2s are not required for survival of the organism; however, these mice may now be vulnerable to normally benign insults and more late-point time points are warranted. Finally, as the ratio of labeled AEC2s did not diminish after multiple depletion rounds, it appears that no other epithelial progenitor is recruited to replenish the AECs pool.

Together, these data suggest a role for AEC2s as a homogenous self-sustaining population of epithelial stem cells that may have diminished self-renewal capacity after continuous lung injury. This principle of stem cell exhaust is well established in other organs as a source of pathologies later in life. By beginning to understand the stem cell capacities AEC2s, we may gain insights to maladaptive repair mechanisms underlying other lung diseases.

4.4 Methods

Mice:

All mice were bred and maintained in a specific-pathogen-free barrier facility. Mice of both sexes were used and studies were started when mature at 8 weeks of age. All mouse strains were congenic on a C57BL/6 background and included *Sftpc*^{tm1(cre/ERT2)Blh} (hereafter *Spc-CreER*; Rock et al., 2011), *Gt(ROSA)26Sor*^{tm1(CAG-EGFP)Blh} (hereafter *Rosa-fGFP*; Rawlins et al., 2009), and

Gt(ROSA)26Sor^{tm1(DTA)Lky} (hereafter *Rosa-DTA*, Jackson Laboratories). Mice were crossed to generate heterozygous animals containing alleles for *Sftpc-CreER* and *Rosa-fGFP* to lineage trace AEC2s. Mice were crossed to contain alleles for *Sftpc-CreER*, *Rosa-fGFP*, and *Rosa-DTA* for targeted AEC2s depletion studies.

Targeted AEC2 Labeling and Depletion:

To specifically and temporally target AEC2s for depletion, mice heterozygous for *Sftpc-CreER*, *Rosa-fGFP*, and *Rosa-DTA* alleles were given 2 doses of tamoxifen separated by 48 hours. tamoxifen (Sigma-Aldrich, catalog #T5648) was dissolved in corn oil and administered to mice via intraperitoneal injection at 0.125 mg of Tamoxifen per kg of mouse weight. For repeated AEC2 depletion, tamoxifen was dosed as before every 19-21 days after the first tamoxifen regimen.

Proliferation studies:

See detailed methods in Chapter 3 of this dissertation.

Tissue processing for immunostaining:

See detailed methods in Chapter 3 of this dissertation.

References:

- Barkauskas, C.E., Cronce, M.J., Rackley, C.R., Bowie, E.J., Keene, D.R., Stripp, B.R., Randell, S.H., Noble, P.W., and Hogan, B.L. (2013). Type 2 alveolar cells are stem cells in adult lung. *J. Clin. Invest.* 123, 3025–3036.
- Jain, R., Barkauskas, C.E., Takeda, N., Bowie, E.J., Aghajanian, H., Wang, Q., Padmanabhan, A., Manderfield, L.J., Gupta, M., Li, D., et al. (2015). Plasticity of Hopx(+) type I alveolar cells to regenerate type II cells in the lung. *Nat Commun* 6, 6727.
- Kanegai, C.M., Xi, Y., Donne, M.L., Gotts, J.E., Driver, I.H., Amidzic, G., Lechner, A.J., Jones, K.D., Vaughan, A.E., Chapman, H.A., et al. (2016). Persistent Pathology in Influenza-Infected Mouse Lungs. *Am. J. Respir. Cell Mol. Biol.* 55, 613–615.
- Vaughan, A.E., Brumwell, A.N., Xi, Y., Gotts, J.E., Brownfield, D.G., Treutlein, B., Tan, K., Tan, V., Liu, F.C., Looney, M.R., et al. (2015). Lineage-negative progenitors mobilize to regenerate lung epithelium after major injury. *Nature* 517, 621–625.
- Zuo, W., Zhang, T., Wu, D.Z., Guan, S.P., Liew, A.-A.A., Yamamoto, Y., Wang, X., Lim, S.J., Vincent, M., Lessard, M., et al. (2015). p63(+)Krt5(+) distal airway stem cells are essential for lung regeneration. *Nature* 517, 616–620.

Figure 1. Genetic depletion model for lung alveolar epithelial stem cells. (A) Adult mice heterogeneous for *Spc-CreER;Rosa-fGFP* or *Spc-CreER;Rosa-fGFP;Rosa-DTA* were given 2 doses of tamoxifen (TAM) at 0.125 mg/kg by intraperitoneal injection separated by 48 hours. AEC2 loss was assessed 3-7d after the last dose of tamoxifen and AEC2 recovery was assessed 21d or more after the last dose of tamoxifen. (B). Immunofluorescence stains on lung tissue sections from *Spc-CreER;Rosa-fGFP* mice shows <10% of lineage labeled SPC+GFP+ AEC2s without tamoxifen (control) and >85% lineage labeled SPC+GFP+ AEC2s 3d after two tamoxifen doses. Scale bar = 200 μ m. (C) Immunofluorescence stains on lung tissue sections from *Spc-CreER;Rosa-fGFP;Rosa-DTA* mice given 2 doses of tamoxifen shows depletion of SPC+ AEC2s by 3d and recovery of SPC+ AEC2 by 24d. Scale bar = 200 μ m. (D) Quantification of lineage labeled SPC+GFP+ AEC2s from immunofluorescence stains on lung tissue sections from tamoxifen injected *Spc-CreER;Rosa-fGFP* and *Spc-CreER;Rosa-fGFP;Rosa-DTA/+* mice or uninjected controls. The recombination efficiencies for lineage labeled AEC2s are comparable in mice with or without DTA. (E) Quantification of total SPC+ AEC2s from immunofluorescence stains on lung tissue sections from tamoxifen injected *Spc-CreER;Rosa-fGFP;Rosa-DTA/+* mice or uninjected controls shows greater than 75% of AEC2s are lost 3d after the last tamoxifen injection.

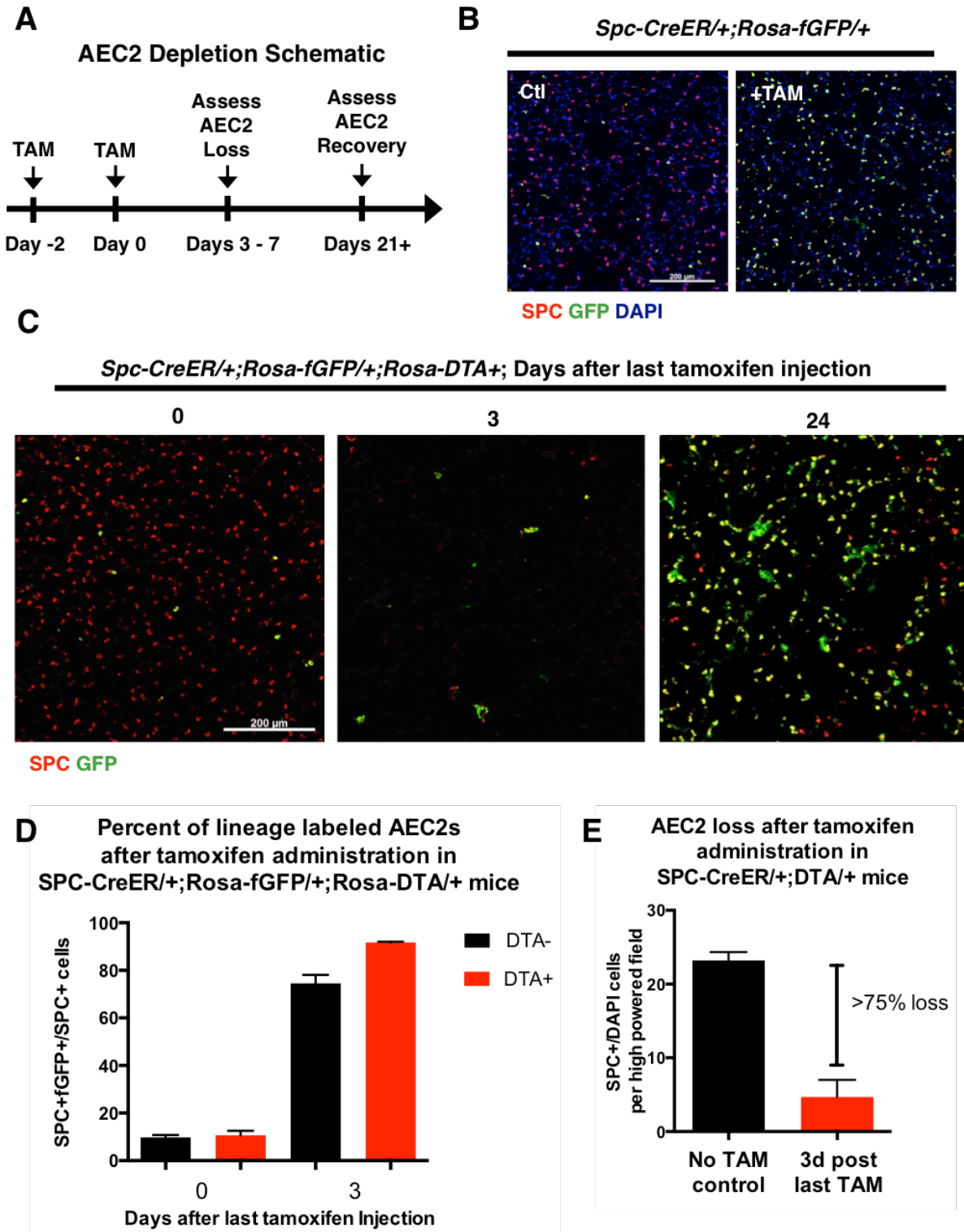
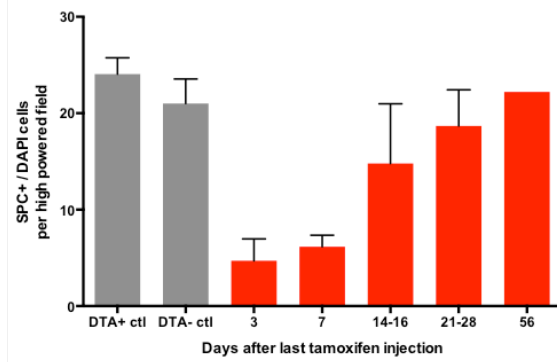
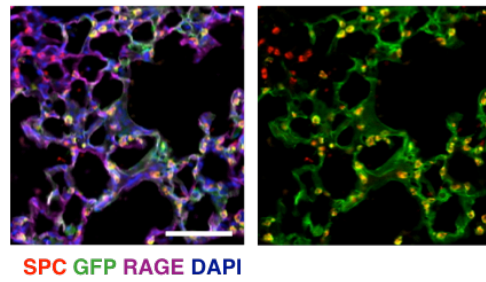


Figure 2. Lung alveolar epithelial stem cells recover after targeted depletion. (A) Quantification of SPC+ AEC2s over time after tamoxifen injection in *Spc-CreER/+;Rosa-fGFP/+;Rosa-DTA/+* or control mice (*Spc-CreER/+;Rosa-fGFP/+;Rosa-DTA/+* without tamoxifen or *Spc-CreER/+;Rosa-fGFP/+* mice with tamoxifen). After depletion, the number of AEC2s recovered to near control levels by 21-28d after the last tamoxifen injection, with complete recovery by 56d. (B) Immunofluorescence stains on lung tissue sections from *Spc-CreER/+;Rosa-fGFP/+;Rosa-DTA* mice 24d after the last tamoxifen dose show increased numbers of lineage traced AEC2-derived (GFP+RAGE+) AEC1s. Scale bar = 100 um. (C,D) Quantification of lineage labeled and unlabeled AEC2s (SPC+GFP+ and SPC+GFP- respectively) from immunofluorescence stains on lung tissue sections from *Spc-CreER/+;Rosa-fGFP/+;Rosa-DTA* mice after tamoxifen injections. While lineage labeled AEC2s are initially absent, their numbers spike immediately after tamoxifen injection, and gradually increase over time. (E) Quantification of proliferating lineage labeled and unlabeled AEC2s (SPC+GFP+EDU+ and SPC+GFP-EDU+ respectively) from immunofluorescence stains on lung tissue sections from *Spc-CreER/+;Rosa-fGFP/+;Rosa-DTA* mice after tamoxifen injections. Both labeled and unlabeled AEC2s proliferate early after tamoxifen injections. (F) Immunofluorescence stains on lung tissue sections from *Spc-CreER/+;Rosa-fGFP/+;Rosa-DTA* mice 5d after the last tamoxifen dose show no Krt5 cysts or pods identified in influenza infectious models.

A AEC2 Depletion & Recovery in *Spc-CreER/+;Rosa-DTA/+* mice**B**

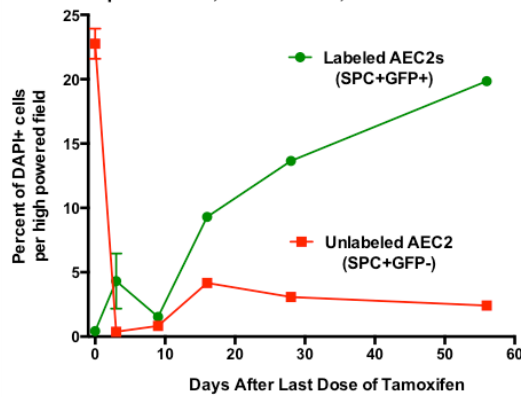
Spc-CreER/+;Rosa-fGFP/+;Rosa-DTA/+
24 days after last TAM injection



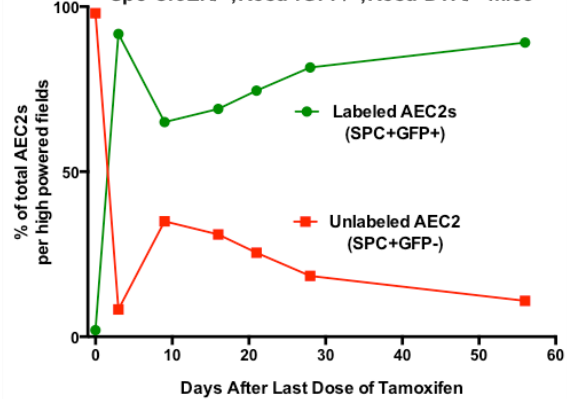
SPC GFP RAGE DAPI

C

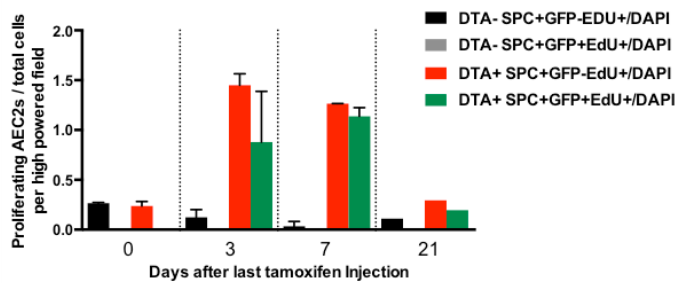
Labeled & Unlabeled AEC2s After Tamoxifen Administration in *Spc-CreER/+;Rosa-fGFP/+;Rosa-DTA/+* mice

**D**

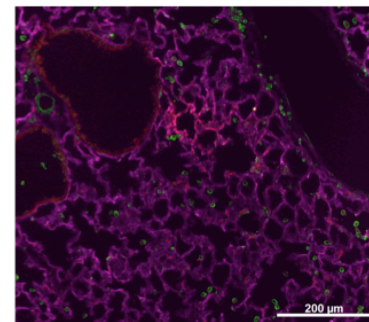
Labeled & Unlabeled AEC2s After Tamoxifen Administration in *Spc-CreER/+;Rosa-fGFP/+;Rosa-DTA/+* mice

**E**

Proliferation of labeled and unlabeled AEC2s after tamoxifen administration in *Spc-CreER/+;Rosa-fGFP/+;Rosa-DTA/+* mice

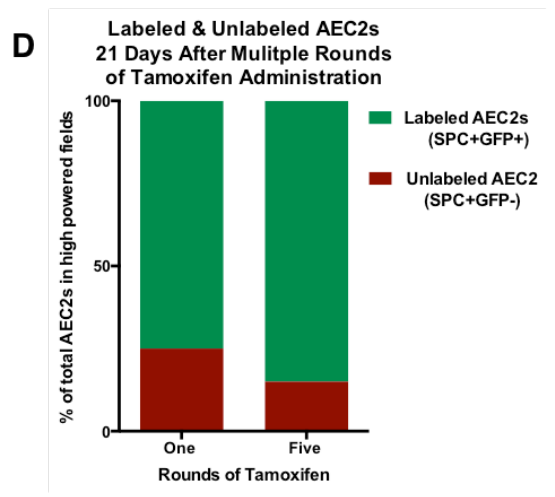
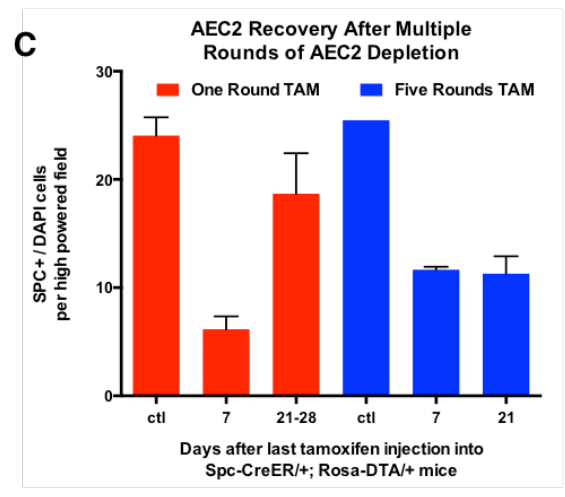
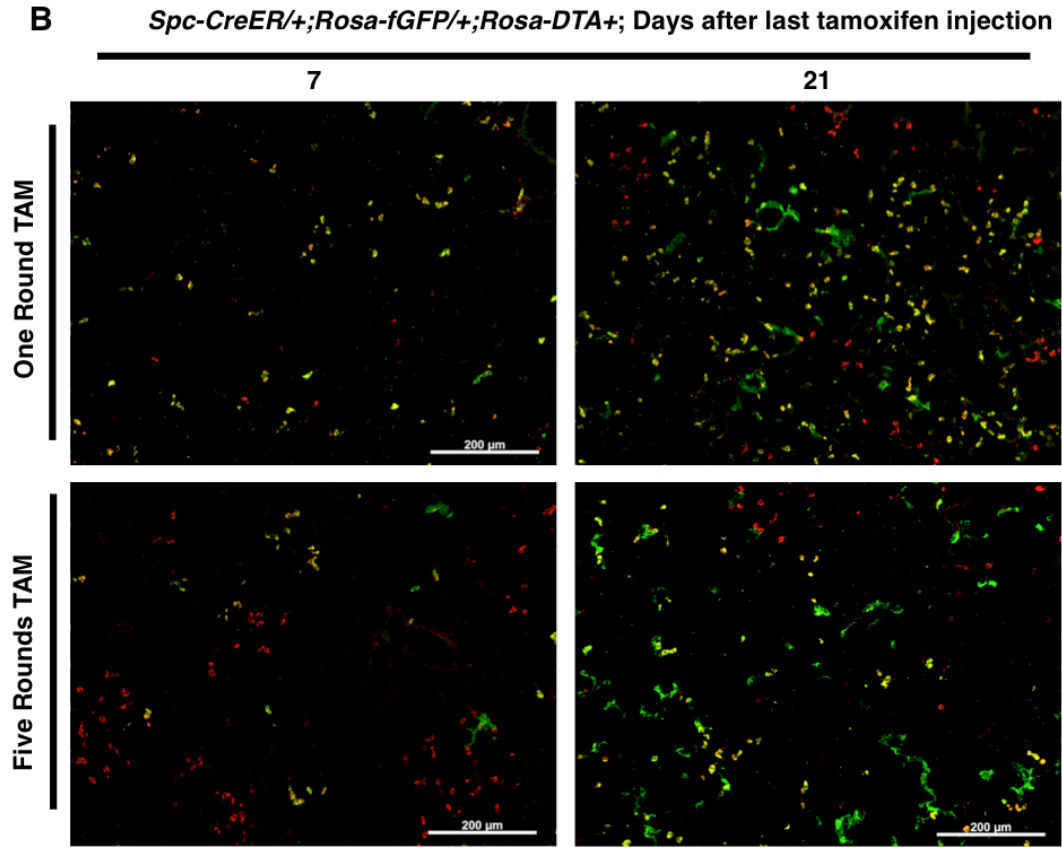
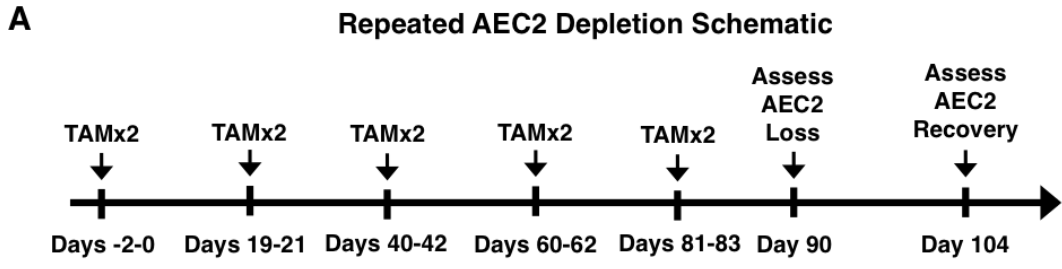
**F**

Spc-CreER/+;Rosa-fGFP/+;Rosa-DTA/+
5 days after last TAM injection



Krt5 CD45 T1a DAPI

Figure 3. Repeated AEC2s depletion results in diminished AEC2 recovery. (A) For repeated AEC2 depletion, two tamoxifen injections were given every three weeks for five rounds of tamoxifen total. AEC2 depletion was assessed 7d after the last round and AEC2 recovery was assessed 21d after the last round. (B). Immunofluorescence stains on lung tissue sections from *Spc-CreER/+;Rosa-fGFP/+;Rosa-DTA* mice after one or five rounds of tamoxifen injections. AEC2s are still depleted in *Spc-CreER/+;Rosa-fGFP/+;Rosa-DTA* mice after five rounds of tamoxifen, although the depletion frequency is less than mice given one round of tamoxifen. AEC2s do not show recovery at 21d compared to mice given one round of tamoxifen. Scale bar = 200 um. (C) Quantification of SPC+ AEC2s from immunofluorescence stains shown in A & B. (D) Quantification of lineage labeled and unlabeled AEC2s (SPC+GFP+ and SPC+GFP- respectively) from immunofluorescence stains on lung tissue sections from *Spc-CreER/+;Rosa-fGFP/+;Rosa-DTA* mice after one or five rounds of tamoxifen injections. The proportion of lineage labeled AEC2s increases after multiple rounds of AEC2 depletion.



Chapter 5
Conclusions

5.1 Conclusions:

Mounting evidence demonstrates that myeloid cells have versatile functions beyond their established roles in host defense. We are only beginning to understand how manipulation of these cells could ameliorate disease states and improve tissue repair. Furthermore, because immune cells widely disseminate and are easy to transplant, one can envision harnessing their potential to enhance proliferative processes within the regenerative lung stem cell niche. The intersection of immunology and stem cell biology is yielding new and testable ideas about altering disease processes previously considered irreversible, and stimulating adult organogenesis that will lead to development of urgently needed clinical therapies. The experiments conducted in this thesis dissertation will advance our understanding of how lung epithelial stem cells respond to external cues in their microenvironment, and the roles played by macrophages during regeneration of the respiratory epithelium.

The main body of this work establishes the groundwork for understanding how the immune system interacts with lung alveolar epithelial stem cells (AEC2) to generate new alveolar tissue. We show that inflammatory bone-marrow derived CCR2+, Ly6C+ monocytes and anti-inflammatory Arginase1+ M2-like macrophages promote lung regeneration. Optimal regeneration in the liver, skeletal muscle, heart and nervous system also relies on recruited monocytes or M2-polarized macrophages (Arnold et al., 2007; Boulter et al., 2012; Gibbons et al., 2011; Heredia et al., 2013; Nishiyama et al., 2015; Ramachandran et al., 2012; Ruffell et al., 2009; Shechter et al., 2013; Shiraishi et al., 2016; Wang and Kubes, 2016). In our model, the simultaneous activity of pro-inflammatory monocytes and anti-inflammatory M2-like macrophages suggests that lung regeneration relies on the coordination of opposing immune signals (Godwin et al., 2013).

Inflammatory monocytes promote scarring after myocardial infarction in the heart and contribute to bleomycin-induced fibrosis and influenza-induced pathology in the lung (Dutta et al., 2015; Aurora et al., 2014; Epelman et al., 2014; et al., 2014; Nahrendorf et al., 2007). On the

contrary, inflammatory monocytes also reverse fibrosis and toxin-induced injury in the liver and promote angiogenesis (Gibbons et al., 2011; Nishiyama et al., 2015; Ramachandran et al., 2012; Willenborg et al., 2012). Often inflammatory monocytes become pro-regenerative and anti-inflammatory after arriving at the site of injury (Arnold et al., 2007; Boulter et al., 2012); however, we do not yet know if this switch occurs during pneumonectomy. Conversion of recruited macrophages towards a pro-regenerative M2 phenotype often occurs after macrophage apoptosis of injured cells (Boulter et al., 2012; Ruffell et al., 2009). While this process is unlikely in PNx-induced lung regeneration, we did find that innate lymphoid group 2 cells (ILC2s) produce IL13, a type-2 cytokine that directly polarizes macrophages towards an M2 phenotype. It must be noted that IL13 also directly stimulates epithelial proliferation and therefore future studies must assess if ILC2s directly promote PNx-induced lung regeneration. Collectively our studies and others demonstrate the importance of macrophage origin, activation signals, and type of injury in dictating the role of macrophages in regeneration.

As we did not find a role for adaptive immune cells in PNx-induced lung regeneration, our studies provide more evidence that innate immunity has a greater ability to influence tissue regeneration (Aurora and Olson, 2014). Macrophages may be ideal immune cells for tissue repair because their normal immune functions, like phagocytosis, can be repurposed for tissue remodeling. Furthermore, macrophages have an incredible ability to produce a wide repertoire of both regenerative signals and matrix proteins that may orchestrate and organize tissue regeneration (Wynn and Vannella, 2016). Although we did not find macrophage-derived signals that directly stimulate AEC2s, PNx-induced macrophages are activated to remodel the matrix. Macrophage-derived matrix metalloproteinases may indirectly stimulate AEC2s and other alveolar niche cells by releasing sequestered growth factors or macrophage-derived collagens may provide a scaffold for cell migration.

Future studies will use lineage-tracing techniques to determine if monocytes directly generate M2-like macrophages or merely support their formation by modulating the immune

microenvironment after pneumonectomy. Looking upstream of the ILC2-macrophage pathway, we hope to interrogate what signals promote ILC2 activation after pneumonectomy. Unpublished data from our laboratory shows that post-PNX AEC2s increase expression of IL-33, a potent activator of ILC2s. Finally, while we have begun to understand macrophage-AEC2s interactions during alveologenesis, we have not investigated how macrophages affect other alveolar niche cells such as fibroblasts or endothelial cells. Our work demonstrates that lung macrophages promote matrix remodeling after pneumonectomy and this may enhance migration or activation of other alveolar niche cells required for lung regeneration.

The second project of this dissertation, AEC2 depletion and recovery, explored the long-term regenerative capacity of type 2 alveolar epithelial stem cells. We find that direct injury to this distal lung stem cell pool stimulates AEC2s to independently replenish themselves through self-renewal and to differentiate into AEC1s to replace the lost epithelial cells. Moreover, we find that continued depletion of AEC2s diminished their long-term regenerative capacity. Future studies will investigate if this model promotes AEC2 senescence and if taxing AEC2s increases the incidence of other lung diseases or the likelihood of failed epithelial repair in other injury models.

References:

- Arnold, L., Henry, A., Poron, F., Baba-Amer, Y., van Rooijen, N., Plonquet, A., Gherardi, R.K., and Chazaud, B. (2007). Inflammatory monocytes recruited after skeletal muscle injury switch into antiinflammatory macrophages to support myogenesis. *J. Exp. Med.* *204*, 1057–1069.
- Aurora, A.B., Porrello, E.R., Tan, W., Mahmoud, A.I., Hill, J.A., Bassel-Duby, R., Sadek, H.A., and Olson, E.N. (2014). Macrophages are required for neonatal heart regeneration. *J. Clin. Invest.* *124*, 1382–1392.
- Boulter, L., Govaere, O., Bird, T.G., Radulescu, S., Ramachandran, P., Pellicoro, A., Ridgway, R.A., Seo, S.S., Spee, B., Van Rooijen, N., et al. (2012). Macrophage-derived Wnt opposes Notch signaling to specify hepatic progenitor cell fate in chronic liver disease. *Nat. Med.* *18*, 572–579.
- Dutta, P., Sager, H.B., Stengel, K.R., Naxerova, K., Courties, G., Saez, B., Silberstein, L., Heidt, T., Sebas, M., Sun, Y., et al. (2015). Myocardial Infarction Activates CCR2(+) Hematopoietic Stem and Progenitor Cells. *Cell Stem Cell* *16*, 477–487.
- Epelman, S., Lavine, K.J., Beaudin, A.E., Sojka, D.K., Carrero, J.A., Calderon, B., Brija, T., Gautier, E.L., Ivanov, S., Satpathy, A.T., et al. (2014). Embryonic and adult-derived resident cardiac macrophages are maintained through distinct mechanisms at steady state and during inflammation. *Immunity* *40*, 91–104.
- Gibbons, M.A., MacKinnon, A.C., Ramachandran, P., Dhaliwal, K., Duffin, R., Phythian-Adams, A.T., van Rooijen, N., Haslett, C., Howie, S.E., Simpson, A.J., et al. (2011). Ly6Chi monocytes direct alternatively activated profibrotic macrophage regulation of lung fibrosis. *Am. J. Respir. Crit. Care Med.* *184*, 569–581.
- Godwin, J.W., Pinto, A.R., and Rosenthal, N.A. (2013). Macrophages are required for adult salamander limb regeneration. *Proc. Natl. Acad. Sci. U.S.A.* *110*, 9415–9420.
- Herold, S., Steinmueller, M., von Wulffen, W., Cakarova, L., Pinto, R., Pleschka, S., Mack, M., Kuziel, W.A., Corazza, N., Brunner, T., et al. (2008). Lung epithelial apoptosis in influenza virus

pneumonia: the role of macrophage-expressed TNF-related apoptosis-inducing ligand. *J. Exp. Med.* *205*, 3065–3077

Heredia, J.E., Mukundan, L., Chen, F.M., Mueller, A.A., Deo, R.C., Locksley, R.M., Rando, T.A., and Chawla, A. (2013). Type 2 innate signals stimulate fibro/adipogenic progenitors to facilitate muscle regeneration. *Cell* *153*, 376–388.

Knipper, J.A., Willenborg, S., Brinckmann, J., Bloch, W., Maaß, T., Wagener, R., Krieg, T., Sutherland, T., Munitz, A., Rothenberg, M.E., et al. (2015). Interleukin-4 Receptor α Signaling in Myeloid Cells Controls Collagen Fibril Assembly in Skin Repair. *Immunity* *43*, 803–816.

Lavine, K.J., Epelman, S., Uchida, K., Weber, K.J., Nichols, C.G., Schilling, J.D., Ornitz, D.M., Randolph, G.J., and Mann, D.L. (2014). Distinct macrophage lineages contribute to disparate patterns of cardiac recovery and remodeling in the neonatal and adult heart. *Proc. Natl. Acad. Sci. U.S.A.* *111*, 16029–16034.

Nahrendorf, M., Swirski, F.K., Aikawa, E., Stangenberg, L., Wurdinger, T., Figueiredo, J.-L.L., Libby, P., Weissleder, R., and Pittet, M.J. (2007). The healing myocardium sequentially mobilizes two monocyte subsets with divergent and complementary functions. *J. Exp. Med.* *204*, 3037–3047.

Nishiyama, K., Nakashima, H., Ikarashi, M., Kinoshita, M., Nakashima, M., Aosasa, S., Seki, S., and Yamamoto, J. (2015). Mouse CD11b+Kupffer Cells Recruited from Bone Marrow Accelerate Liver Regeneration after Partial Hepatectomy. *PLoS ONE* *10*, e0136774.

Ramachandran, P., Pellicoro, A., Vernon, M.A., Boulter, L., Aucott, R.L., Ali, A., Hartland, S.N., Snowden, V.K., Cappon, A., Gordon-Walker, T.T., et al. (2012). Differential Ly-6C expression identifies the recruited macrophage phenotype, which orchestrates the regression of murine liver fibrosis. *Proc. Natl. Acad. Sci. U.S.A.* *109*, E3186–95.

Ruffell, D., Mourkioti, F., Gambardella, A., Kirstetter, P., Lopez, R., Rosenthal, N., and Nerlov, C. (2009). A CREB-C/EBP β cascade induces M2 macrophage-specific gene expression and promotes muscle injury repair. *Proceedings of the National Academy of Sciences* *106*, 17475–

17480.

Shechter, R., Miller, O., Yovel, G., Rosenzweig, N., London, A., Ruckh, J., Kim, K.-W.W., Klein, E., Kalchenko, V., Bendel, P., et al. (2013). Recruitment of beneficial M2 macrophages to injured spinal cord is orchestrated by remote brain choroid plexus. *Immunity* 38, 555–569.

Shiraishi, M., Shintani, Y., Shintani, Y., Ishida, H., Saba, R., Yamaguchi, A., Adachi, H., Yashiro, K., and Suzuki, K. (2016). Alternatively activated macrophages determine repair of the infarcted adult murine heart. *J. Clin. Invest.*

Wang, J., and Kubes, P. (2016). A Reservoir of Mature Cavity Macrophages that Can Rapidly Invade Visceral Organs to Affect Tissue Repair. *Cell* 165, 668–678.

Wynn, T.A., and Vannella, K.M. (2016). Macrophages in Tissue Repair, Regeneration, and Fibrosis. *Immunity* 44, 450–46

Willenborg, S., Lucas, T., van Loo, G., Knipper, J.A., Krieg, T., Haase, I., Brachvogel, B., Hammerschmidt, M., Nagy, A., Ferrara, N., et al. (2012). CCR2 recruits an inflammatory macrophage subpopulation critical for angiogenesis in tissue repair. *Blood* 120, 613–625.

Publishing Agreement

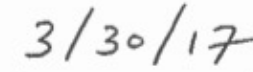
It is the policy of the University to encourage the distribution of all theses, dissertations, and manuscripts. Copies of all UCSF theses, dissertations, and manuscripts will be routed to the library via the Graduate Division. The library will make all theses, dissertations, and manuscripts accessible to the public and will preserve these to the best of their abilities, in perpetuity.

Please sign the following statement:

I hereby grant permission to the Graduate Division of the University of California, San Francisco to release copies of my thesis, dissertation, or manuscript to the Campus Library to provide access and preservation, in whole or in part, in perpetuity.



Author Signature



Date